DEVELOPMENT OF HYBRID GRAPHITIC CARBON NANOCOMPOSITES AS SENSING PLATFORM FOR PHARMACEUTICAL DRUGS IN-VITRO IN BIOLOGICAL FLUIDS

THESIS

SUBMITTED IN PARTIAL FULFILMENT OF THE REQUIREMENTS

FOR THE AWARD OF THE DEGREE OF

Doctor of Philosophy

IN

CHEMISTRY

BY

SHEKHER K

(Roll No. 716060)

RESEARCH SUPERVISOR

Dr. K. V. GOBI

Professor, NITW

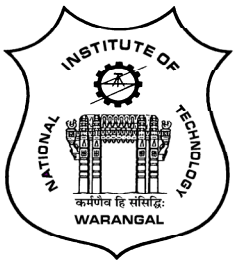

DEPARTMENT OF CHEMISTRY

NATIONAL INSTITUTE OF TECHNOLOGY WARANGAL

WARANGAL – 506 004, TELANGANA, INDIA

JULY – 2021

DECLARATION

This is to declare that the work presented in the thesis entitled ***"Development of Hybrid Graphitic Carbon Nanocomposites as Sensing Platform for Pharmaceutical Drugs in-vitro in Biological Fluids"*** is a bonafide work done by me under the supervision of **Prof. K. V. Gobi**, Professor in the Department of Chemistry and was not submitted elsewhere for the award of any degree.

I declare that this written submission represents my ideas in my own words and where others' ideas or words have been included, I have adequately cited and referenced the original sources. I also declare that I have adhered to all principles of academic honesty and integrity and have not misrepresented or fabricated or falsified any idea/data/fact/source in my submission. I understand that any violation of the above will be a cause for disciplinary action by the Institute and can also evoke penal action from the sources which have thus not been properly cited or from whom proper permission has not been taken when needed.

Date: (**SHEKHER KUMMARI)**

Place: **NIT Warangal** Roll Number: **716060**

CERTIFICATE

This is to certify that the work presented in the thesis entitled ***"Development of Hybrid Graphitic Carbon Nanocomposites as Sensing Platform for Pharmaceutical Drugs in-vitro in Biological Fluids"*** is a bonafide work carried out by **Mr. SHEKHER KUMMARI** under my supervision and was not submitted elsewhere for the award of any degree.

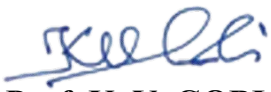

Prof. K. V. GOBI

(Research Supervisor)

ACKNOWLEDGEMENTS

ACKNOWLEDGEMENTS

During the course of my Doctoral Research work, I have received the assistance and support from the following people:

First and foremost, I am truly indebted and I express my earnest gratitude for my Research Supervisor ***Professor K. V. Gobi,*** Department of Chemistry, National Institute of Technology Warangal for his inestimable expertise and astute guidance. His unabated enthusiasm, which stems from his absolute command over the subject, has been a constant source of inspiration for me to work hard and the outcome is expressed in the form of this thesis. I consider myself as very fortunate for being his Doctoral Research Student and it would have been impossible to achieve this goal without his sturdy support and care.

I am grateful to ***The Director***, National Institute of Technology Warangal, for giving me the opportunity to carry out the research work and allowing me to submit in the form of thesis. I greatly acknowledge ***Ministry of Education, Govt. of India*** for the financial support in the form of Institute fellowship.

I express my gratitude to the Doctoral Scrutiny Committee members: ***Dr. Vishnu Shanker***, Chairman and Head, Department of Chemistry, ***Dr. Raghu Chitta***, Department of Chemistry and ***Dr. Abdul Azeem***, Department of Physics, NIT Warangal for their detailed review, constructive suggestions and excellent advice during the progress of this research work.

My sincere thanks are due to ***former Heads*** of the Department of Chemistry during the period of my research work.

I want to thank all the faculty members from the Department of Chemistry, namely Prof. A. Ramachandraiah, Prof. V. Rajeswar Rao, Dr. Vishnu Shanker, Dr. D. Kashinath, Dr. Venkatathri Narayanan, Dr. Raghu Chitta, Dr. B. Srinivas, Dr. K. Hari Prasad, Dr. S. Nagarajan, Dr. M. Raghasudha, Dr. Ch. Jugun Prakash, Dr. Ravinder Pawar, Dr. Mukul Pradhan, Dr. Rajeshkhanna Gaddam, Dr. V. Rajeshkumar and all the other faculty members for their valuable advice and encouragement throughout the research work.

I convey my special thanks from the bottom of my heart to my senior ***Dr. K. Koteshwara Reddy, Dr. M. Satyanarayana***, ***Dr. K. Yugender Goud, Dr. V. Sunil Kumar, Dr. V.V.N. Phani Kumar, Ms. S. Manasa*** and my juniors ***Mr. K. Sampath*** and ***Ms. G. Aarti*** for their continuous support and encouragement in each and every step of my research work.

With all happiness, I acknowledge the cheerful assistance rendered by all my research colleagues, Dr. K. Vimal Kumar, Dr. A. Varun, Dr. A. Ajay Kumar, Dr. K. Ramaiah, Dr. M. Sai, Dr. Chirra Suman, Dr. P. Vinay, Mr. S. Suresh, Mr. G. Ambedkar, Mr. K. Sathish, Mr. M. Srikanth, Mr. R. Venkatesh, Mr. Neeli Satyanarayana, Mr. P. Babji, Mr. K. Vijendhar Reddy, Mr. Ch. Raju, Mr. T. Dhanunjay Rao, Mr. A. Naveen reddy, Mr. A. Bhargava Sai, Mr. P. Venkatesham, Mr. B. Prashanth, Mr. B. Anjaiah, and my friends for their munificent support. I am grateful to the lab assistants *Mr. Praveen, Mr. Srinivas, Mr. G. Santhosh* and ***other supporting staff*** of the Department of Chemistry, NIT Warangal for their cooperation.

My heart goes to my beloved ***Family Members*** who with all their patience, prayers and faith in the Almighty, waited all these long years to see me reaching this stage. Their blessings and care always gave me new fervour and gusto to do something more with perfection.

I always remember and cherish the encouragement and inspiration provided by all my friends and well-wishers during the course of my research work.

Date: **SHEKHER KUMMARI**

CONTENTS

Table of Contents

SYMBOLS AND ABBREVIATIONS

IUPAC	:	International Union for Pure and Applied Chemistry
cm	:	Centimeter
s	:	Seconds
nm	:	Nanometer
i	:	Current
E	:	Potential
υ	:	Scan Rate
µA	:	Microampere
mV	:	Millivolt
µM	:	Micromolar
nM	:	Nanomolar
M	:	Molarity
F	:	Faraday Constant
R	:	Gas Constant
T	:	Absolute Temperature
A	:	Surface Area of Electrode
Z'	:	Real Impedance
Z''	:	Imaginary Impedance
R_{CT}	:	Charge Transfer Resistance
Z_W	:	Warburg Impedance
Ω	:	Ohm
Da	:	Dalton
λ_{max}	:	Absorption maximum
AuNPs	:	Gold Nanoparticles
AHP	:	3-Amino-5-hydroxypyrazole
B-R Buffer	:	Britton-Robinson Buffer
CA	:	Chronoamperometry
Chit	:	Chitosan
CME	:	Chemically Modified Electrodes
CNF	:	Carbon Nano Fiber

CVD	:	Chemical Vapour Deposition
CV	:	Cyclic Voltammetry
CA	:	Chronoamperometry
DPV	:	Differential Pulse Voltammetry
EDX	:	Energy Dispersive X-Ray Spectroscopic Analysis
EIS	:	Electrochemical Impedance Spectroscopy
5-FU	:	5-Fluorouracil
GCE	:	Glassy carbon electrode
5-HT	:	Serotonin
LDL	:	Low-detection-limit
MTX	:	Methotrexate
MWCNT	:	Multiwall Carbon Nanotubes
NFT	:	Nitrofurantoin
PBS	:	Phosphate buffer solution
RSD	:	Relative Standard Deviation
SWV	:	Square Wave Voltammetry
SEM	:	Scanning Electron Microscopy
SPCE	:	Screen Printed Carbon Electrode
VAL	:	Valacyclovir
XRD	:	X-ray Diffraction

CHAPTER 1

INTRODUCTION

1. Introduction

Extreme increases in industrial advancement and in public health criteria have formulated current modern trends in health industry such that the science need be extremely advanced to detect and quantify trace levels of various analytes from complex sample matrices with hands-free sophisticated point-of-care analytical systems at sub-nanogram levels. Thus, enhanced performances in analytical methods for quick and reliable monitoring are required. In order to reciprocate/comply with severe norms in worldwide legislations, rapid, sensitive, specific and portable on-site analytical tools need be developed for the target analyte to attain accurate results.

The main aim for the development of new chemical sensors and biosensors is the detection of specific target molecules with sensitive, selective, rapid and cost-effective process in a wide range of fields spanning from pharmaceutical, environmental and agriculture/food applications to health care including clinical diagnosis and treatment of diseases amongst others. Fabrication of electrochemical and biosensors by incorporation nanomaterials is showing significant enhancements in their performance during the past decades.

Electrochemical methods are powerful and resourceful analytical tools which offer excellent sensitivity, accuracy and precision. These techniques also useful in onsite analysis with wide linear determination range, moreover the instrumentation is low-cost. Electrochemical measurement techniques can be understood as two dimensional in which the potential is generally being correlated with qualitative properties and the current measurements are being correlated with quantitative properties. This selectivity depends on the available potential range and the number of analyte molecules that are active in this range.

A study on the state of art of sensors with a special attention to the electrochemical sensors for small molecules is given in this chapter. A brief demonstration of various types of chemical sensors classified by their transduction techniques will be followed by the role of nanocomposites such as conducting polymers, CNTs, graphene and metal nanoparticles, etc. as a recognition layer in sensors with a comprehensive literature report. Then, with a description on the literature reports of the use of chemically modified electrodes (CMEs) in the analyses of pharmaceutical drugs, the objectives followed by research framework will be presented.

The detection of sub-micro or sub-nanogram levels of pharmaceutical drugs at various stages of medical diagnosis is very crucial. For an example, it is important in the study of anticancer drugs in cancer patients for dosage selection and dosing intermissions in clinical applications. Once the drug is administered, it undertakes several metabolic steps, and to determine those steps, we must have some different analytical approaches to follow the administered drug in biological samples. There are two prime classical analytical methods: high performance liquid chromatography (HPLC) and gas chromatography (GC), which are very sensitive and promising in order to quantify the various targeted molecules. Sabourian and research group published an important review on HPLC methods for quantifying anticancer drugs in human samples[1]. Klimczak et al. determined sub-microgram levels of vitamin C by HPCL method[2]. Jiping Ma proposed a metal organic framework (MOF)-based magnetic solid-phase extraction from environmental water samples for the detection of pesticides by HPLC-DAD with a very low detection limit[3]. Yilmazn et al. developed voltammetric and gas chromatographic methods for the diclofenac detection in pharmaceutical drugs [4].

But these methods are laboratory based techniques involving bulky non-transportable instrumentation and a number of tedious time-consuming separation and purification protocols. For modern world applications, it is essential to fabricate ready-to-use portable novice-friendly methods for direct determination of trace levels of pharmaceutical compounds from complex sample matrices.

Chemical sensors

Chemical sensor is a device that transforms chemical information (activity, concentration, partial pressure) into a measurable signal. A chemical sensor is mainly divided in to two parts, recognition part and a transducer part. Recognition element comprised in the recognition zone undergoes chemical reactions or binding interactions with the target analyte molecule, and then the chemical information is converted into a readable physical signal at the transduction element of the transducer zone. When the readable output signal is of electrical nature, then the sensing systems is defined as electrochemical sensors, which are classified into potentiometric, amperometric and conductometric sensors. Electrochemical sensors are continuously advanced and becoming important analytical tools for the process of analysis.

1.1. Transduction methods

There are many analytical techniques available and applied to the development of sensors. From the all available techniques, spectroscopic, piezoelectric, optical and electrochemical methods have been employed as transduction methods in developing electrochemical and biosensors. In the past years, plenty of articles and reviews were published by using different types of transduction methods in biosensors development. Those are: electrochemical[5–12], fluorescence[13–18], luminescence[19–22], chemiluminescence[23–25], Raman spectroscopy[26–31], quartz crystal microbalance[32–36], capillary electrophoresis[28,37–39], surface plasmon resonance[40–43] and cantilever biosensor[44–46]. Various transduction methods explored for the development of biosensors are shown in Fig. 1.1.

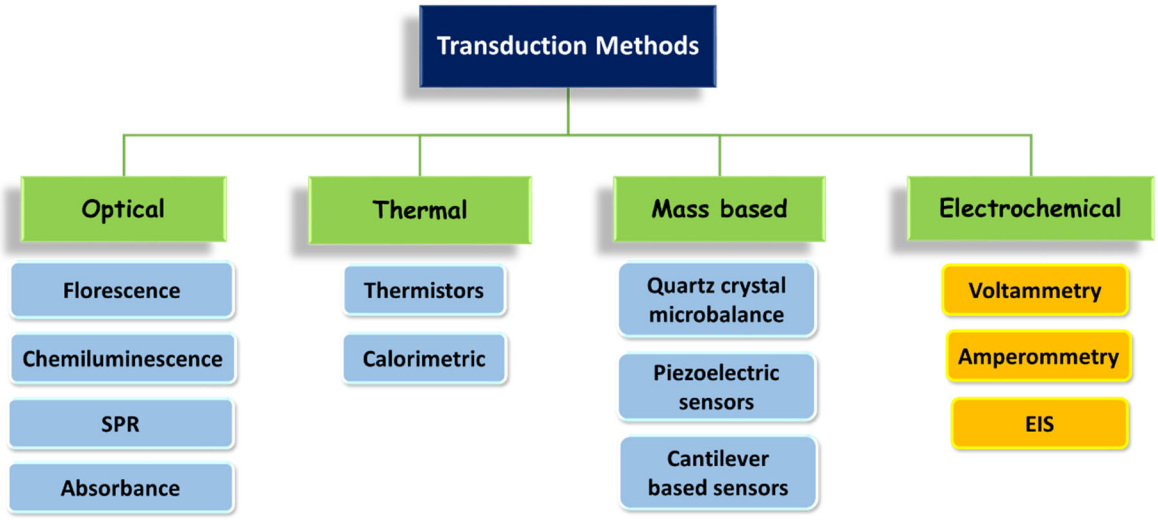

Fig. 1.1. *Various transduction techniques applied in chemical sensor systems.*

1.1.1. Optical sensors

Optical biosensors have brought many advances and opportunities for biosensing in medicine, life science and relevant areas. Optical transducers were investigated for regular medical diagnostics and research applications also[47]. Optical sensors quantify different properties of analyte molecules and provide a real-time, label-free comparable detection. There are many variety of optical spectroscopy techniques (e.g., fluorescence, Raman, phosphorescence, luminescence and absorbance) working in various types of biosensors.

The continuous monitoring of an analyte through optical means can be considered into two subcategories, one is direct sensing scheme and the other is a reagent-mediated sensing scheme. In direct sensing scheme, an intrinsic optical property (such as absorption, fluorescence, etc.) of the analyte is monitored. Based on the direct sensing methods to design and make an optical sensor, they divided into various subcategories:

- Absorption – based Sensing
- Fluorescence – based Sensing
- Raman and Surface Enhanced Raman Scattering (SERS) – based Sensing

The second one reagent-mediated sensing scheme is applicable when the analyte does not have an adequate intrinsic optical property which could be monitored directly. Here, sensing can be achieved by employing a suitable indicator whose spectral properties imply the analyte's concentration. These are broadly divided into two categories.

- Indicator – mediated Colorimetric Sensing
- Indicator – mediated Luminescence Sensing

1.1.2. Thermal sensors

The heat generation during enzyme/substrate reactions can be used in a calorimetric biosensor. Recently, Wang and colleagues described a thin film cantilever thermal biosensor by using high Seebeck coefficient material silicon to design a highly sensitive thermal sensor, and the thermocouple thermal sensor with silicon and metal needs heat treatment to realize ohmic contact for high sensitivity[48]. Xie et al. explained briefly the principles and features of thermal biosensors and included a discussion on the different types of thermal transducers[49]. Satoh et al. have demonstrated calorimetric microsensors in 1995 for the detection of cholesterol in blood serum by enzymatically produced heats of oxidation and decomposition[50]. Recently, Xiao et al. developed calorimetric biosensor for detection of cancer biomarkers by Au nanoparticles-decorated Bi_2Se_3 nanosheets[50].

1.1.3. Mass sensors

Quartz crystal microbalance (QCM) sensors is one type of mass sensor which responds to the changes of micro- and nanogram quantities of mass adsorption or desorption with the change

in the frequency of the resonating quartz crystal. The piezoelectric AT-cut quartz crystal is inserted between two electrodes. The electrodes are combined to an oscillator and applied an AC voltage over the electrodes. Due to the piezoelectric effect, the quartz crystal oscillates at its resonance frequency. Adsorption of analyte molecules on the quartz crystal modulates the resonance frequency of the crystal, and the change in resonance frequency indicates the mass adsorbed, leading to quantitative analysis [51–54].

Cantilever sensor systems are composed of multiple micron-thick cantilevers that respond by bending due to changes in mass [55–57]. Specific coatings are applied to the cantilevers to adsorb the chemicals of interest selectively.

Compared to all other transduction methods (*optical, thermal and mass sensors*), electrochemical methods are providing great advantages in terms of time, cost and operating process in many fields since its introduction. So, in the introduction, electrochemical techniques which were investigated in my research for the development of electrochemical sensors have been focussed along with thorough literature review (Fig. 1.2).

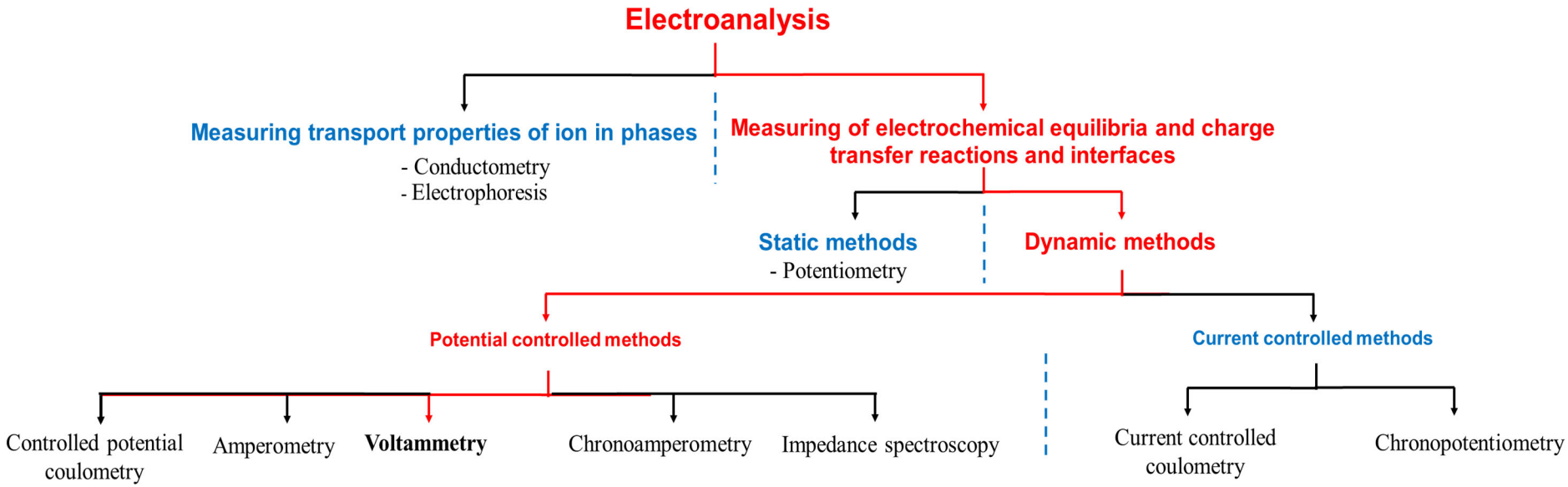

Fig 1.2. *A possible subunit of electroanalysis. ''Dynamic techniques'' are those in which the electrochemical equilibrium is shifted with the help of an excitation (current changes or potential changes), whereas in the ''static techniques'' the electrochemical equilibrium at the electrode is not affected. Sometimes, the dynamic techniques are described as active, and the static techniques as passive techniques.*

1.1.4. Electrochemical sensors

Extensive research investigations are going on for the fabrication of sensor systems towards various specific targets by using electrochemical analytical techniques[58–65]. The sensor systems operate by reacting with the analyte and produce electrical signal proportional with the analyte concentration. The sensor consists of minimum two electrodes – working and counter electrodes to create complete system. The main advantages of these systems are easy construction, the possibility of portability and miniaturization, high sensitivity, selectivity and comparatively low costs. Related to other methods, electroanalytical methods offer advantages such as portable and rugged instrumentation without any movable mechanical parts, on-site analysis and pocket size analyzers. The combination of nanomaterials with electrochemical transducers led to promising sensor systems for detection of numerous analytes of low- and high-molecular weight compounds[66–70]. The electrochemical sensors are mainly classified as: potentiometric, conductometric, voltammetric and amperometric sensors.

Potentiometric sensors

Toko and his group has designed an electronic tongue based on potentiometric sensing first time in 1998 called "taste sensor'' by using eight potentiometric electrodes made of different lipid–polymeric membranes[71]. Since early 1930's, potentiometric sensors have found most extensive practical applicability due to their ease, familiarity and cost. The potentiometric sensors has measured the potential difference between the two electrodes, reference and indicator electrodes. The measured potential used to determine the analytical quantity of interest, in general, the concentration of some components of the solution. Actually, in this system, we measured the potential difference of reference and indicator electrodes without separating the electrochemical cell. While the half-cell potential of the reference electrode remains constant, potential of the indicator electrode reciprocates the analyte concentration. In results, the change in the cell potential could be interrelated to the concentration of the analyte in logarithmic manner. Mainly three types of potentiometric devises are there:

- Ion-selective electrodes (ISE)

- Coated wire electrodes (CWE)
- Field effect transistors (FET)

The ion-selective electrode is an indicator electrode, which is proficient to selectively measure a particular ionic species. ISEs consist of semi-permeable membrane, which separate the test sample from the inside contents of the electrode but allows the permeation of particular type of ions selectively across the membrane. One of the electrodes is the working electrode whose potential is determined by its environment, while the second electrode is a reference electrode. The cell potential can be related to the concentration of the dissolved ions[72–74]. Under classical CWE design, a conductor is directly coated with an appropriate ion-selective polymer to form an electrode system that is sensitive to electrolyte concentration [75]. The field effect transistor (FET) is a solid-state device that exhibits high input impedance and low output impedance, hence it is capable of monitoring charges build up on the ion sensing membrane. Polymer matrix (electrode modifiers) of the potentiometric sensors can be altered by the immobilization of biological materials leading to the development of potentiometric biosensors[76,77].

Voltammetric/Amperometric sensors

Voltammetry/Amperometry is one of the electroanalytical methods in which the signal of interest is current that depends on the concentration and characteristic of the analyte. At the inert electrode, some chemical components are oxidized or reduced while electrons are exchanged between the working electrode and analyte. The direction of the electron-flow depends upon the properties of the analyte and is controlled by the electric potential applied to the working electrode. electrochemical cell consists of working, reference and counter electrodes. The working electrode is the electrode at which the reaction takes place, the reference electrode provides stable potential components to the working electrode and an inert conducting material (e.g. platinum) used as counter electrode. Supporting electrolyte is added to remove electromigration effects, to decrease the resistance of the solution and to maintain the ionic strength constant in controlled potential experiments.

Cyclic voltammetry

In CV analysis, the potential of the working electrode is changed at a fixed potential ramp in the forward and backward directions while the current is monitored, and the resultant current

profile against potential is called voltammogram. During the measurement of cyclic voltammetry, the potential is ramped to a more positive or negative side, but at the end of the sweep, the direction of the potential scan is reversed. The potential is applied between the reference and working electrodes, and the current at the working electrode against the counter electrode (auxiliary electrode) is measured. The results are plotted as current versus potential. Based on the initial scan direction, the forward scan produces a current peak for a specific analyte that can be either reduction or oxidation current.

Differential pulse voltammetry

Among the various pulse voltammetry techniques developed, DPV is the most important and widely used technique [78,79]. The main idea used in DPV is to subtract the current measured before the step from the measured current at the end of a potential step (Fig. 1.3 A). For this, potential pulses are applied to the electrode as staircase ramp.

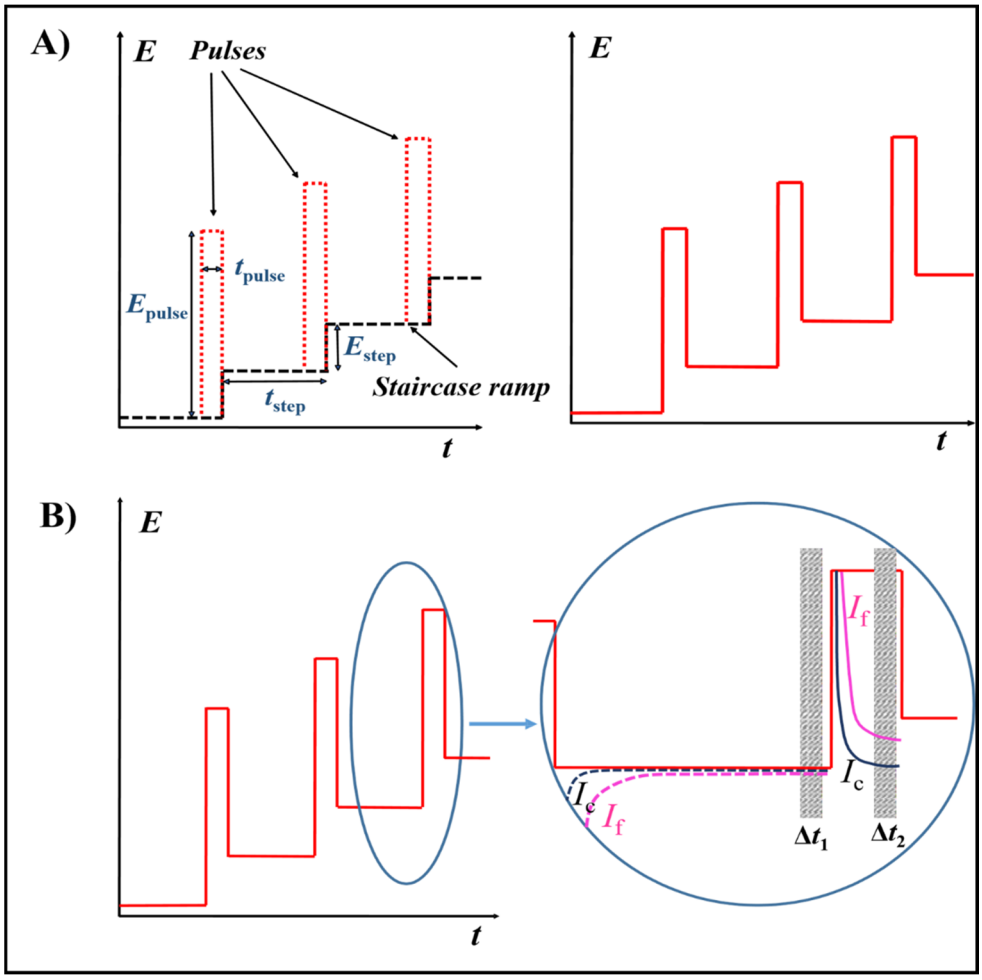

Fig. 1.3. **A)** *Left side: with the potential pulses of the superposition staircase ramp. Right side: the potential–time function resulting from superposition. B) Potential–time function in differential pulse voltammetry. On the right side, the time periods* Δt_1 *and* Δt_2 *for current measurements are shown and also the capacitive and faradaic currents before the pulse (dashed lines) and at the end of the pulse (full lines).*

The potential–time function provides the possibility to subtract the current shortly before the pulse from the current sampled at the end of the pulse (Fig. 1.3 B). Each and every pulse will produce one measuring point according to the equation:

$$I_{n2} - I_{n1} = \Delta I_{n,dp}$$

Here, number of individual pulse is *n*. DPV contains of discrete $\Delta I_{n,dp}$ data plotted against the applied potential of the working electrode. This curve be similar to the first derivative of the direct current voltammogram, but it should be highlighted that it is not simply the mathematical first derivative. Figure 1.4 shows a schematic differential pulse voltammogram. DPV employed widespread because it is possible to determine electroactive compounds below nanomolar levels also.

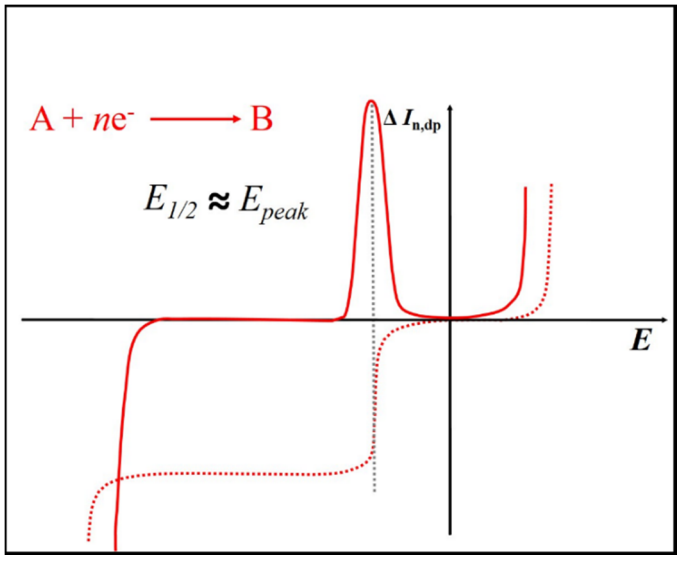

Fig. 1.4. *Differential pulse voltammogram (solid line), and the relevant polarogram (dotted line)*

Electrochemical impedance spectrometry (EIS)

Electrochemical impedance spectroscopy (EIS) or ac impedance methods have seen remarkable increase in popularity in recent years. Actually, in initial days, it was used for the

double-layer capacitance determination[80], The application of EIS studies has extended its range in recent years and widely used as a characterization technique in various systems for instance in the electrode and complex interfaces. The EIS, studies the response of system by applying a small ac potential to the system, this sinusoidal ac signal has been applied to the system at different ac frequencies. Therefore, these studies have been named as Impedance spectroscopic studies. The response of the system for the applied ac potential at different frequencies is a characteristic property of that particular system. Hence the information about the system will be obtained from these studies.

Macdonald, in his review[81], outlined the foundation of EIS. Electrochemical impedance spectroscopy is an outstanding, non-destructive, accurate technique for examining processes occurring at the surface of the electrode. In this technique, a small amplitude of sinusoidal voltage the electrochemical system will be given and the system current response to the input voltage will be measured as faradaic impedance. The EIS studies consist of two different plots, the former one is Nyquist plot and the later one is Bode plot. In Nyquist plot the imaginary value of impedance and the real value of the impedance were plotted. These system characteristic plots contain lot of information about the system for instance the electrified interfaces and electron transfer reactions through the interfaces.The Nyquist plots for charge transfer systems generally exhibits a depressed semi-circular pattern and a straight line making a 45° angle with the x-axis. The depressed semi-circular region at high frequencies implies the electron transfer limited process. The occurrence of a straight line indicates the Warburg impedance which mainly occurs because of the diffusion process. Using this Niquist plot we can obtain information about the electron transfer kinetics at the interface and diffusion processes. For example, if there is only a straight line was observed in the Nyquist plot indicates the occurrence of fast electron transfer reactions at the system. Whereas, large depressed semicircular pattern gives information about slow electron transfer processes. Impedance parameters such as solution resistance (Rs), charge transfer resistance (Rct), double layer capacitance (Cdl), CPE exponent (n) and Warburg impedance (W) etc, were obtained by fitting the experimental data with appropriate equivalent circuit models. the second EIS plot is called Bode plot, in which the logarithm of frequency(X-axis) is plotted with total impedance (Y-axis) value of the system and the logarithm of frequency(X-axis) is also plotted with phase angle shift (Y-axis).

1.2. Recognition elements

1.2.1. Biological recognition materials

A biological recognition element or bioreceptor is a biological element (e.g. enzyme) which is very sensitive and selective towards recognizing the specific analyte that could be enzyme substrate, antigen, complementary DNA. It is essential for a bioreceptor to be highly sensitive to the specific analyte to avoid interference by other elements from the sample medium[82].

Enzymes In 1962, Leland Clark first time introduced the enzyme-based biosensor and they fabricated an electrochemical biosensor for detection of glucose in blood, depending on the enzyme glucose oxidase [83]. Enzyme-based biosensors developed widely since then have exposed. Enzymes that can recognize specific analytes are proficient biocatalysts such as urease [84], peroxidase[85] and redox enzymes[86]. The working principle is depends on a catalytic reaction and binding abilities for the specific molecules[87]. There are several possible mechanisms for analyte recognition process:

1) Enzyme converting the analyte into a sensor-detectable product

2) Detection of an enzyme inhibited or activated via the analyte; and

3) Monitoring the modification of enzyme properties

Recently, Yang et al. had constructed a potentiometric glucose biosensor by successfully anchoring the synthesized Fe_3O_4-enzyme-Ppy nanoparticles on the magnetic glassy carbon electrode (MGCE) surface[88]. Das and research group published an important review article on recent advances on developing third generation enzyme electrodes for the applications of biosensor development[89]. R. B. Rakhi el al. reported a sensitive enzymatic glucose detection based on a biosensor platform of Au/MXene nanocomposite[90]. Nguyen and group published review article which examines the operating principle of enzymatic biosensors utilizing electrochemical, thermistor, optical and piezoelectric measurement methods[91]. As well, enzyme-based biosensors could be employed for extended time period because enzymes are stable and not consumed, while the stability of the enzyme decides the lifetime of the sensor.

Antibodies Electrochemical immunosensors (EIs) are one more type of biosensors which have recently fascinated a lot of attention for initial diagnosis and medical analysis of diseases[92].

In EIs, antigens and antibodies can be used as bioreceptors, and EIs are suitable for the clinic diagnostics of many diseases. Nakhjavani et al. recently introduced a simple and ultrasensitive immunosensor to the detection of the lowest alteration of CA 15-3, the standard biomarker of breast cancer, by modifying gold electrode where anti-CA 15-3 antibody was immobilized[93]. Khan et al. reported a novel, label-free impedimetric immunosensor for sensitive and rapid detection of myoglobin by immobilizing anti-myoglobin antibody on multiwalled carbon nanotube coated screen-printed electrode [94]. Ferreira et al. described an interdigitated immunosensor for cystatin C detection based on polypyrrole/carbon nanotube electrochemical capacitor[95]. Tang et al. has designed an important integrated automatic electrochemical immunosensor array for the simultaneous detection of hepatitis A, hepatitis B, hepatitis C, hepatitis D, and hepatitis E[96]. But, in terms of the sensing mechanism, all immunosensors depended on the sensitivity of the molecular recognition to create a stable antigen–antibody complex[97].

Nucleic acids Nucleic acid based biosensors use the paired components of nucleic acids as the biological recognition element. For example, the binding reaction from two single-strand DNA (ssDNA) chains to establish double-stranded DNA (dsDNA) was used. The sequences that are complementary to a recognized target nucleic acid sequence can be generated, tracked and eventually immobilized on the sensor.

Aptamer Aptamer sensor is a typical bioderivative biosensor, and aptamer is chemically related to nucleic acid probes but based on the principle of antibody and antigen [98]. Aptamer sensors have few advantages compared to antibody-based biosensors, which include a high binding efficiency, use of a smaller size recognition element, needs less sophisticated process and avoids animal source components.

Zhu et al. developed a conducting polymer/gold self-assembled nanocomposite based aptamer sensor for highly sensitive label-free detection of kanamycin. The sensing surface was immobilized with an in-vitro selected DNA aptamer onto a gold nanoparticle-comprised conducting polymer[99]. Recently, in 2020, Shaoguang Li et al. demonstrated a re-engineered electrochemical aptamer-based biosensors to tune their useful dynamic range via distal-site mutation and allosteric inhibition[100]. Kim et al. proposed a flexible three-dimensional carbon nanoweb (3DCNW)-based aptasensor for the detection of the oncogenic biomarker, platelet-induced growth factor (PDGF)[101].

Despite of these advantages, some of the problems associated with aptasensors is the reduction in the assay efficiency that results from the properties of nucleic acids such as chemical simplicity and structural pleomorphic.

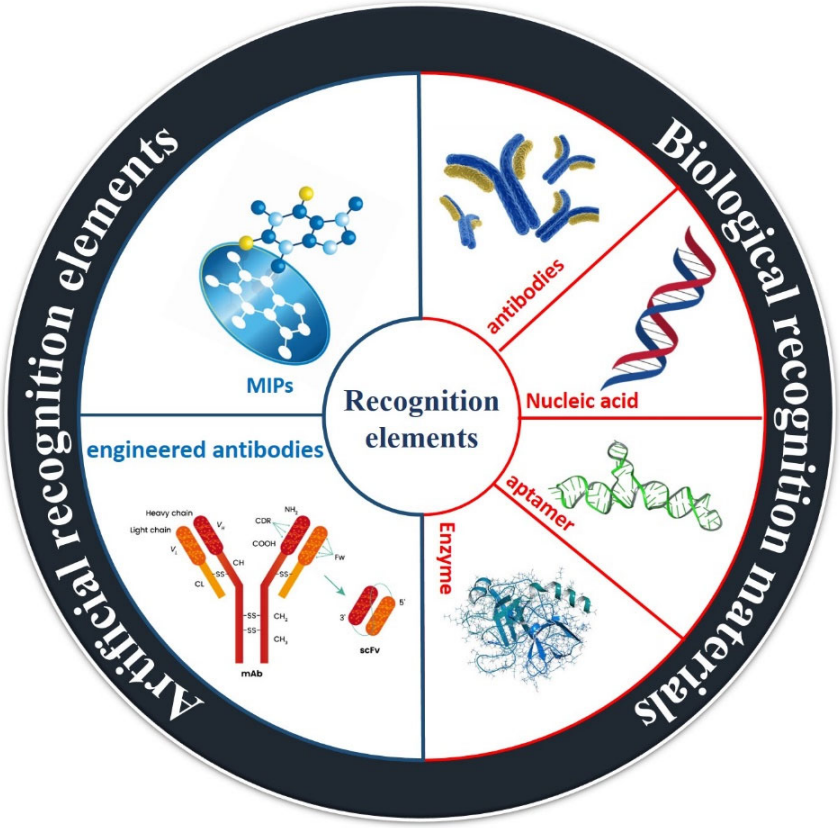

Fig. 1.5. *Representation of recognition elements: artificial (MIPs, engineered antibodies) and biological (antibodies, nucleic acids, aptamers and enzymes).*

1.2.2. Artificial recognition elements

Molecularly imprinted polymer (MIP) It is a polymer that is processed/synthesized using the MIP technique which leaves cavities in the polymer matrix with an affinity for a chosen "template" molecule. Alexander and research group have reported a thorough study on the development of molecular imprinting science and technology from the unexpected discovery of Polyakov in 1931 to the report on applications of imprinted polymers in 2003[102]. Joseph et al. have described in his recent review the production processes of imprinted polymer, method and the applications of the reported sensors. An in-depth survey of new applications to gas-phase

sensing also carried out, but the attention is mainly on the advancement of sensors for targets in solution. Literature reports included among the applications are those designed to detect toxic chemicals, drugs, toxins in foods, pathogens, and explosives [103]. Blooming et al. provided a critical review for inclusive overview of the present research on electrochemical sensors depending on MIPs on nanostructured carbon material surfaces for applications towards electrochemical detection[104]. In 2020, Hatamluyi et al. established an electrochemical sensor depending on MIP technique coupled with carbon quantum dots unified hexagonal boron nitride nanosheets for determination of trace levels of oxaliplatin[105]. Cao and group published a critical review on recent advances of MIP based sensors in the determination of food safety hazard factors[106].

Engineered antibodies These antibodies have made a huge progression in antibody production technologies in the past few decades. Engineered antibody is referred to the modified molecule obtained by processing recombinant antibody and reassembled antibody gene via recombinant DNA and protein engineering technology. According to the antibody production technology and application field, engineered antibodies are categorised into four main categories:

- Recombinant antibodies
- Biospecific antibodies
- Therapeutic antibodies
- Antibody-drug conjugates

Torrance et al. successfully carried out the covalent attachment of functional C-terminal cysteine residue (scFvCLcys) and demonstrated a surface plasmon resonance-based sensor[107]. Fahie and group have engineered oligomeric protein nanopores with rigid structures for the determination of a wide range of molecules including small analyts and biological species such as DNA and proteins[108]. Rajesh and research team demonstrated a CVD-graphene modified platinum nanoparticles (PtNPs) embedded functionalized engineered antibody nanohybrid transistor for the determination of breast cancer biomarker, HER3[109].

1.3. Literature on electrochemical sensors using nanocomposite materials

1.3.1. Carbon based materials

Carbon nanotubes

Carbon nanotubes (CNTs) found as most important and promising material from carbon group since discovered by Iijima 1991 [110], because of its significant physical and electrical properties: high electrical conductivity, high aspect ratio and good chemical stability. CNTs establish a new structure of graphitic carbon consisting of one or several concentric tubules and can be divided into multi-wall carbon nanotubes (MWCNT) and single wall carbon nanotubes (SWCNT).

Carbon nanotubes can easily promote the electron transfer reaction when used for electrode modification in the sensor system. In addition to the enhanced electrochemical reactivity, CNT-modified electrodes were helpful to accumulate very important biomolecules (e.g., nucleic acids) and to improve surface fouling effects. Research has been expanded to various areas on the applications, since the first use of CNT based electrode for dopamine detection by Britto et al. [73]. A very usual process to modify the electrode with CNTs is direct drop-cast on the electrode (mostly glassy carbon electrode) or abrasive immobilization (mostly on pyrolytic graphite electrode) method. The extraordinary sensitivity of CNT conductivity to the surface adsorbates made CNTs as highly sensitive nanoscale sensors. Because of these properties, CNTs are tremendously attractive for sensors ranging from amperometric enzyme electrode to DNA hybridization biosensor. To make use of such a remarkable properties of these unique materials, CNTs have to undergo proper functionalization and immobilization.

Graphene/Graphene oxide

Very recently Wang Yu et al. published a review on the progress in the functional modification of graphene/graphene oxide materials [111]. Ambrosi et al. reported an important review on the electrochemistry of graphene and related materials[112]. Mao et al. have reported a critical review on the advantages, facts, challenges and opportunities involved in graphene development[113]. Brownson et al. reported a tutorial review on electrochemical aspects of graphene, starting from fundamental concepts to prominent applications[114]. Pumera reported a review on electrochemistry of graphene-based nanomaterials and their applications[115]. A critical

review was reported by Liu et al. on the research articles relevant to the applications of graphene materials in biological and chemical sensors[116]. Guo and Dong have reported a critical review on the synthesis, molecular engineering, thin film hybrids and applications of graphene nanosheets in energy and analytical fields [117]. Georgakilas et al. have done an extensive review on the functionalization of graphene and discussed covalent and non-covalent approaches involved in graphene functionalization and applications of graphene derivatives in electrochemical biosensors[118]. Chen et al. have reported a critical review on the preparation, functionalization and electrochemical applications of graphene oxide [119].

1.3.2. Conducting polymers

From the discovery of organic conducting polymers, these materials have seen a wide range of applications in many branches of science and technology, such as primary and secondary batteries, metallization of dielectrics, electromagnetic shielding, electronic systems, antistatic coatings, supercapacitors, chemical sensors, biosensors, etc. Every conducting polymer have an extended p-orbital system, which is responsible to electron transfer from one end of the polymer to other[120,121]. Linear backbone "polymer blacks" such as polyacetylenes, polypyrroles, polyanilines, poly-(3-alkylthiophene), poly-(p-phenylene sulphide), polyindoles, etc., and their copolymers are the main class of the conducting polymers. One of the most important properties of conducting polymer is their ability to catalyze some electrodic reactions, and it can enhance the kinetic process of electrode when it have a thin polymer layer on their surface[121–123].

In general, there are three methods for electropolymerization, galvanostatic (constant current), potentiostatic (constant potential) and potentiodynamic (potential scanning). These methods are easier to be described quantitatively and therefore have been commonly utilized to investigate the nucleation mechanism and also the macroscopic growth. Potentiodynamic technique has been mainly used to get a qualitative information of the redox processes involved in the beginning of polymerization reaction and to observe the electrochemical behaviour of the polymer film after deposition by electrochemically. Polymer modified electrodes (PMEs) fabricated by electropolymerization technique have received extensive attention in the detection of analyte because of their easiness to fabricate, controlled growth of polymer films, and thin sub-micron films apart from sensitivity, selectivity, homogeneity in electrochemical deposition and chemical stability of the film[62,124]. Selectivity of PMEs as sensors depends on the combinations

of different mechanisms such as ion exchange, size exclusion, hydrophobic and electrostatic interaction.

1.3.3. Metal nanoparticles

The design and synthesis of new nanoscale materials has attained great interest from last two decades due to their wide-range applications in various fields. Among all the nanoscale materials, metal nanoparticles of gold, silver, platinum, palladium, etc. have received great attention owing to their significant properties and many promising applications. Metal nanoparticles have unique chemical, electrical, optical properties and varying size-dependent characteristics and are very promising for practical applications in different fields[125–127]. Nanoparticles behave different from bulk materials and their physical and chemical properties vary with their quantum scale dimensions. The electrocatalytic performance of metal nanoparticles were controlled by their size, composition, surface area and morphology [128,129]. In recent years, noble metal nanoparticles have been widely utilized, due to their extraordinary catalytic activities for both oxidation and reduction reactions. To avoid aggregation and to obtain high surface area, the metal nanoparticle catalysts are dispersed in organic polymers such as Nafion, colloids, porous substrates and surfactants, which ensure high dispersion and disaggregation of the nanoparticles [130–132]. The use of metal nanoparticle-based superstructures to design electrochemical devices is a very promising prospect. Till now, various methods have been used for tailoring metal nanoparticles on electrode surfaces, which include the anchoring by covalent attachment, electrostatic binding, electrochemical deposition, etc.

The catalytic activity of metal nanoparticles depends on their dispersibility and surface properties, while the high degree of dispersibility and large surface area are desirable for many catalytic processes usually. So, conducting polymers considered to be useful matrices for the immobilization of the dispersed nano metal catalysts[133]. Because of a relatively high electrical conductivity of some polymers, it is possible to shuttle the electrons through polymer chains between the electrodes and dispersed metal nanoparticles, where the electrocatalytic reaction occurs.

In addition to linker molecules, capping reagents would also affect the electron-transfer reactions and electrocatalytic functions of metal NPs. In the synthesis of AuNPs, the Brust-

Schiffrin method would be really a great advantage to prepare a very small AuNPs with uniform-size in large amounts by utilizing thiols. Since the synthesized metal nanoparticles can get easily segregated, the thiol-capped gold or silver NPs might be desired to be a component of the MNP-modified electrode [134,135]. However, the thiol capping is too strong to find good results in electrochemical activity, and the electrochemistry of thus-formed monolayer-protected Au/Ag clusters was extensively studied. Along with thiol capping, NPs stabilization by amine functional groups could also enhance the electrocatalytic activity[18,19].

We can also increase the electrochemical activity of modified electrodes by making the composites of metal nanoparticles along with different other electroactive materials such as graphenes, CNTs, conducting polymers, metal oxide frameworks, etc [138–140]. Along with CNTs, graphenes, conducting polymers and metal nanoparticles, researchers focused on the combinations with a number of other materials and molecular recognition elements for the development of electrochemical sensors.

1.4. Electrochemical sensors for pharmaceutical drugs

Anti-bacterial

Cefixime is an antibiotic prescription used to treat different types of bacterial deceases. These infections include strep throat, otitis media, urinary tract infections and Lyme disease. Karimian et al. proposed a molecularly imprinted polymer (MIP) immobilized MWCNT surface for the selective detection of cefixime by a voltammetric analysis. In this study, a covalent bonding was first established between cefixime and carboxyl-functionalized multiwall carbon nanotube modified GCE[141]. Dehghani and research group published an article based on electropolymerized polyaniline MIP layer on surface of graphene oxide and gold nanowires modified GCE for the detection of the cefixime[142]. Sagar et al. has reported cefixime detection up to nanomolar range by using the voltammetric method, and the cefixime detection is validated on MoS_2QD–AuNP fabricated screen-printed carbon electrode (SPCE) [143]. Abrishamkar et al. demonstrated nano zeolite modified carbon paste electrode for cefixime electrocatalytic oxidation [144].

Nitrofurantoin is most extensively recommended antibiotic prescription used to treat bladder infections, ear infections and minor skin infections, but it is not as effective for kidney infections. Muthusankar et al. developed a novel sensor system for simultaneously detection of

antibiotic drug nitrofurantoin and anticancer drug flutamide using the N-CQD@Co_3O_4/MWCNTs hybrid composite electrode and the electro-kinetics of the fabricated sensor system was analysed by using the cyclic voltammetry technique[145]. Dechtrirat and his research group successfully synthesised molecularly imprinted polymer (MIP) nanocomposite based on poly-(3,4-ethylenedioxythiophene)/poly(styrene sulfonate) (PEDOT:PSS) with the deposition of gold nanoparticles (AuNP) as topmost layer on SPCE for the detection of nitrofurantoin by voltammetric method[146]. He and Li published an article based on reduced graphene oxide/Fe_3O_4 nanorod composite electrode for detection of 1-aminohydantoin and nitrofurantoin[147]. Baby et al. synthesised phase-pure magnesium ferrite nanoparticles by deep eutectic-mediated solid-state synthesis at a temperature of 500 °C for the simultaneous determination of 4-nitrophenol and nitrofurantoin[148]. Recently, Kokulnathan and research team established a facile method for the preparation of a $LuVO_4$/graphene sheet (GRS) composite to form a hierarchical structure $LuVO_4$/GRS, and $LuVO_4$ was encapsulated within ultrathin GRS sheets. The synthesised electrocatalyst exhibited superior electrochemical sensing nature for the detection of nitrofurantoin (NFT)[149]. By utilizing an eco-friendly sonochemical method, flower-like nickel oxide trapped on boron doped carbon nitride (NiO/BCN) nanocomposite was synthesized for the electrochemical detection of NFT [150]. Karuppaiah et al. prepared lanthanum molybdate nanospheres (LMNSs), and their electrocatalytic activity towards NFT was demonstrated[151]. Annalakshmi developed a novel nickel stannite ($NiSnO_3$; NSO) nanoparticles via a facile sonochemical synthetic method and applied for electrocatalytic detection of nitrofurantoin[152].

Anti-viral

Valacyclovir is an important anti-viral drug, and it is pro-drug of acyclovir used against Herpes simplex virus (HSV) and Varicella-zoster virus. Todakar et al. investigated electrochemical detection of valacyclovir at the modified carbon paste sensor with reduced graphene oxide (rGO/CPE) by using square wave voltammetry [153]. Devarushi and research group reported an article to observe the electrochemical behaviour of the anti-viral drug valacyclovir at carbon paste electrode and its catalytic application with differential pulse voltammetry[154]. Adhikari et al. published an important review and emphases on the recent strategy and use of carbon nanomaterials such as single-walled carbon nanotubes, Bucky paper, graphene and their composites as sensing materials for the electroanalysis of pharmaceuticals and representative

biological compounds, acetaminophen, methylglyoxal, valacyclovir and glucose[155]. Jain and Pandey published a research article based on graphene/bismuth oxide/glassy carbon electrode (GRP-Bi_2O_3/GCE) as a sensor material for sensitive, selective detection of valacyclovir by using two important electroanalytical techniques, cyclic and square wave voltammetry techniques[156]. Saleh et al. reported a simple and rapid technique for the fabrication of a disposable sensor system depends on the electro polymerization of porous Cu-microparticles on pencil graphite electrode (Cu-PGE) for the electrochemical detection of valacyclovir[157]. Adhikari et al. developed a highly sensitive electrochemical sensor based on graphene nanosheets for simultaneous analysis of valacyclovir and acetaminophen through the concurrent electrochemical reduction and deposition of graphene oxide onto a glassy carbon electrode[158].

Acyclovir Dorraji et al. electropolymerised Eriochrome black T on the pre-treated GCE for the sensitive detection of acyclovir by DPV [159]. Shetti and group has designed a nano clay modified carbon paste sensor for determination of nanogram levels of acyclovir by square wave voltammetry[160]. Tarlekar et al. have proposed for the first time a single-walled carbon nanotube-Nafion composite electrode for the monitoring of antiviral drug acyclovir employing square wave voltammetry[161]. Hamtak et al. designed a new sensor system by anchoring multi-walled carbon nanotubes (MWCNTs) and TiO_2 nanoparticle into the polymeric matrix on nanoporous glassy carbon electrode[162]. Very recently, Shetti and research team developed a sensor based on bentonite and γ-Fe_2O_3 nanoparticles for the quantification of acyclovir[163]. Atta et al. introduced a novel sensor surface acquired by adapting a GCE surface by multi-walled carbon nanotubes layers, graphene, an ionic liquid crystal (ILC) and MnO_2, and the designed sensor (GCE/CNT/ILC/RGO/MnO_2) exhibited outstanding current responses for sofosbuvir, ledipasvir and acyclovir in human serum[164]. Ranganathan et al. developed a polystyrene:β-cyclodextrin inclusion complex-supported yttrium oxide (Y_2O_3)-modified glassy carbon electrode (PS:β-CD IC/Y_2O_3/GCE) for the simultaneous determination of two important antiviral drugs, acyclovir and 4-aminoantipyrine[165].

Anti-cancer

Anticancer or chemotherapy drugs are used to treat cancer and to control the growth of cancerous cells. There are many types of electrochemical sensors developed for the determination of anticancer drugs by modifying the working electrode.

5-Fluorouracil is an antineoplastic agent which acts as an antimetabolite to uracil and used primarily for the treatment of solid tumours of breast, colon and rectum. Bukkitgar et al. developed a sensor for the detection of 5-fluorouracil by using the carbon paste electrode modified with electrodeposited methylene blue thin film [166]. A highly effective electrochemical sensor for the analysis 5-fluorouracil was fabricated based on silver nanoparticles-polyaniline nanotube by Zahed and group[167]. Lima et al. described the application of modified carbon paste electrode with porphyrin-capped gold nanoparticles to detect 5-fluorouracil[168], and an "ON/OFF" switchable temperature-controlled electrochemical sensor was developed based on a microgel consisting thermo-sensitive conductive poly-(3,4-ethylenedioxythiophene) and poly-(N-isopropylacrylamide) by Mutharani et al. in recent time[169]. Hatamluyi et al. successfully synthesized graphene quantum dots-polyaniline/ZnO and developed highly selective and sensitive electrochemical sensor for determination 5-fluorouracil and irinotecan simultaneously [170]. Pattar and research group developed chemically reduced graphene oxide and chitosan (CRGO/CS) modified glassy carbon electrode and used to determine 5-fluorouracil by using cyclic, staircase and square wave voltammetric techniques[171]. Fouladgar reported amplified voltammetric sensor for the detection of doxorubicin and 5-fluorouracil using CuO-CNT nanocomposite/ionic liquid modified sensor[172]. Rahimi-Nasrabadi et al. demonstrated a praseodymium-erbium tungstate (Pr:Er) nanoparticles modified carbon paste electrode for the sensitive voltammetric determination of 5-fluorouracil[173].

Methotrexate is an anti-folate and chemotherapy agent for the treatment of neoplastic disorders, cancers including breast cancer, lymphoma, osteosarco and leukemia. Ensafi et al. fabricated an electrochemical sensor based on $CoFe_2O_4$/reduced graphene oxide (rGO) and ionic liquid modified-glassy carbon electrode for electrochemical determination of methotrexate by differential pulse voltammetric technique[174]. Šelešovská et al. described a novel sensitive voltammetric method for methotrexate determination by using differential pulse voltammetric technique at bare boron-doped diamond electrode[175]. Chen and research group established an electrochemical sensor for determination of methotrexate based on DNA and GO, and adsorptive voltammetric performances of methotrexate at the DNA sensor were studied using differential pulse voltammetry[176]. Wei et al. reported a simple method by using poly(L-lysine) modified glassy carbon electrode (PLL/GCE) to detect methotrexate in the presence of organic compounds [177]. Jandaghi et al. constructed a sensor system based on Ce-doped ZnO nano-flowers for the

detection of methotrexate[178]. Chen et al. fabricated a graphitic carbon nitride covered vanadium oxide nanocomposite (V_2O_5@g-C_3N_4) by a simple sonochemical approach for the electrochemical detection of methotrexate[179]. Zhou et al. developed an important analytical device for methotrexate sensing in whole blood by anchoring electrode surface with tungsten phosphide embedded nitrogen-doped carbon nanotubes (WP/N-CNT) [180]. Recently, Jandaghi et al. reported GCE altered by cerium-doped ZnO nanoflowers to develop a sensor for immediate detection of the two cancer drugs, methotrexate and epirubicin [181], and Deng et al. developed a novel acetylene black (AB) sensor modified with stearyltrimethylammoniumbromide (STAB) and applied to the determination of methotrexate in serum [182].

1.5. Aims and objectives

Quality of a drug is determined after establishing its authenticity by testing its purity and quality of the pure substance in the drug and its formulations. Various analytical methods including chemical, physical, physico-chemical and biological ones are employed for establishing the drug quality. Electrochemical methods are the most widely used one among the all physico-chemical methods. Following the development of spectrophotometric and electrochemical methods for detection of pharmaceutical drugs in our laboratory, the present study investigates the fabrication of electrochemical sensors for drugs such as Methotrexate, Serotonin, Nitrofurantoin and Valacyclovir. Influences of various analytical parameters on the sensor performance have been explored together with response range, effect of pH, scan rate, detection limit and interference for all the developed sensor systems. Mechanistic aspects of the electrodic reactions of the pharmaceutical drugs such as electrochemical transfer rate, number of electrons, diffusion coefficient and reaction mechanism. The developed sensors have been then applied for the determination of the drugs in pharmaceutical formulations, artificial physiological solutions and in serum samples to establish the applicability of these sensors for direct, on-site determination in real-world samples.

The main ***objectives*** of the present study are as follows. The overall aim of the present study is to design and present a novel electrochemical sensor technology that can rapidly detect the specified pharmaceutical drugs in real samples such as drug formulations, urine samples and blood serum at applicable/physiological concentration limits.

1. To fabricate an electrochemical sensor for the detection of **Methotrexte** using functionalized carbon nanotubes paste electrode (f-CNTPE).

2. To develop an electrochemical sensor for the detection of **Serotonin** by electrochemical deposition of gold nanoparticle onto conducting polymer layer on carbon nanotube based electrode.

3. To develop an electrochemical sensor for the detection of **Nitrofurantion** using electrochemically reduced GO-CNT based electrode.

4. To fabricate an electrochemical sensor for the detection of **Valacyclovir** using electrodissolution-induced deposition of nanoAu particle on *poly*-(3-amino-5-hydroxypyrazole) coated carbon paste electrode.

The developed sensor systems with the above stated objectives would offer a substantial opportunity towards the real time analyses of the specified drug molecules from artificial urine samples, human serum and pharmaceutical formulations successfully.

1.6. Thesis organization

The outline of the total research work taken up in the present study is schematically depicted in Scheme 1.1.

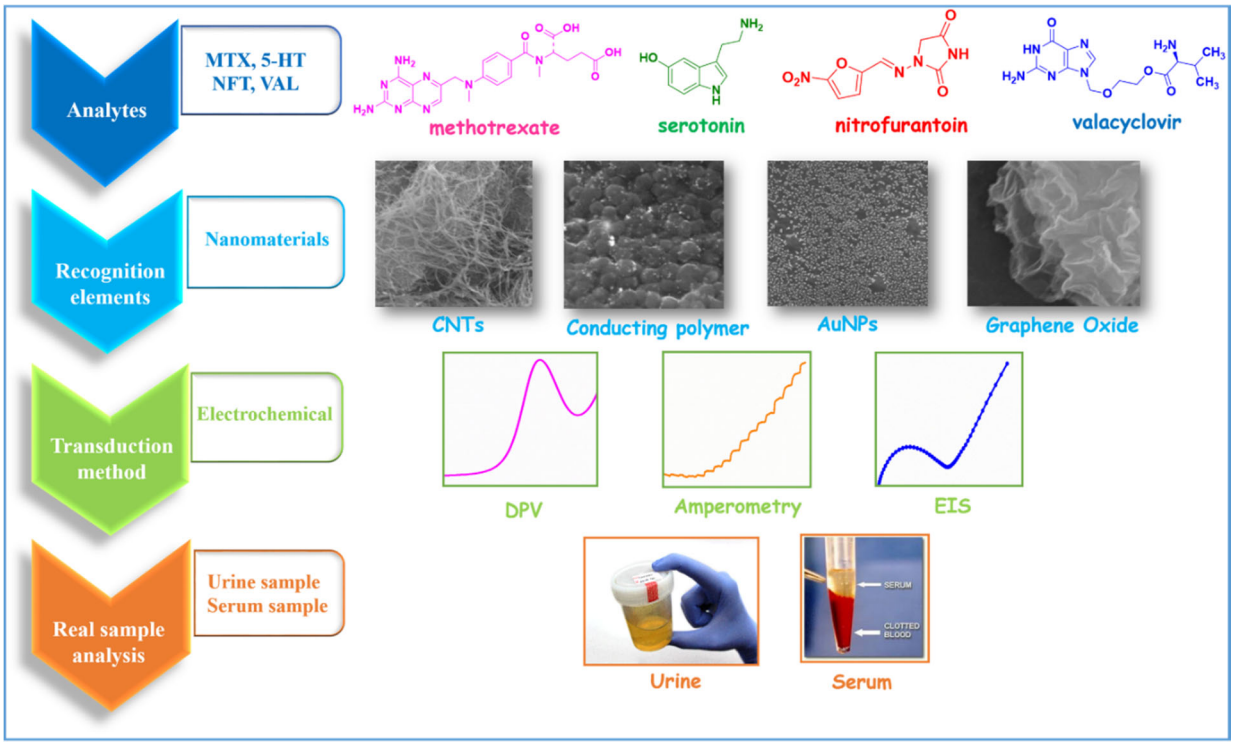

Scheme 1.1. Research framework

CHAPTER 2

Direct electrochemical determination of methotrexate using functionalized carbon nanotube paste electrode as biosensor for *in-vitro* analysis of urine and dilute serum samples

2.1. Introduction

Chemotherapy is one of the predominant methods followed for the treatment of cancers. Chemotherapy is usually applied in addition with the other therapies, such as surgery, hormone or radiation treatments. It is an aggressive treatment using pharmaceutical drugs in heavy doses to destroy rapidly increasing cancerous cells in our body. Methotrexate (2,4-diamino-N_{10}-methyl pteroylglutamic acid; MTX) is an anti-folate and chemotherapy agent for the treatment of neoplastic disorders, cancers including breast cancer, lymphoma, osteosarco and leukemia[183–186]. On the other hand, MTX leads to certain severe side effects, such as hepatic failure, bone marrow suppression and hypo albuminuria [184,185,187,188]. Because of the high dose levels and long duration of treatments of chemotherapy, it becomes very important to develop a simple, rapid and cost-effective method for timely on-site analysis of physiological samples for the quantitative analysis of active MTX concentration. Though a few analytical techniques are available for highly sensitive detection of MTX, such as HPLC [189,190], fluorimetry [191,192] and capillary electrophoresis [193,194], they are exceedingly disadvantageous and highly impractical due to extensive time consuming processes, complicated laborious procedures, need of technical experts to apply and highly expensive bulky instrumentation [195–198]. To overcome these difficulties, electroanalytical methods such as stripping voltammetry [199,200], pulse voltammetry, electrochemical impedance analysis, etc. are promising candidates because of their low-cost instrumentation, portable for on-site analysis, high sensitivity and novice-friendly [186,201–203]. In this work, an electrochemical sensor system for highly sensitive and selective detection of trace quantities of MTX from real-world samples has been developed.

From the past few decades, different types of nanomaterials have been effectively used for the development of biosensors such as nanographites, CNTs [204], graphene [205,206], metal nanoparticles [207,208] and core–shell nanoparticles [209]. Multi-walled carbon nanotubes (MWCNTs) are extensively probed, in recent years, because of their superior performance in electrochemical sensors and other fields[210–212]. MWCNTs can excellently promote electron transfer between the electroactive species and the electrode due to their high surface area and unique long nano-thread like geometry with high aspect ratio [213,214]. The remarkable electron-transfer ability of CNTs would promote the fabrication of nanoscale sensor using CNTs. Eventually the use of CNTs would lead to the decrease in response time, increase in surface area

and thus sensitivity, fabrication of micro sensors and multiplex analysis. CNTs will reduce electrode fouling and thus would highly improve prolonged usage, reusability and storage ability of such sensors [215–217]. Functionalized MWCNT has been used in the fabrication of carbon paste electrodes for effective reusability of the sensor in multiple analyses.

In recent years, various combinations of metal nanoparticles and carbon nanomaterials were explored for the development of electrochemical biosensors for MTX [175,218–223]. Boron-doped diamond electrode explored by DPV analysis exhibited a linear determination range of 0.05 - 20 μM MTX [175]. Anti-MTX polyclonal antibody anchored onto a self-assembled cysteamine monolayer was explored by electrochemical immittance spectroscopy and multivariate data analysis for the detection of MTX [218]. Single-walled carbon nanotube wrapped with dsDNA was cast to fabricate the electrode, and the developed sensor was found to exhibit a linear determination range of 0.02 - 1.5 μM MTX [219]. NanoAu particles adsorbed onto self-assembled monolayer electrode showed a low-detection-limit of 0.01 μM MTX by SWV analysis [220]. Copper nanoparticle deposited carbon black electrode was explored for the determination of methotrexate by SWV analysis, and a linear determination range of 0.25 - 2.2 μM with a low-detection-limit of 90 nM was obtained [221].

In this manuscript, we investigated the fabrication and development of a simple, low-cost MWCNT based carbon paste electrode without any metallic nanoparticles, so as to avoid aggregation based deactivation and to ensure stability and long-time storability. Selective detection of MTX in the presence of physiological electroactive interferents, ascorbic acid, dopamine, etc. has been investigated. Comprehensive analyses for the direct determination of MTX from pharmaceutical dosages, artificial urine and human serum samples without any time-consuming purification or extraction steps prior to the drug assay are carried out, and high recovery limits have been observed. Steady-state current–time analysis under hydrodynamic conditions mimic to flow-cell analysis for multiple samples has been investigated.

2.2. Experimental

2.2.1 Chemicals

Methotrexate, uric acid, ascorbic acid, dopamine and serotonin of >99.8% purity were procured from TCI, Japan. Chitosan (deacetylation 85%, 60–120 kDa), MWCNT (purity 95%, 10–

30 μm length and 20–30 nm OD) were purchased from SRL, India. All other chemicals were of analytical grade reagents with a minimum of 99.5% purity. Double-distilled water treated with Ultrahigh water purifier (Thermo Fisher Scientific, USA) with the final resistance of 18 Mohm was utilized all throughout the investigation and for the preparation of aqueous solutions. Phosphate buffer solution (PBS) was prepared by using 0.2 M H_3PO_4, followed by the addition of 0.1 M NaOH to adjust the pH to 3.2. Artificial urine solution was prepared according to the procedure reported elsewhere in the literature [224], by mixing 1.1 mM lactic acid, 2.0 mM citric acid, 170 mM urea, 90 mM NaCl, 25 mM NH_4Cl, 10 mM sodium sulphate, 25 mM sodium bicarbonate, 2.5 mM calcium chloride, 7.0 mM KH_2PO_4 and 7.0 mM K_2HPO_4, and then the pH was adjusted to 3.2 with NaOH.

Direct determination of MTX spiked in serum samples was carried out using human serum samples collected from a healthy donor, and aliquots of the collected serum samples were stored at -20 °C prior to use. MTX solution in PBS buffer (pH 3.2) was added to serum samples to prepare MTX-spiked serum samples.

2.2.2 Functionalization of MWCNT

MWCNTs were functionalized following the procedure reported earlier [225,226] with little modifications. MWCNT (120 mg) was added to 10 mL 3 M HNO_3, sonicated for few minutes and heated to 60 °C for 24 h under constant stirring. During the treatment, it is oxidized at side-wall defect sites and at nanotube ends to form carboxyl groups. The obtained black solid precipitate was centrifuged, and the centrifugate was washed repeatedly with water until the supernatant becomes neutral (pH = 7). The resultant functionalized MWCNT was dried at 80 °C in hot-air oven.

2.2.3. Fabrication of *f*-CNTPE electrodes

Functionalized MWCNT paste electrodes (*f*-CNTPE) have been prepared as follows: Functionalized MWCNT (50 mg) was mixed with paraffin oil at 5:1 wt. ratio in mortar. The paste was filled compact into 4.0 mm diameter Teflon tube, and the electrical contact was made from the other side of the tube using Cu wire. Surface of the electrodes was polished with butter paper before the experiment. Steps involved in the fabrication of *f*-CNTPE electrodes have been illustrated in Scheme 2.1.

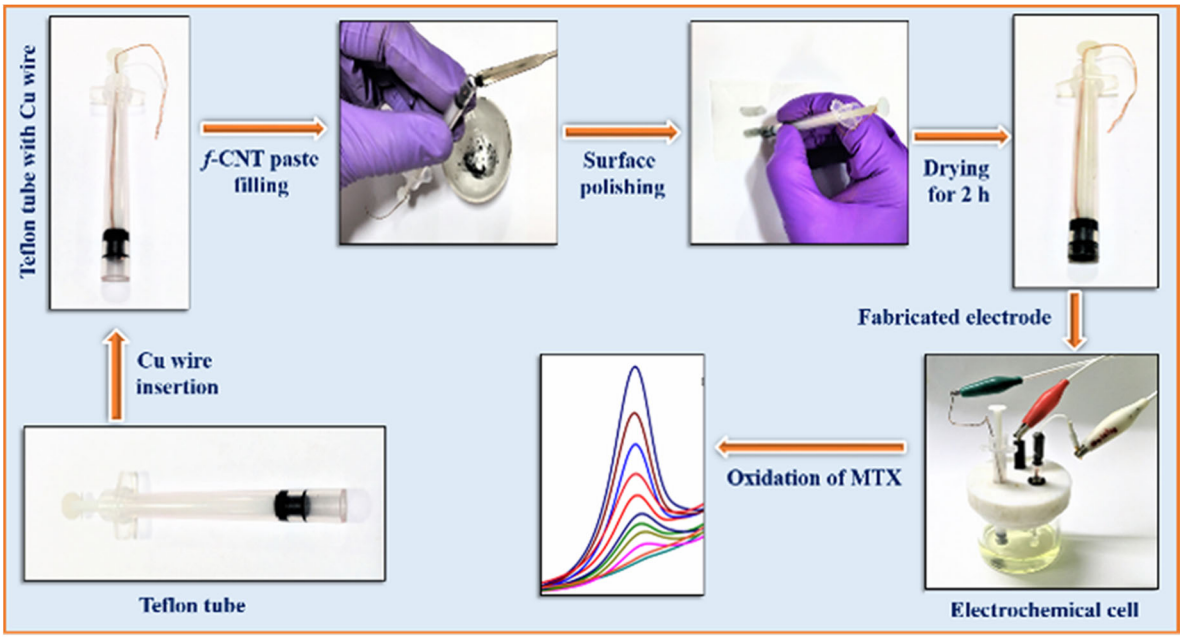

Scheme 2.1. Schematic representation of the fabrication of *f*-CNTPE electrode.

2.2.4 Electrochemical and SEM experiments

For electrochemical experiments, CHI 619d (CH International, USA) electrochemical workstation and three-electrode two-compartment cell with functionalized CNT paste electrode as working electrode, Pt wire counter electrode and Ag|AgCl (3 M KCl) reference electrode. Electrode potentials were referred against Ag|AgCl (3 M KCl). Experimental solutions were purged with nitrogen gas for 10 min before electrochemical analyses. All electrochemical measurements were carried out at room temperature of ca. 25 °C.

Scanning electron microscopic images of the sensor surface were recorded with TESCAN VEGA-3 SEM (Czech Republic) equipped with magnetron sputter coater (Quorum, SC7620 sputter Coater). Prior to the imaging, a conductive nano-film of Au (~5 nm thick) was sputtered on the electrode surface using Sputter coater. Morphological images of the sensor surface were recorded at a reduced pressure of 0.10 milli Pascal with magnification levels of up to 35,000 times.

2.3. Results and discussion

2.3.1. Characterization of *f*-MWCNT surface

Functionalized MWCNT was studied by vibrational Raman spectroscopy, which exhibits high potential for the analysis of graphitic nature of carbons [227,228]. The structural changes

occurred with MWCNT by the functionalization can be analyzed from the changes in vibrational Raman spectroscopy bonds. The Raman spectra of pristine MWCNT and *f*-MWCNT were recorded and shown in Fig. 2.1. They exhibit D-band (~1,340 cm^{-1}) related to the structural disorders and conversion of graphitic carbons leading to -COOH groups at CNT ends and defect sites, G-band (~1,570 cm^{-1}) related to graphitized carbon and G^{I}-band (~2,650 cm^{-1}) related to the first overtone of the D-band. The quantitative measurement of the functionalization of MWCNT would be indicated by the intensity ratio of I_D/I_G. The increase in the I_D/I_G value for *f*-MWCNT (1.10) compared to pristine MWCNT (0.951) clearly proves the decrease in graphitic carbon content and the functionalization of MWCNT.

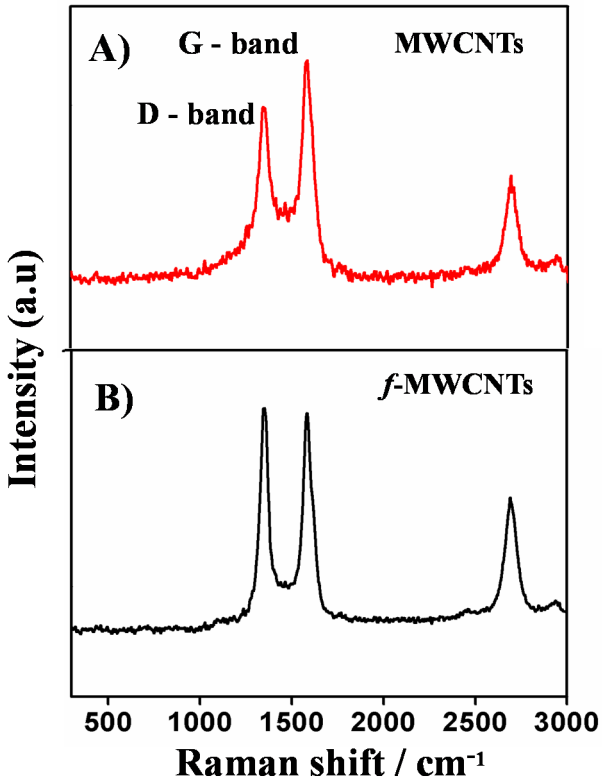

Fig. 2.1. *Raman spectra of (A) MWCNTs and (B) f-MWCNTs.*

Surface morphology of *f*-CNTPE was investigated by scanning electron microscopy at different magnifications. Before the imaging, a conductive nano-film of Au (~5 nm thick) was sputtered on the electrode surface, and the SEM images recorded at different magnifications are shown in Fig. 2.2. The electrode surface is comprised of long nano-thin thread like structures of CNTs, and individual CNTs are randomly oriented all over the electrode surface. The SEM images show that the CNTs are ribbon like structure of ~30 nm diameter. The SEM images of *f*-CNTPE

show an intense network of nano-threads of CNTs all over the surface along with high porosity simultaneously, and thus the effective electroactive surface area would increase enormously.

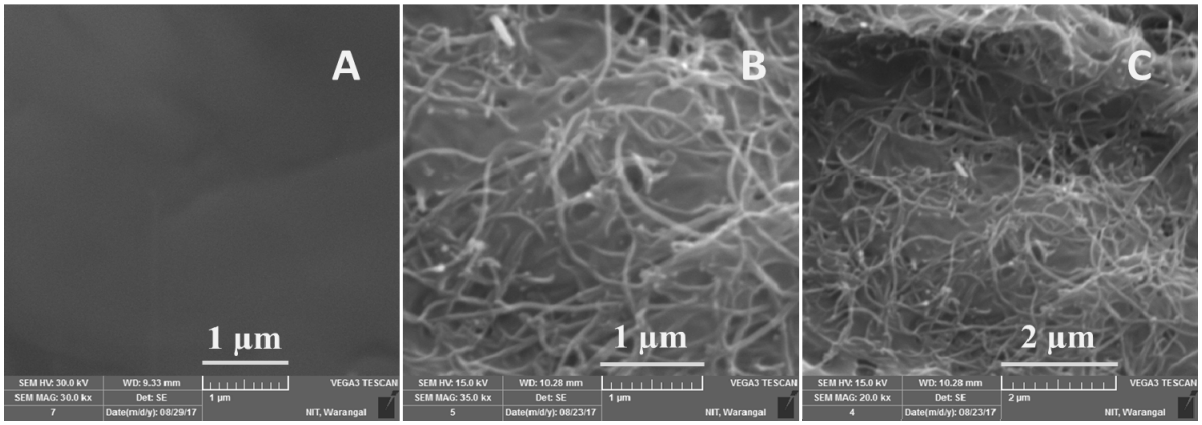

Fig. 2.2. *SEM images of CPE (A) and f-CNTPE (B, C) at different magnifications.*

2.3.2. Electrochemical behavior of MTX at *f*-CNTPE

Cyclic voltammetry is a basic and prime technique employed for the study of electrochemical characteristics of electrodes, analytes, electrode-solution interfaces, etc. To determine the electroactive surface area of *f*-CNTPE and control CPE electrodes, cyclic voltammetric studies of $K_3[Fe(CN)_6]$ were carried out in aq. 2.5 mM $K_3[Fe(CN)_6]$ + 0.1 M KCl using *f*-CNTPE and control CPE electrodes at different scan rates. We observed a higher peak current with *f*-CNTPE compared to the control CPE. The plots of the peak current against the square root of the scan rate were linear and passing through the origin, as shown in Fig. 2.3 (A). Electroactive surface area of the electrodes were determined using the Randles-Sevcik equation, employing the diffusion coefficient of $K_3[Fe(CN)_6]$ as 6.7 x 10^{-6} cm^2 s^{-1} [226,229]. Functionalized MWCNT paste electrode, *f*-CNTPE, exhibited an electroactive surface area of 0.210 cm^2, which is nearly two times higher compared to the geometric surface area of the electrode, 0.126 cm^2, and the control CPE electrode exhibited a surface area of 0.110 cm^2. From the observations, we conclude that the use of *f*-MWCNT enhanced the electroactive surface area of *f*-CNTPE electrode effectively.

Cyclic voltammetric measurements of MTX were carried out at *f*-CNTPE and CPE in 1.0 × 10^{-5} M MTX solution in PBS (pH 3.2), and the CVs recorded at 100 mV s^{-1} are shown in Fig. 2.3 (B). An irreversible oxidation peak was obtained in the potential range of +0.6 to +1.0 V with

no sign of peaks in the cathodic scan. Compared to the control experiments at CPE, the anodic peak current of MTX at *f*-CNTPE electrode is about two times higher and the anodic peak potential has been shifted to a less positive potential region by ~70 mV. The electrocatalytic effect is due to the enhanced surface area of *f*-CNTPE and the functionalization of CNT with reactive sites.

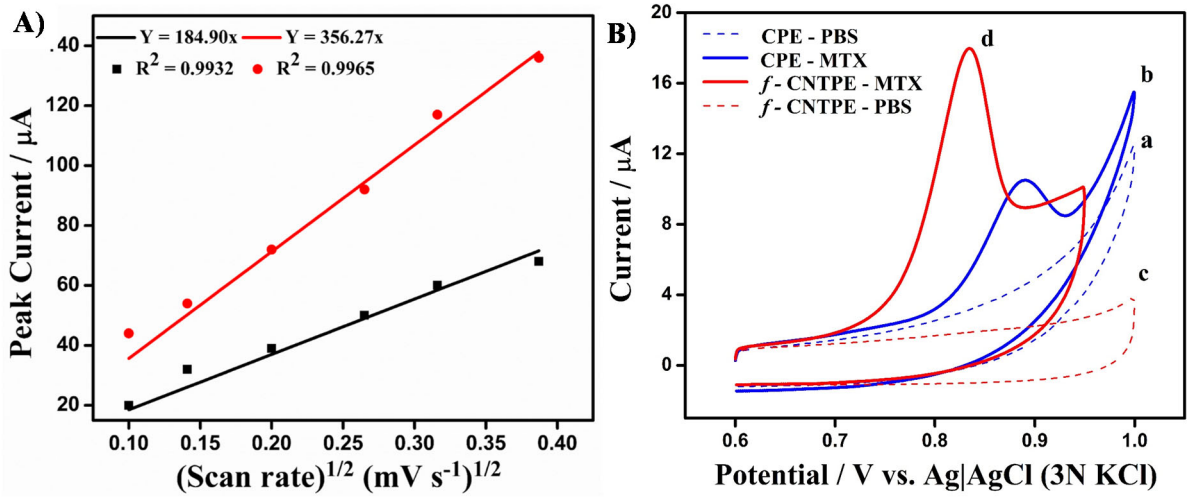

Fig. 2.3. *A) Plot of the anodic peak currents obtained at (a) bare CPE and (b) f-CNTPE in aq. 2.5 mM $K_3[Fe(CN)_6]$ + 0.1 M KCl against the square root of scan rate. B) CVs recorded at (a, b) CPE and (c, d) f-CNTPE in the (a, c) absence and (b, d) presence of 1.0 × 10^{-5} M MTX in PBS (pH 3.2). Scan rate 100 mV s^{-1}.*

Effect of the potential scan rate on the cyclic voltammograms of MTX at *f*-CNTPE was studied, and the observed results are given in Fig. 2.4. Cyclic voltammograms of MTX recorded at different scan rates of 10 – 300 mV s^{-1} are shown in Fig. 2.4 (A), and the peak currents increased gradually along with the scan rate. The anodic peak currents were plotted against the square root of sweep rate ($\upsilon^{1/2}$), and a linear plot was obtained with a regression coefficient of 0.9859 (Fig. 2.4 (B)). These results infer that the oxidation of MTX at the modified *f*-CNTPE is a diffusion controlled process. With the increase in the scan rate, the anodic peak shifts to more positive potentials. The peak potential was linearly dependent on ln(scan rate) (Fig. 2.4(D)). From the dependence of peak potential vs. ln(scan rate), the number of electrons involved in the electrodic process could be calculated using the Laviron's equation [230]. The slope of the E_p vs. ln(scan rate) plot, $b = (RT/\alpha n_\alpha F)$, where 'b' is the slope and 'α' is the electron transfer coefficient, and, according to Laviron's equation, the electron transfer coefficient 'α' for an irreversible electrodic reaction is

0.5 [230,231]. From the slope of the plot (Fig. 2.4(D)), the value determined for n_α is nearly 2, which evidences that two electrons are involved in the oxidation process of MTX.

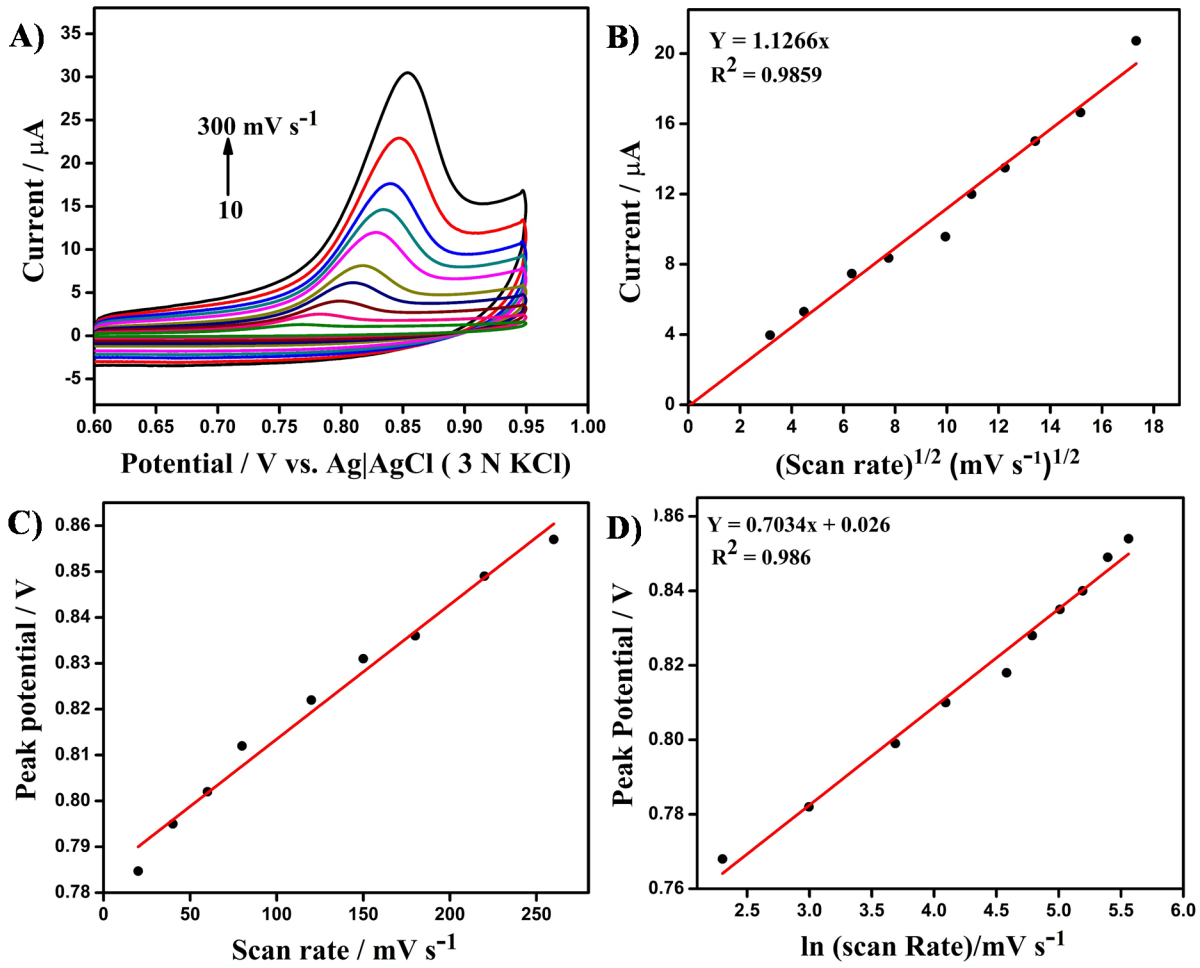

Fig. 2.4. *(A) CVs of 1.0 × 10^{-5} M MTX in PBS buffer (pH 3.2) at f-CNTPE; scan rate = 10, 20, 40, 70, 100, 130, 170, 210, 250 and 300 mV s^{-1}. (B) Plot of i_p vs. square root of scan rate. (C) Plot of E_p vs. scan rate. (D) Plot of E_p vs. ln(scan rate).*

2.3.3. Determination of MTX by differential pulse voltammetry (DPV)

The electrochemical sensing of *f*-CNTPE towards MTX detection was investigated by differential pulse voltammetry (DPV). The anodic peak observed at +0.730V was monitored and a good voltammetric profile was obtained with the optimum parameters of 120 mV pulse amplitude, 50 ms pulse width, 5 ms sample width, 5 mV step increment and 150 ms cycle period. DPVs were recorded using *f*-CNTPE at different concentrations of MTX (0.4–5.5 µM), and the obtained DPVs are shown in Fig. 2.5 (A). The peak current is linearly proportional to MTX

concentration, as shown in Fig. 2.5 (B). The plot of peak current vs. C_{MTX} is linear, passing through the origin, and the low detection limit is determined to be 4.0×10^{-7} M MTX.

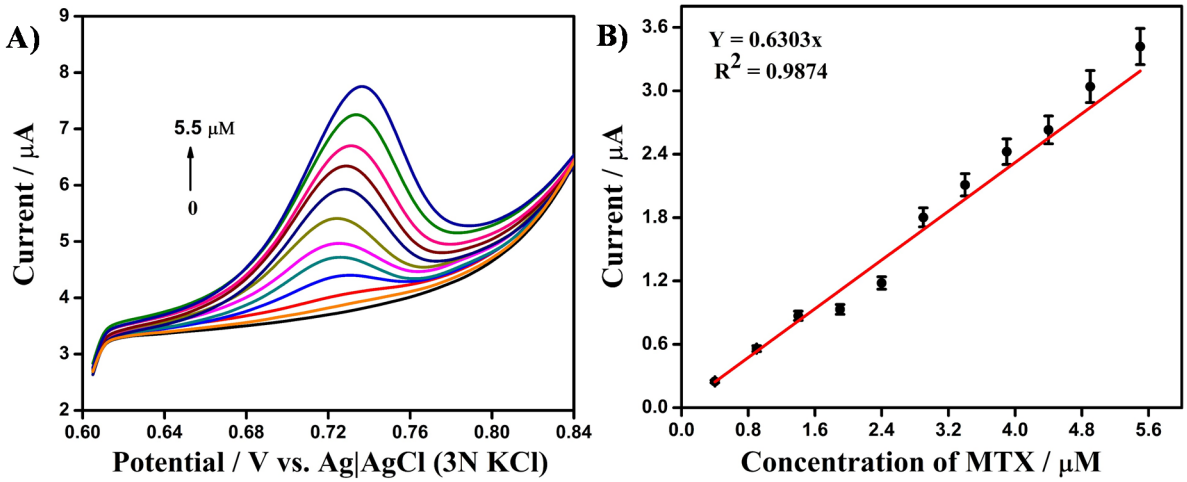

Fig. 2.5. *(A) DPVs of MTX (0 and 0.4 to 5.5 µM) in PBS (pH 3.2) at f-CNTPE. (B) Plot of the peak current against the concentration of MTX.*

2.3.4. Square wave voltammetry (SWV) of methotrexate at *f*-CNTPE

SWV was employed then to investigate the detection limit of MTX under the best possible parameters: potential window +0.60 to +0.95 V, 4 mV step height, 0.025 V amplitude, 15 Hz frequency. SWVs were recorded with *f*-CNTPE in the presence of MTX at 10 - 1500 nM (Fig. 2.6 (A)). The calibration plot of peak current vs. concentration of MTX is shown in Fig. 2.6 (B). The peak current increased in parabolic manner along with MTX concentration, and two linear regions were observed (Fig. 2.6 (B)). Such a parabolic plot could be attributed to a slow heterogeneous interfacial electron-transfer, and the peak current did not increase proportionately with MTX concentration. The slope of the linear region in the low concentration range of 10 – 80 nM is high compared to the other, and the linear regression equations are: $i(\mu A) = 3.598\ C_{MTX}(\mu M)$ with $R^2 = 0.998$ in 10 – 80 nM range, and $i(\mu A) = 0.247 + 1.046\ C_{MTX}(\mu M)$ with $R^2 = 0.9943$ in 100 – 1500 nM range. The RSD obtained at 10 nM concentration and the slope of the plot in the low concentration range were employed to determine the low-detection-limit (3σ/slope) to be 2.9 nM. Linear concentration range is 1.0×10^{-8} – 1.5×10^{-6} M. Performance of the fabricated sensor has been compared with other electrochemical sensors and analytical methods reported in the literature (Table 2.1). The low-detection-limit using simple *f*-CNTPE is 2.9×10^{-9} M by SWV and is highly comparable to the low-detection-limits reported previously by using various electrochemical

methods with various modified electrodes utilizing nanoAu, nanoCu, anti-MTX antibody, boron-doped diamond electrode, etc. (Table 2.1). Further, the present sensor system exhibits an equivalent low-detection-limit of 10 nM by steady-state current–time analysis method (*vide infra*) under hydrodynamic conditions, which could be extended to repeated analysis of multiple samples using flow-cell analysis. The developed biosensor system has been established for successful determination of MTX selectively in the presence of other interferents and from impregnated urine and serum sample s (*vide infra*).

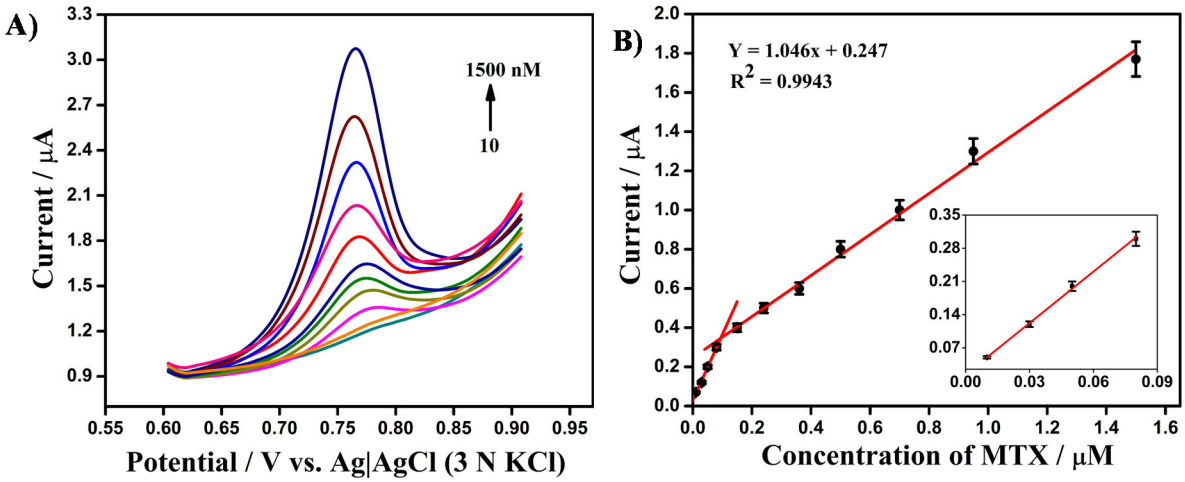

Fig. 2.6 *(A) SWVs of MTX 10 to 1500 nM in PBS (pH 3.2) at f-CNTPE. (B) Plot of the peak current against the concentration of MTX. Inset shows the plot of peak current at low concentrations of MTX.*

Table 2.1. Detection of MTX using electrochemical and various analytical methods.

Electrode	Method	Linear range	Low-detection-limit (nM)	Reference
BDDE	DPV	50 nM – 20 μM	10.0	[175]
PLL/GCE	SWV	5 nM – 200 nM	1.7	[232]
MWCNTs-DHP/GC	DPADSV	50 nM – 5 μM	33.0	[217]
DNA/SWCNT/Nafion/GCE	SWAS	20 nM – 1.5 μM	8.0	[219]
DNA/GCE (ox)	SWV	20 nM – 4 μM	5.0	[201]
NanoAu/LC/GCE	SWAS	40 nM – 2 μM	10.0	[220]
NanoCu/Carbon black	SWV	2.2 μM – 25 μM	90.0	[221]
MWCNT–SPE	_	0.5 μM – 100 μM	100.0	[212]
f-CNTPE	SWV	10 nM – 1.5 μM	2.9	Present work
	i-t analysis	10 nM – 1.5 μM	10.0	Present work

BDDE - Boron-doped diamond electrode; PLL – poly(L-lysine); DHP – dihexadecylhydrogenphosphate; LC - L-cysteine; SPE - Screen printed electrode.

2.3.5. Steady-state current–time analysis

Sensitivity of the present sensor system was examined by the steady-state current–time analysis mimic to hydrodynamic flow-cell experiments towards the detection of MTX. Experimental solution was stirred with a magnetic bar at a constant non-turbulent rotation rate of 400 rpm. Figure 2.7 (A) shows the i–t curve of *f*-CNTPE obtained for the addition of MTX with a uniform stirring at the applied potential of + 0.85 V. The current response of *f*-CNTPE with each addition of MTX at an interval of ~ 60 s at various concentrations is shown in Fig. 2.7 (A). Following MTX addition, the current increased anodically and attained a plateau within 10 s. The increase in anodic current was plotted against MTX concentration, and the linear plot obtained from 10 to 1500 nM MTX is given in Fig. 2.7 (B). The addition of MTX as low as 10 nM produced a current response with a signal-to-noise ratio (S/N ratio) of ~ 8 (Fig. 2.7 (A) inset). The performance of the present sensor system was further examined towards MTX detection in presence of various biological interferents and in pharmaceutical and physiological samples.

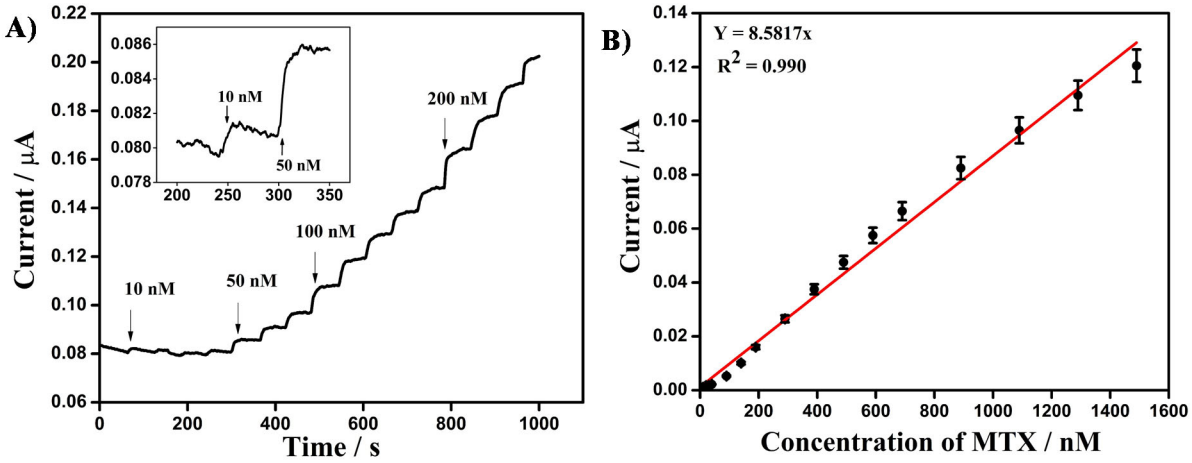

Fig. 2.7. *(A) Steady state current–time analysis at f-CNTPE in PBS (pH 3.2) to the additions of MTX. Every addition increases the concentration of MTX at regular intervals of ~1 min.* E_{app} *= + 0.85 V. (B) Plot of the increase in anodic current vs. MTX concentration.*

2.3.6 Interference studies

Electrochemical responses of methotrexate in the presence of interferents that co-exist in real samples such as ascorbic acid (AA), uric acid (UA), and important neurotransmitters such as dopamine (DA) and serotonin (5-HT) were investigated at *f*-CNTPE modified electrode. Figure 2.8 shows the DPVs obtained in the presence of a mixture of AA, UA, DA and 5-HT 1.5 µM each

along with the presence of MTX at different micromolar levels (1.0 – 4.0 μM) in PBS (pH 3.2). At the modified *f*-CNTPE, distinct peaks were observed for MTX and for the other components, and thus selective determination of MTX could be achieved. The peak currents for MTX increased with MTX concentration irrespective to the presence or absence of these interferents. A very good peak-to-peak separation was observed between MTX and the other compounds. It is clear that the fabricated sensor platform is good for selective MTX detection despite the presence of interferents.

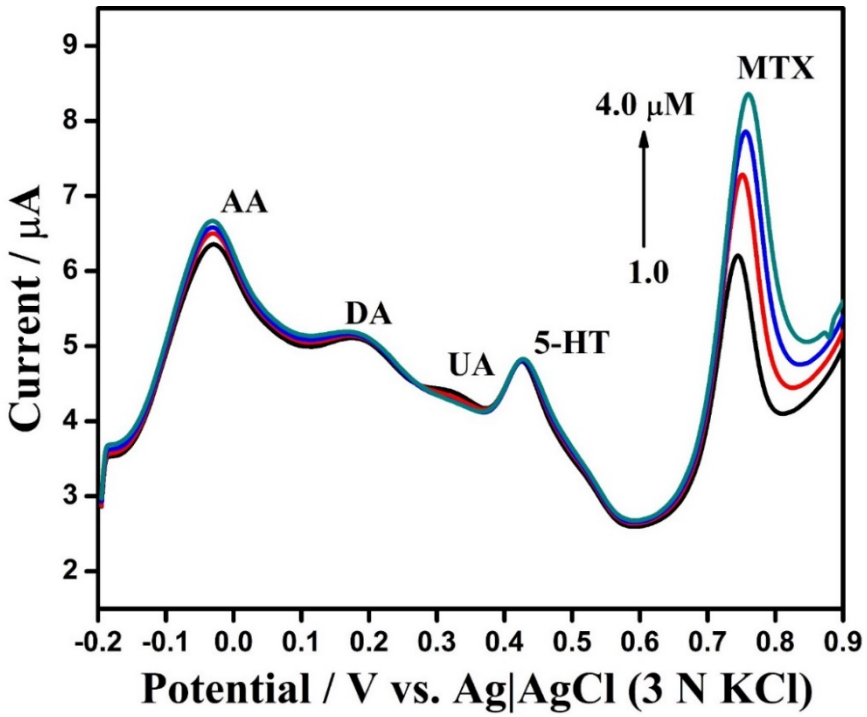

Fig. 2.8. *DPVs at f-CNTPE with MTX at different concentrations (1.0, 2.0, 3.0 and 4.0 μM) in the presence of AA, DA, UA and 5-HT 1.5 μM each in PBS (pH 3.2).*

2.3.7 Repeatability and reproducibility

Repeatability of the fabricated *f*-CNTPE has been examined by recording SWVs of 1.0 μM MTX repetitively by using the same electrode. In a time period of 15 days, we successively measured the anodic peak current response for 25 times and found that the anodic peak current decreased by ~ 4.5%, indicating that the present sensor has good stability and repeatability for multiple usage. Reproducibility of the present biosensor electrode has been examined by recording the anodic peak current of 1.0 μM MTX using six independent *f*-CNTPE electrodes. The RSD of the anodic peak currents of these electrodes was found to be 2.6% for the detection of MTX in multiple experiments, showing excellent reproducibility of the present biosensor. From these

evidences, we conclude that the present sensor is highly reproducible and reusable for the detection of MTX.

2.3.8 Determination of MTX in pharmaceutical, artificial urine and human blood serum

Finally the sensor was examined for practical applicability. Pharmaceutical samples of MTX (5 mg tablet) were analyzed by the standard addition method. In Fig. 2.9 (A), the curves "a and b" show the DPVs of the experimental solutions having 0.5 μM pure MTX + 0.5 or 1.5 μM MTX from pharma drug. Recovery of MTX from artificial urine was examined by the addition of MTX into undiluted artificial urine of pH 3.2. The biosensor has been tested in artificial urine samples and in diluted serum samples of healthy donors, and thus the pharmaceutical drug MTX initially is not present at all in these samples. MTX is impregnated at different concentration levels, and the DPVs were recorded. In curves "c - f", the DPVs recorded at *f*-CNTPE in pure buffer and in artificial urine with the presence of 1.0 and 2.0 μM MTX were shown. In urine samples, the oxidation peak of MTX occurred at a less positive potential, + 0.65 V (e, f), and it could be attributed to the high ionic strength of the urine solution. The recovery values of MTX determination in pharmaceutical and urine samples are given in Table 2.2, and the recovery values are quite satisfactory, ranging from 96.8 to 102.5%.

The electrochemical response of MTX at *f*-CNTPE electrode was recorded in human serum obtained from a healthy donor with a dilution by 30 times using the supporting electrolyte. DPVs in the presence of impregnated MTX at different concentrations (0.0 –3.0 μM) in the diluted serum are shown in Fig. 2.9 (B). In the absence of MTX, a weak anodic peak was observed at + 0.36 V, and it will be characteristic to uric acid (*vide supra,* Fig. 2.8) present in the real sample of human serum. In the presence of 1.0 μM MTX, the anodic peak corresponding to the oxidation of MTX appears at +0.81 V, and the peak current increased with the concentration of MTX. Both in artificial urine samples and in diluted serum samples, the DPVs observed at 1.0 μM MTX exhibit a prominent peak (Fig. 2.9 (A) (e) and 2.9 (B)), and the ratio of the anodic peak current against the noise of the DPV response is very high (S/N ratio > 3). From the results in Fig. 2.9 (A) and 2.9 (B), it can be readily assumed that the low-detection-limit of the present biosensor could be ≤ 1.0 μM MTX from pharmaceutical tablets, artificial urine and diluted serum samples.

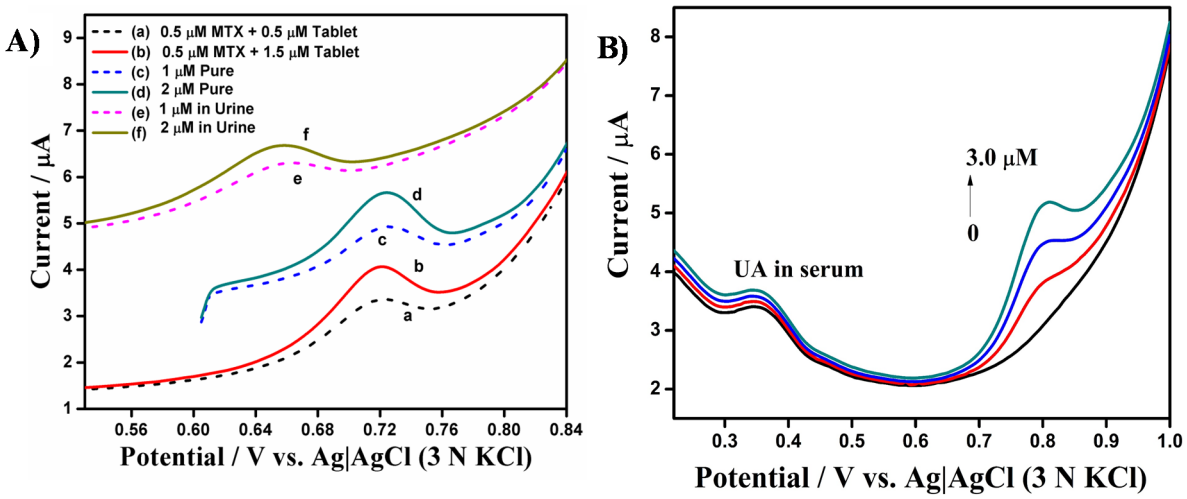

Fig. 2.9. *(A) DPVs recorded at f-CNTPE in the presence of a mixture of 0.5 μM pure MTX + 0.5 μM (a) and + 1.5 μM (b) MTX from a pharmaceutical formulation in PBS buffer (pH 3.2), pure MTX in PBS (pH 3.2; c, d) and in artificial urine (pH 3.2; e, f); [MTX] = 1.0 μM (c, e) and 2.0 μM (d, f). (B) DPV analysis in diluted human serum (30 times) at various concentrations of MTX (0, 1.0, 2.0 and 3.0 μM).*

Table 2.2 Recovery limits for the determination of MTX in pharmaceutical tablet, artificial urine and in serum samples.

Sample	MTX ($\times 10^{-6}$ M)	Tablet added ($\times 10^{-6}$ M)	Found ($\times 10^{-6}$ M)	Average recovery (%)	RSD (%)
Tablet (5 mg/100 mL)	0.5	0.5	0.97	96.8	1.3
	0.5	1.5	2.05	102.5	0.9
Urine	1.0	-	0.97	96.8	1.2
	2.0	-	1.97	98.5	1.7
Serum	1.0	-	0.97	97.4	1.4
	2.0	-	1.91	95.5	0.7
	3.0	-	2.97	99.0	1.8

2.4 Conclusions

In the present work, we described a simple and cost-effective method for quantitative determination of sub-micromolar levels of MTX based on *f*-CNTPE. The developed biosensor is the first electrochemical sensor, to the best of our knowledge, for the determination of trace quantities of MTX from pharmaceutical samples, urine and diluted serum. Linear determination range and low-detection-limit, respectively, were 1.0×10^{-8} M – 1.5×10^{-6} M and 2.9×10^{-9} M in SWV investigations. Steady-state current – time analysis demonstrated the determination of MTX as low as 10 nM (S/N ratio ~ 8) in less than 10 s. The developed sensor system is excellent for the detection of MTX at sub-micromolar concentrations in presence of other physiological electroactive interferents. The proposed method was successfully employed for the determination of methotrexate *in-vitro* in real sample analyses of pharmaceutical dosage, urine and diluted human serum samples with the recovery limits of 95.5 to 102.5%. The developed electrochemical sensor system and the methodology could be extended for other drug compounds and for practical applications in the analyses of pharmaceutical dosages and clinical samples.

CHAPTER 3

Electrodissolution-induced deposition of nanoAu particle on *poly*-(3-amino-5-hydroxypyrazole) coated carbon paste electrode for highly sensitive detection of Valacyclovir in physiological samples

3.1. Introduction

Valacyclovir is an important anti-viral drug. It is pro-drug of acyclovire and useful for the usage against Herpes simplex virus (HSV) and Varicella-zoster virus (VZV) virus. This compound is rapidly converted into an essential amino acid L-valine and acyclovir (active antiviral state of valacyclovir) by hydrolysis in the liver and intestine, primarily mediated by enzyme valacyclovir hydrolase via first-pass metabolism [233]. Acyclovir and valacyclovir are activated by the phosphorylation of virus-specific thymidine kinase. There are several traditional chromatographic and spectrophotometric techniques such as RP-HPLC [234,235], HPLC [236,237], spectrophotometry[238,239] and LC-MS [240] proposed for valacyclovir detection from physiological and pharmaceutical samples. But these techniques are time consuming, expensive and even handling also difficult. Electrochemical techniques received high attention for the detection of different types of small molecular analytes in various fields due to their highly sensitive, selective, rapid analysis and easy to operate with a miniaturized portable system. In past years, only a few reports are available in the literature for the detection of valacyclovir by electrochemical techniques with the use of single-walled carbon nanotube modified GCE[233], single-walled carbon nanotube-rGO nanohybrid [155], and self-assembled dopamine nanolayers wrapped carbon nanotube [241]. It is extremely warranted to develop a highly sensitive and selective sensor for portable, miniaturized, rapid, on-site detection of valacyclovir.

In recent years, conducting polymers received special attention in electrochemical materials [242], corrosion protection[243], photocatalysis [244] and sensors[245,246]. Fabrication of electrodes by using a conducting polymer is an emerging method in sensors due to their high compatibility with metal nanoparticles and biological molecules [247,248]. Conducting polymers have extended π-orbital system which can easily promote the flow of electrons from one end of the polymer to the other, which enhances the catalytic properties of the sensor system. Kinetics of the electrodic processes can be improved by depositing a thin film of conducting polymer. The efficiency and biocompatibility of the sensor system is influenced by the polymer thickness over the surface of the electrode. Compared to other methods, the electrochemical polymerization method is simple and best technique for the formation of polymer on the electrode surface with desirable thickness.

Composite of metal nanoparticles with different types of materials such as carbon nanotubes [231,249], graphenes and polymers [250,251] have been used in nanoscience and technology. Especially gold nanoparticle composites show a significant role in biosensors due to their high strength and stability, excellent electron conductivity and unique surface chemistry. Gold nanoparticles freely allow the electron flow into the materials and demonstrated catalytic activity towards oxidation and reduction. Prime difficulty with nanoparticles is particle aggregation, which is responsible for the decrease in conductivity and effective surface area. To overcome this difficulties, several approaches have been introduced, such as surfactant stabilizers, polymer thin-film coatings, thiol-ligand coating and polymer capping agents [252–254].

The main aim of the present studies is to propose a conventional, sensitive and selective method for detection of the important anti-viral drug VAL by using voltammetric techniques. In the present work, the electrochemical oxidation of VAL has been investigated at AuNPs decorated conducting polymer interface. The detection of VAL in artificial urine and pharma samples showed that the sensor system proposed in this study might be adopted in quality control as well as therapeutic drug monitoring in clinical and hospitals.

3.2. Experimental

3.2.1. Chemicals

Valacyclovir, ascorbic acid, uric acid, dopamine and serotonin were obtained from Tokyo Chemical Industry, Japan and $HAuCl_4$ from Sigma-Aldrich, USA. (3-Amino-5-hydroxypyrazole) and graphite nanopowder were purchased from SRL, India. Other chemicals were analytical grade (min. 99% purity). PBS buffer was prepared by mixing of 1 M potassium dihydrogen phosphate (KH_2PO_4) and dipotassium hydrogen phosphate (K_2HPO_4) to pH 7.0. Artificial urine was prepared as per the literature procedure [25]. Double-distilled water filtered with 0.2-µm filter was used for aqueous solutions.

3.2.2. Synthesis of chitosan protected AuNPs

The chitosan protected AuNPs was prepared according to the literature report with a small adaptation [255], and we reduced $HAuCl_4$ by using chitosan. A homogeneous chitosan solution of 1% w/v was obtained by dispersing chitosan in 1% v/v aq. acetic acid with ultra-sonication for 10

min, then added 3 mL 10 mM aq. $HAuCl_4$ and heated at 80 °C for 1 h. Here, we optimized the concentration of gold by varying the volume between 1.0, 2.0, 3.0 and 4.0 mL. We observed that the solution changed from yellow colour to wine red, which confirms the growth of nanoAu particles, and the nanoAu solution was stored at 4 °C for further usage.

3.2.3. Fabrication of AuNPs/poly-AHP/CPE

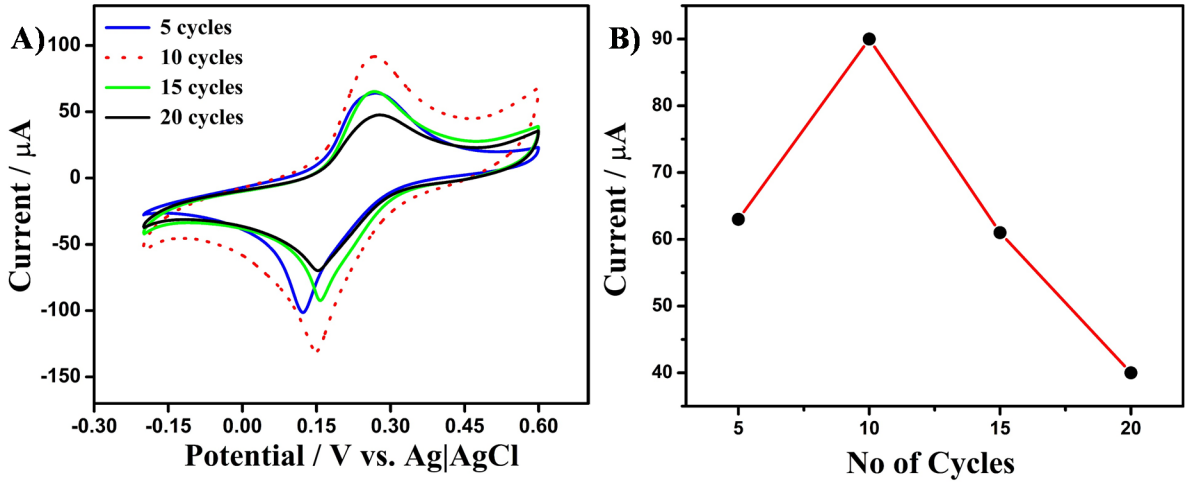

Fig. 3.1. *(A) CVs of 1 mM $K_3[Fe(CN)_6]$ in 0.1 M KCl at different poly-AHP/CPE electrodes formed by potentiodynamic polymerization with various number of cycles (5, 10, 15 and 20).*

Carbon paste electrode (CPE) was prepared as follows. 5 µL paraffin oil added to 30 mg of graphite nanopowder and mixed until a homogenous paste was obtained. The paste was filled into a 4 mm diameter Teflon tube, and a copper wire was inserted from the top of the tube to establish electrical contact. Surface of the CPE was smoothened using a clean butter paper before the experiment is started. Finally, the electrodes were kept for drying at room temperature overnight and denoted as CPE. Then, 5, 10, 15 or 20 consecutive potential cycles were applied on four independent fabricated CPEs placed in 10 mM 3-amino-5-hydroxypyrazole (AHP) with 0.1 M sulphuric acid, and the potential range was - 0.2 to + 1.1 V at 25 mV s^{-1} scan rate. A thin film of *poly*-AHP formed on CPE surface, and the electrode is denoted as *poly*-AHP/CPE. We observed that the *poly*-AHP/CPE electrode formed with 10 potential cycles for electropolymerization has shown highest current response in 1.0 mM $K_3[Fe(CN)_6]$, as shown in (Fig. 3.1 (A)). Subsequently, synthesized chitosan biopolymer protected colloidal gold

nanoparticle (AuNPs) was deposited on *poly*-AHP/CPE at +0.3 V for 20 s, and the total steps involved in biosensor fabrication was described schematically (Scheme 3.1.).

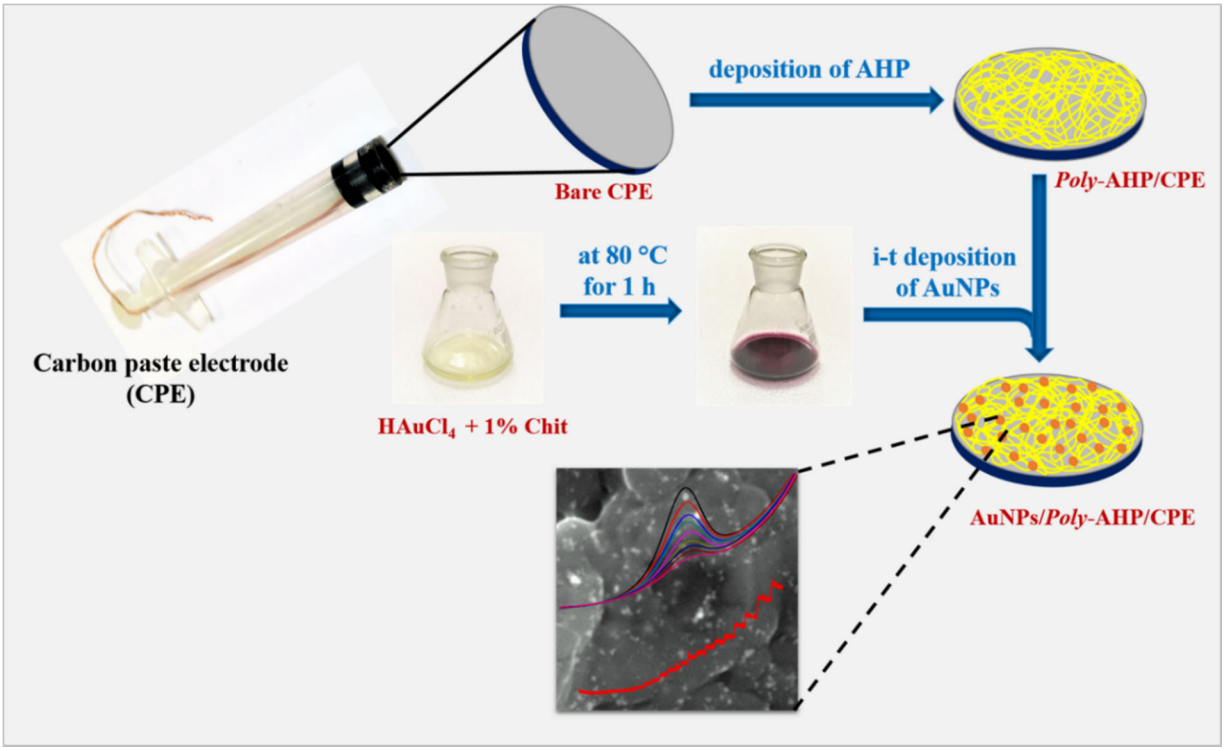

Scheme 3.1. *Schematic representation of electrode fabrication*

3.2.4. Characterization

UV-Visible spectral studies were carried out on PerkinElmer LAMBDA25 spectrophotometer for colloidal gold solution. XRD spectrum of all the electrodes was recorded using Bruker AXS D8 diffractometer in the 2θ range of 10° - 90° with Cu Kα source of 1.5406 Å, step size of 0.01 deg and 0.3 s per step. For surface morphological studies by SEM using TESCAN VEGA 3 SEM operating at 10-30 kV, *poly*-AHP/CPE and AuNPs/*poly*-AHP/CPE films were cut nearly 2 to 3 mm thickness from the electrodes. Here, the films were attached on Cu stub using a conductive carbon adhesive tape, and then a thin film of Au of ~5 nm thick was coated on the films by sputtering to avoid charging and thus blurring during the SEM imaging.

3.2.5. Electrochemical analysis

Electrochemical workstation (CHI 619d, USA) was employed for all voltammetric and impedimetric experiments. Electrode potential has been referred against Ag|AgCl (3 N KCl). PBS (pH 5.0-9.0) was used for all electrochemical experiments as the supporting electrolyte.

3.3. Results and discussion

3.3.1. Electrodeposition of AuNPs/*poly*-AHP film on CPE

A thin film of AuNPs/*poly*-AHP film was formed on the surface of CPE by applying two layers of deposition using AHP monomer and chitosan protected colloidal gold suspension. For the electrochemical deposition of poly-AHP, the CPE placed in 10 mM AHP with 0.1 M H_2SO_4 was swept ten potential cycles between -0.2 to +1.1 V at 25 mV s^{-1}, and the CVs recorded are shown in Fig. 3.2(A). The oxidation peak of AHP appeared at + 0.84 V in the first cycle, and, in the very next cycle, it shifted to +0.79 V with a considerable decrease in peak current. From the 2^{nd} to 5^{th} potential cycles, we observed a slight decrease in peak current for each cycle, which indicates that the oxidative AHP monomer undergoes polymerization on the surface of CPE with each additional potential cycle and that the electroactive polymerization decreased and stabilized at cycle 5. For each additional cycle, AHP polymerized constantly to an equal extent on the surface of the electrode. The amine functional group of AHP will generate a radical cation at + 0.85 V during its oxidation process.

These radical cations form the dimer, and the dimers are oxidizable easily than the monomer, subsequent in the polymerization on the surface of CPE. For the deposition AuNPs on the AHP polymerized CPE, *poly*-AHP/CPE was kept in the solution of chitosan protected AuNPs and was applied a potential of -0.2 V for 150 s, resulting in the deposition of AuNPs on the surface of *poly*-AHP/CPE (Fig. 3.2 (B)). The AuNPs present in the solution were deposited on the electrode surface, which was confirmed by XRD and SEM analyses.

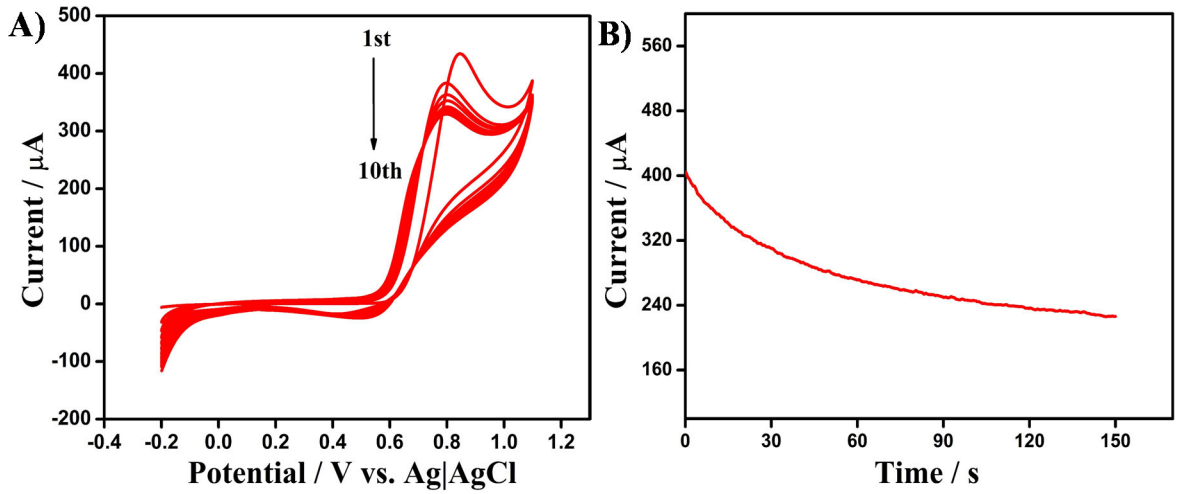

Fig. 3.2. *(A) Potentiodynamic polymerization of AHP (10 cycles) on CPE in 10 mM AHP with 0.1 M H_2SO_4 at a scan rate of 25 mV s^{-1}. (B) Potentiostatic deposition of chitosan protected AuNPs.*

3.3.2. Characterization of AuNPs/*poly*-AHP/CPE

Formation of gold nanoparticles in the colloidal gold solution is first characterized by UV-visible spectroscopy. We recorded the UV-visible spectra of chitosan protected Au NPs, chitosan and aqueous solution of $HAuCl_4$. The absorption maximum was observed for gold NPs (Fig. 3.3 (A)) at 534 nm, which infers that the diameter of Au NPs is about 50 nm.

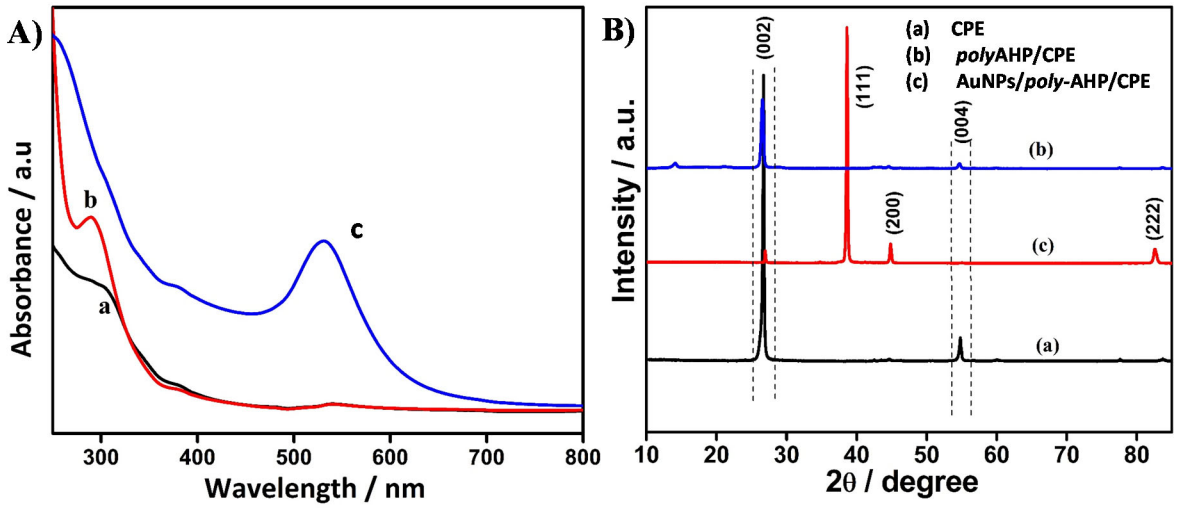

Fig. 3.3. *(A) UV-Visible spectra of a) aq. 1% w/v chitosan, b) aq. HAuCl4, and c) Au NPs in aq. 1% w/v chitosan. (B) Powder XRD patterns of a) CPE, b) poly-AHP/CPE and c) AuNPs/poly-AHP/CPE.*

XRD patterns of CPE and *poly*-AHP/CPE electrodes exhibit the diffraction peaks at 26.56° and 54.66º, which correspond to the characteristic peaks of graphitic carbon of (002) and (004) planes, respectively [166]. It was observed that the intensity of the C (002) diffraction peak decreased from CPE to *poly*-AHP/CPE due to the polymerization, which eventually results in masking of the graphitic nature of CPE (Fig. 3.3 (B)). AuNPs/*poly*-AHP/CPE exhibits diffraction peaks at 38.62º, 44.82° and 82.56° representing (111), (200) and (222) planes, respectively, ascribed to the FCC crystalline Au (JCPDS No. 04 - 0784) besides the C (002) diffraction peak, which clearly depicts the successful formation of Au nanoparticles by electrochemical deposition of $HAuCl_4$. The average crystalline size of nanoAu was calculated using the Scherrer formulae, and it was found to be ~ 35 nm.

The structural morphology of the colloidal gold before and after deposition on *poly-AHP/CPE* has been characterized by SEM analysis. Figure 3.4 (A) is the typical image of the pure synthesized colloidal gold in solution, and Fig. 3.4 (B, C) shows SEM images after deposition of nanoAu on *poly-AHP/CPE* at different magnifications. In Fig. 3.4 (B, C), we can clearly observe the homogeneous uniform distribution of AuNPs on the surface of *poly-AHP,* which is already formed as a well-sheet like structure on CPE and is well responsible for efficient fast electron-transfer. Figure 3.4(C) shows that the AuNPs*/poly-AHP/CPE* film is of enormous porous nature between layer-to-layer with high surface area, and in turn it could be increasing the current response of the electrode. By using EDX measurements, the chemical composition of AuNPs*/poly-AHP/CPE* was deduced. EDX elemental mapping of carbon, gold, nitrogen and oxygen in Fig. 3.4(E) clearly reveals that Au is uniformly distributed throughout the AuNPs*/poly-AHP/CPE* matrix. The elemental composition of AuNPs*/poly-AHP/CPE* from EDX analysis (Fig. 3.4 D) shows the presence of C, O, N and Au as major elements at the weight percentages of 63.19 %, 22.24%, 10.14% and 4.02%, respectively, over the whole region of AuNPs*/Poly-AHP/CPE* film surface.

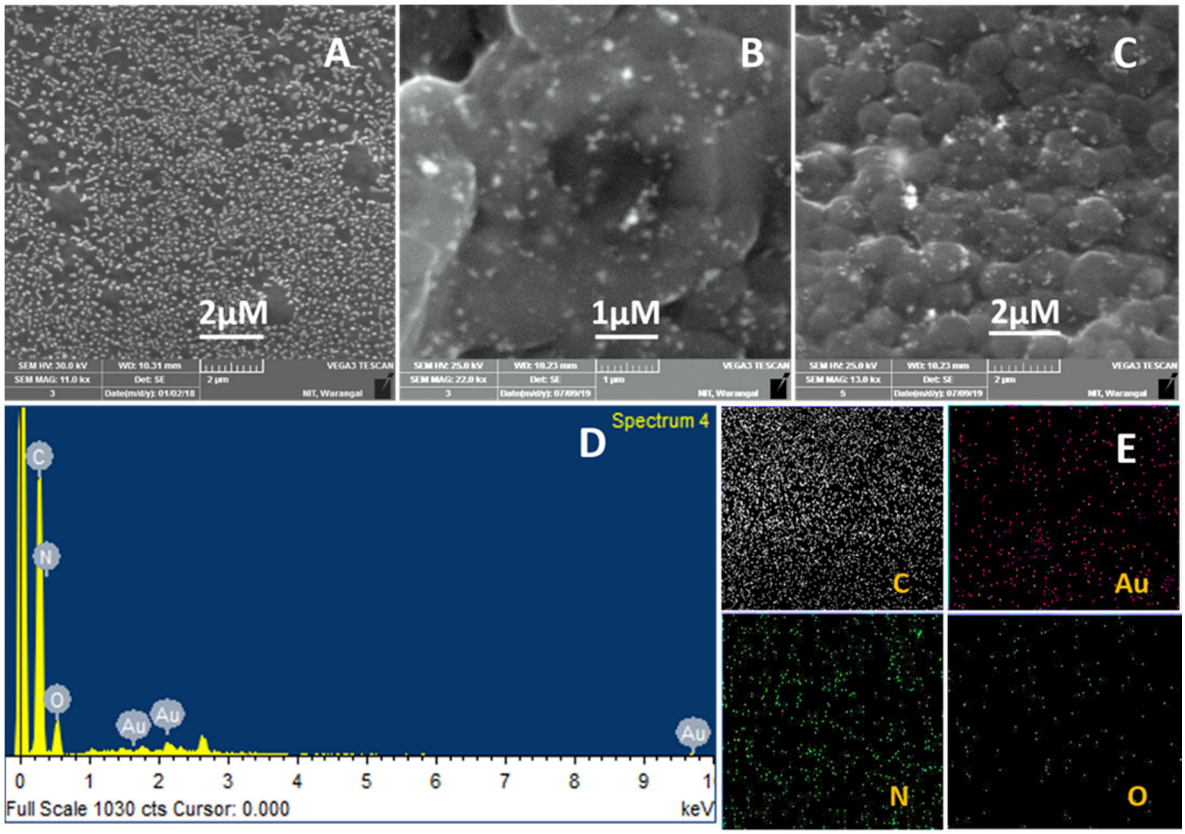

Fig. 3.4. *SEM images of synthesized colloidal AuNPs (A), AuNPs/Poly-AHP/CPE at different magnifications (C, D). EDX spectrum of AuNPs/Poly-AHP/CPE (D) and EDX elemental mapping of carbon, gold, nitrogen and oxygen on AuNPs/Poly-AHP/CPE surface (E).*

3.3.3. Electrochemical oxidation of valacyclovir

CVs of 20 µM VAL in PBS (pH 7.0) were recorded at CPE, *poly*-AHP/CPE and AuNPs/*poly*-AHP/CPE (Fig. 3.5 (A)). In presence of valacyclovir, only one irreversible oxidation peak was identified at all CPE, *poly*-AHP/CPE and AuNPs/*poly*-AHP/CPE electrodes and, in the absence of the drug, no characteristic peak was observed in PBS at any of the electrodes. AuNPs/*poly*-AHP/CPE has shown highest anodic peak current compared to *poly*-AHP/CPE and bare CPE, and it could be connected to the increase in the area of surface, which could be confirmed to the higher capacitive current of AuNPs/*poly*-AHP/CPE electrode. The anodic peak potential of VAL is ~ + 1.02 V at bare CPE, and also a well-defined anodic peak observed at a less positive potential of + 0.97 V for both *poly*-AHP/CPE and AuNPs/*poly*-AHP/CPE electrodes. Moreover, the anodic peak current resulted at AuNPs/*poly*-AHP/CPE is ~ 5 times greater than that at *poly*-AHP/CPE and is ~ 20 times greater than that at bare CPE. AuNPs/*poly*-AHP/CPE is

advantageous towards electrooxidation of VAL with the decrease in overpotential and higher electrocatalytic currents in the oxidation of VAL. All these results are clearly indicating that the AuNPs/*poly*-AHP film on CPE well promoted the electrocatalytic oxidation of VAL.

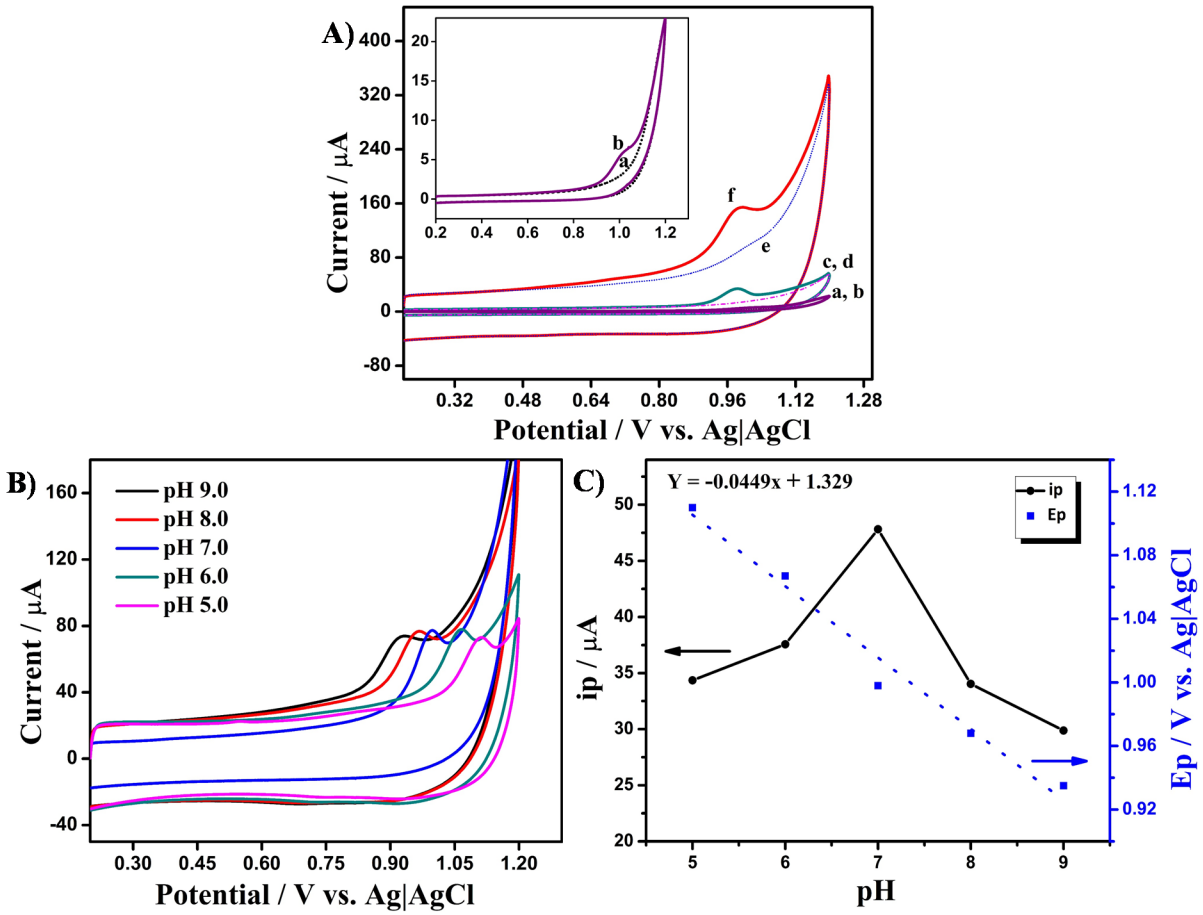

Fig. 3.5. *(A) CVs of VAL recorded in PBS (pH 7.0) in presence (b,d,f) and absence (a,c,e) of 20 µM VAL at bare CPE (a, b), Poly-AHP/CPE (c, d) and AuNPs/Poly-AHP/CPE (e, f). Scan rate = 100 mV s^{-1}. (B) CVs of 20 µM VAL in PBS buffer of different pH values (5 – 9) at AuNPs/Poly-AHP/CPE; scan rate = 100 mV s^{-1}. (C) Plot of peak potential and peak current against pH.*

Effect of pH on the electrochemical oxidation of valacyclovir has been explored by CV at AuNPs/*Poly*-AHP/CPE in the pH range from 5.0 – 9.0, and the obtained CVs are shown in Fig. 3.5 B. The electrooxidation of VAL was obviously influenced by pH. The oxidation peak potential gradually became more negative with the increase in pH of the buffer solution, and the plot of E_p vs pH is shown in Fig. 3.5 C. The peak current was found to be maximum at pH 7.0. From the pH variation studies, we concluded that pH 7.0 is good for further analyses with high peak current and optimum peak potential for VAL oxidation.

Further, we studied the effect of scan rate on the electrooxidation of VAL to describe the electron-transfer mechanism involved at the electrode. We recorded CVs at different potential sweep rates in the range of 20 – 300 mV s^{-1} using AuNPs/*poly*-AHP/CPE in 10 µM VAL. The oxidation peak current of VAL gradually increased with the sweep rate, as seen in Fig. 3.6A. We observed a linear plot passing through origin between the oxidation peak current and the square root of scan rate (Fig. 3.6B). It is clearly indicating that the electrochemical oxidation process of VAL is following a diffusion-controlled mechanism and also that the AuNPs/*poly*-AHP film is porous and superficial to permit the efficient diffusion of VAL across it.

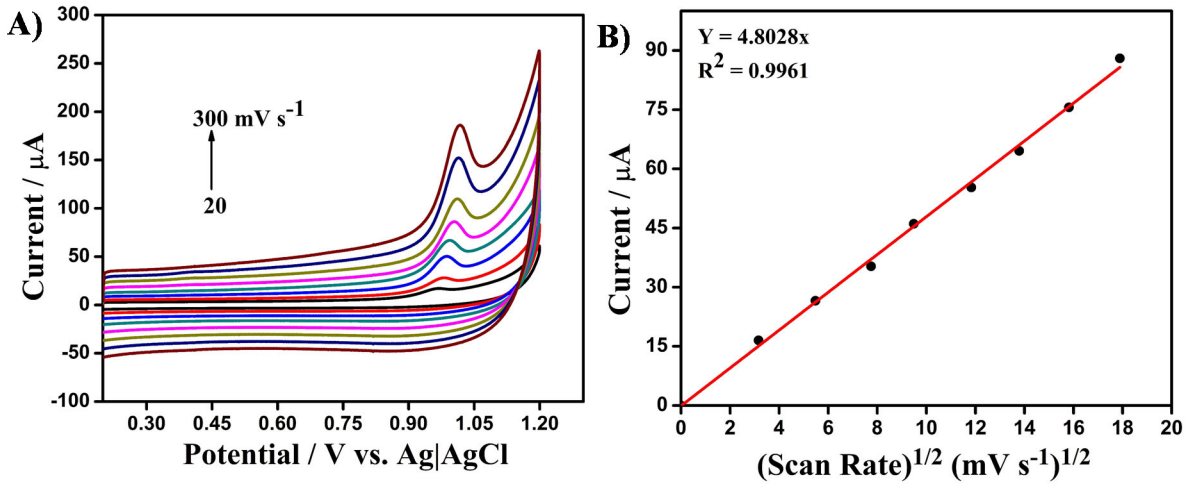

Fig. 3.6. *(A) CVs of* 10 µM VAL *in PBS buffer (pH 7.0) at AuNPs/Poly-AHP/CPE with different scan rates (20, 40, 60, 100, 150, 200, 250 and 300 mV* s^{-1}*). (B) Plot between peak current and square root of scan rate.*

3.3.4. Electrochemical impedance spectrometry (EIS)

Electrochemical impedance spectrometry (EIS) studies of sensor reveals the interfacial properties and characteristics of the nanoparticle coated polymer film. The impedance spectra of CPE, *poly*-AHP/CPE and AuNPs/*poly*-AHP/CPE in aq. 2 mM $K_3[Fe(CN)_6]$ + 0.1 M KCl were recorded at the open circuit potential (OCP) from 100 kHz – 0.01 Hz. Here the charge transfer resistance (R_{ct}) value of the Nyquist plots of CPE, *poly*-AHP/CPE and AuNPs/*poly*-AHP/CPE reveals the electron-transfer efficiency at the interface (Fig. 3.7 A). We analyzed with different types of equivalent circuit models for fitting of the resultant data, and the best fit for the observed results was simple Randles equivalent circuit and is shown in the inset of Fig. 3.7 A. Nyquist plots of CPE, *poly*-AHP/CPE and AuNPs/*poly*-AHP/CPE have shown a semi-circular curve followed

by a linear plot, and the respective R_{ct} values determined from the diameter of the semi-circles are 16.5, 7.6 and 3.5 kΩ, respectively. Compared to CPE and *poly*-AHP/CPE electrodes, AuNPs/*poly*-AHP/CPE has shown very low R_{ct} value, which indicates a very high conductivity and improved the electron-transfer across interface of the electrode of AuNPs-embedded polymer sensor compared to *poly*-AHP/CPE and CPE electrodes.

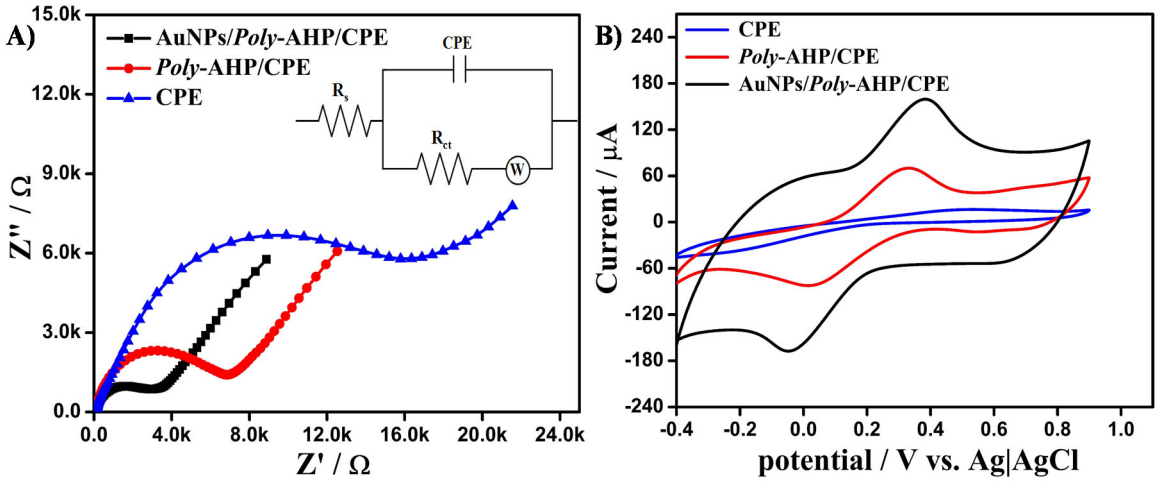

Fig. 3.7. *(A) Nyquist plots and (B) CVs of CPE, Poly-AHP/CPE and AuNPs/Poly-AHP/CPE in aq. 2 mM $K_3[Fe(CN)_6]$ + 0.1 M KCl.*

CV experiments carried out in $K_3[Fe(CN)_6]$ further support the stepwise enhanced interfacial electron-transfer upon the depositions of conductive polymer film and impregnated AuNPs layer on the sensor surface. Figure 3.7 (B) shows the CVs of CPE, *poly*-AHP/CPE and AuNPs/*poly*-AHP/CPE in aq. 2 mM $K_3[Fe(CN)_6]$ + 0.1 M KCl at a scan rate of 100 mV s^{-1}. All three electrodes have shown a pair of anodic and cathodic peaks, and, among all the electrodes, AuNPs/*poly*-AHP/CPE has shown highest peak current response than poly-AHP/CPE and CPE. It indicates that the electron-transfer at the AuNPs/*poly*-AHP/CPE interface is facile and enhanced compared to poly-AHP/CPE and CPE. The observed enhanced electron-transfer at AuNPs/*poly*-AHP/CPE could well be promoted with the lowest R_{ct} of AuNPs/*poly*-AHP/CPE from electrochemical impedance studies.

3.3.5. Differential pulse voltammetry (DPV)

Quantitative analysis of VAL was investigated by differential pulse voltammetry (DPV) using AuNPs/*poly*-AHP film as sensing interface. DPVs were recorded at the optimized conditions of 50 mV pulse amplitude, 40 ms pulse width, 5 mV step increment and 200 ms cycle period.

DPVs of VAL recorded at AuNPs/*poly*-AHP/CPE in PBS (pH 7.0) over the concentration range of 5 – 80 nM VAL are shown in Fig. 3.8A. A well-defined oxidation peak of VAL was observed at + 0.94 V, and the oxidation peak current gradually increased with the concentration. A linear plot of peak current vs. VAL concentration was observed (Fig. 3.8 B). The low-detection-limit is determined to be 1.89 nM. The sensor performance was compared with previously reported articles by various electrochemical, chromatographic and other analytical methods, as shown in Table 3.1. The LOD of the present sensor is superior compared to various electrochemical systems based on single-walled carbon nanotube and boron-doped diamond electrodes and chromatographic analytical systems. Then, we investigated the performance of AuNPs/*poly*-AHP film for VAL detection in presence of interferents and from pharmaceuticals and physiological samples.

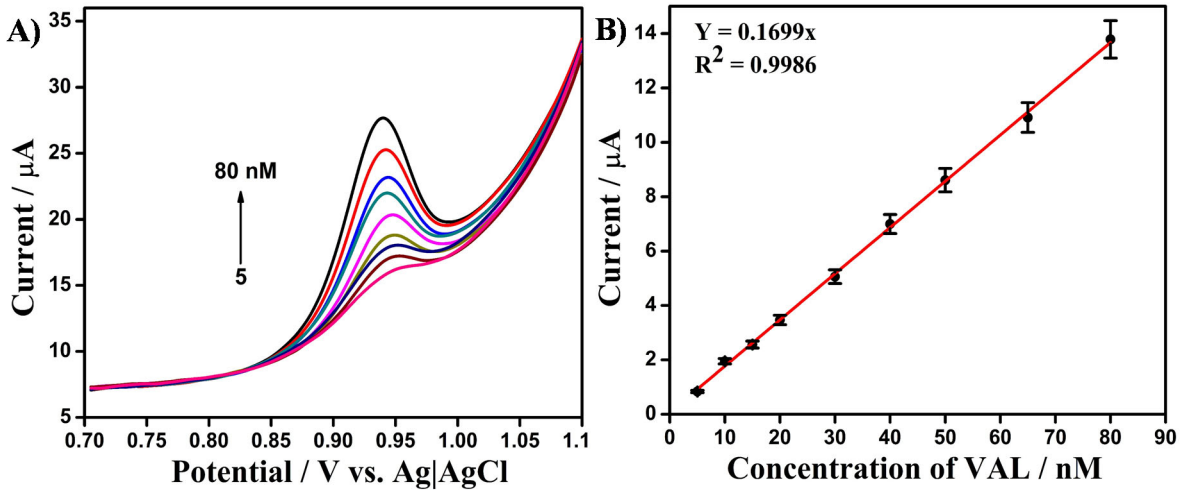

Fig. 3.8. *(A) DPVs of VAL in PBS buffer (pH 7.0) at different concentrations (5.0 to 80 nM) at AuNPs/Poly-AHP/CPE. (B) Plot of peak current against concentration of VAL.*

3.3.6. Steady-state i–t analysis

Further, sensitivity of AuNPs/*poly*-AHP/CPE towards VAL detection was studied by using the steady-state amperometric i-t analysis. Figure 3.9 shows the steady state i-t curve observed with AuNPs/*poly*-AHP/CPE for VAL detection at the applied potential of +1.1 V in PBS under non-turbulent steady stirring condition. AuNPs/*poly*-AHP/CPE electrode showed an anodic increase in the steady-state current for the initial addition of 2.5 nM VAL and also for each further successive additions of various concentrations at an interval of ~40 s. The current increased immediate to the additions of VAL and attained a plateau in ~ 5 s. Figure 3.9 B shows the plot of the current response against the concentration of VAL, and the plot was linear from 2.5 to 220

nM. The addition of VAL as low as 2.5 nM produced a remarkable change in the current with a very good signal-to-noise ratio of ~5 (S/N = ~5; Inset of Fig. 3.9(A)). Performance of AuNPs/*poly*-AHP/CPE sensor was further studied towards VAL detection in presence of interferents and in pharmaceutical and physiological samples.

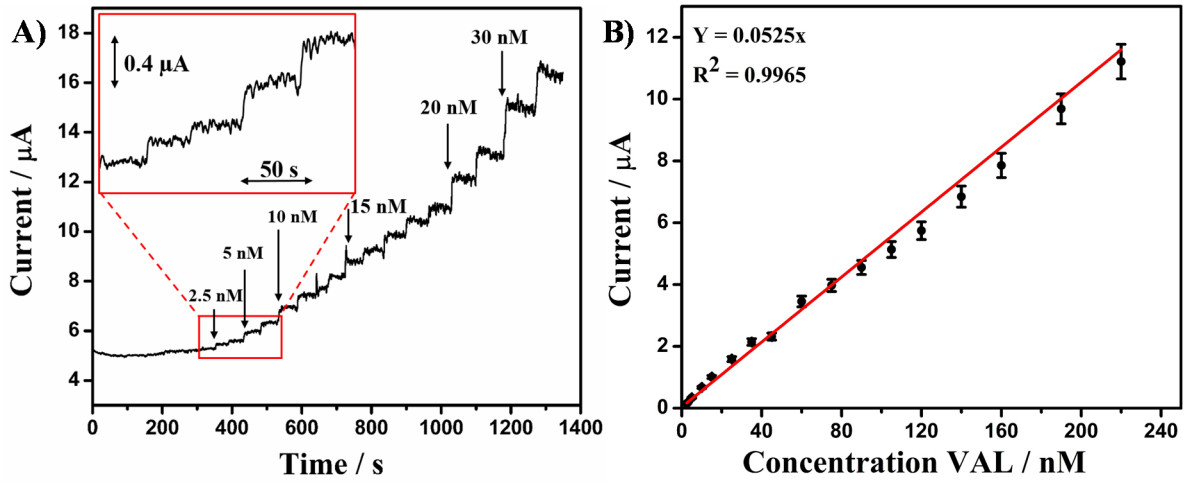

Fig. 3.9. *(A) Steady state current–time analysis at AuNPs/poly-AHP/CPE in PBS (pH 7.0) to the additions of VAL. Every addition increases VAL concentration at intervals of ~ 40 s.* E_{app} *= + 1.1 V. (B) Plot of the anodic current vs. VAL concentration.*

Table 3.1. Detection of VAL using electrochemical methods.

Electrode	Method	Linear range	Limit of detection	Reference
DA@CNT/GCE	Amperometry	3 - 75 nM	2.55 nM	[241]
BDD electrode	DPV	8×10^{-7} to 1×10^{-4} M	1.52×10^{-7} M	[256]
	SWV	2×10^{-6} to 1×10^{-4} M	7.60×10^{-7} M	
-	HPLC	1–250 μg mL^{-1}	0.29 μg mL^{-1} (0.90 μM)	[237]
SWCNT/GCE	DPV	5×10^{-9} to 5.5×10^{-8} M	1.80×10^{-9} M	[233]
rGO/GCE	DPV	0.01–45.1 μM	1.34 nM	[257]
GRP-Bi_2O_3/GCE	SWV	100–700 ng mL^{-1}	4.7×10^{-11} M	[258]
GCE	DPV	4×10^{-6} to 2×10^{-4} M	1.04×10^{-7} M	[259]
	SWV	4×10^{-6} to 2×10^{-4} M	4.60×10^{-8} M	
-	LC-MS-MS	5 – 1,075 ng mL^{-1}	-	[240]
AuNPs/Poly-AHP/CPE	DPV	5 – 80 nM	1.89 nM	present work
	Steady state i-t	2.5 – 220 nM	2.5 nM	

DA@CNT : Dopamine nanolayers wrapped carbon nanotubes, BDD : boron-doped diamond, SWCNT : single-walled carbon nanotubes, rGO : reduced graphene oxide, GRP- Bi_2O_3/GCE: graphene/bismuth oxide/glassy carbon electrode

3.3.7. Interference studies

Electrochemical response of VAL has been investigated against electroactive compounds, e.g. dopamine (DA) and serotonin (5-HT), at AuNPs/*Poly*-AHP/CPE by DPV. Figure 3.10 shows the DPVs resulted in the mixture of DA and 5-HT 4 µM each and VAL at 10 - 40 nM using AuNPs/*Poly*-AHP/CPE in PBS (pH 7.0). The oxidation peak of VAL is not affected by the presence of above interferents. Even high concentrations of DA and 5-HT together were coexist in the test sample, the peak currents of VAL gradually increased by increasing the concentration of VAL and were not at all influenced by the presence of the interferents. From these experimental results, we can clearly confirm that the proposed electrochemical sensor could be implemented for VAL detection even with possible electroactive interferents in the test solution.

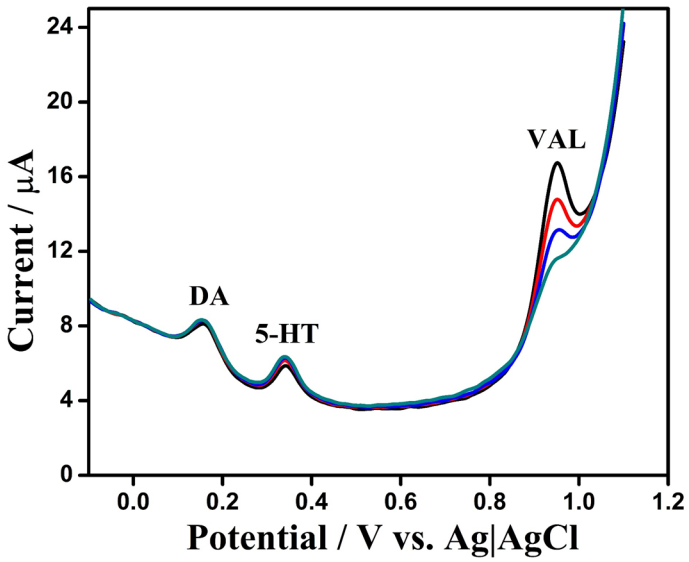

Fig. 3.10. *DPVs recorded at Au NPs/Poly-AHP/CPE with VAL at different concentrations (10, 20, 30, 40 nM) in the presence of DA and 5-HT 4 µM each in PBS buffer (pH 7.0).*

4.3.8. Repeatability and reproducibility

The stability and repeatability of the present sensor system towards the detection of VAL was investigated by recording DPVs of 0.5 µM VAL at a single AuNPs/*Poly*-AHP/CPE electrode. We successfully measured the oxidation peak current response for 20 times over a period of 10 days and observed that there is a meagre decrease in peak current by only 3.9%, showing the stability and repeatability of the present electrode. Reproducibility of the present sensor system was observed by recording DPVs of 0.5 µM VAL with six independent AuNPs/*Poly*-AHP/CPE

electrodes. In the multiple experiments, the RSD of the anodic peak current of these electrodes was 2.8% for the detection of VAL, showing good reproducibility of the present sensor system. From these observations, finally, we concluded that the film of AuNPs/*Poly*-AHP on CPE was highly stable and reproducible for the detection of VAL.

3.3.9. Determination of VAL in pharmaceutical, artificial urine and human serum samples

Finally, the developed electrochemical sensor has been examined for real-world applicability. VAL (1 g tablet) pharmaceutical samples were analyzed by using the developed AuNPs/*Poly*-AHP/CPE sensor system with the help of the standard addition method. In Fig. 3.11(A), the curves "d, e and f" show the DPVs of 10 nM pure VAL together with 10 – 40 nM VAL from pharmaceutical tablets at AuNPs/*Poly*-AHP/CPE. The obtained recovery values from these experimentations varied from 96.8 to 102.3 % (Table 3.2), which are quite acceptable. Also, the VAL recovery from artificial urine samples was studied by adding VAL into artificial urine of pH 6.0 without any buffer. Curves "a, b and c" are showing the DPVs measured in undiluted artificial urine in presence of 20, 30 and 50 nM VAL, respectively, and the recovery varied from 95.2 to 101.2 % (Table 3.2). The recovery limits of the spiked VAL concentration from both the pharmaceutical formulations and artificial urine verified that the developed biosensor is highly proficient for the detection of VAL in real samples.

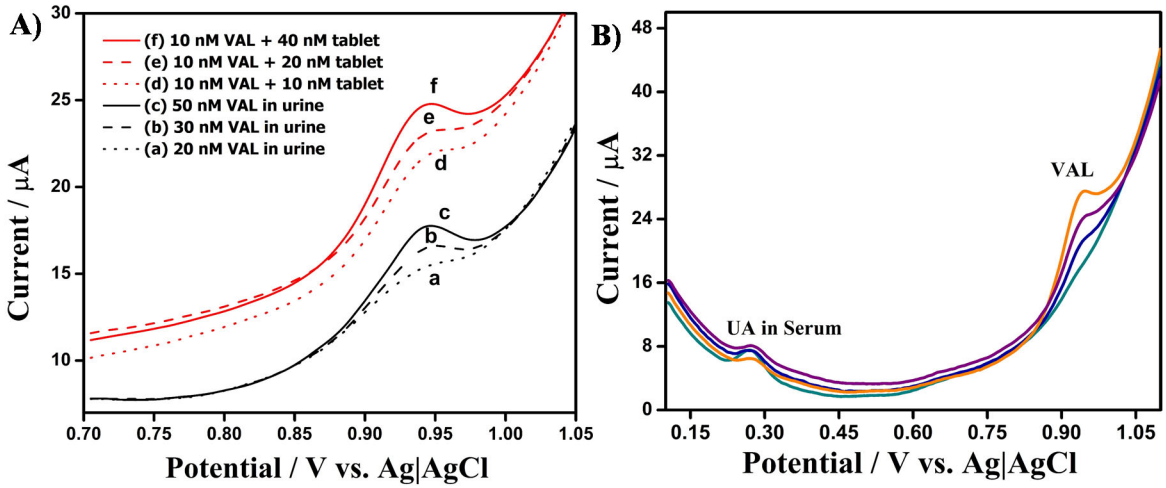

Fig. 3.11. *(A) DPVs recorded at AuNPs/Poly-AHP/CPE in the presence of a mixture of 10 nM pure VAL and different concentrations of VAL (d = 10 nM, e = 20 nM and f = 40 nM) from pharmaceutical formulation in PBS buffer (pH 7.0) and in the presence of (a = 20, b = 30 and c*

= 50 nM) VAL in artificial urine. (B) DPV analysis in diluted human serum (10 times) at various concentrations of VAL (0, 20, 30 and 50 nM).

Further, we investigated the performance of AuNPs/*Poly*-AHP/CPE to the detection of VAL in human serum sample obtained from a healthy donor with a dilution of 10 times in PBS as supporting electrolyte. DPVs recorded at different concentrations (0, 20, 30 and 50 nM) of impregnated VAL in the diluted serum are shown in Fig. 3.11 (B). At the potential of ~ + 0.28 V, a weak anodic peak was observed and was ascribed to the uric acid present in human serum sample [260]. In presence of 20 nM VAL, the anodic peak appeared at + 0.91 V corresponding to the oxidation of VAL, and the peak current increased with increasing VAL concentration. In both samples of urine and serum, the DPVs at 20 nM VAL exhibited a prominent peak (Fig. 3.11(A,B), and the ratio of the peak current against the noise of the DPV response is very high (S/N ratio > 3). From the results in Fig. 3.11 (A, B), we could establish that the low-detection-limit of the sensor could be < 20 nM VAL from a pharmaceutical tablet, artificial urine and diluted human serum sample.

Table 3.2. *Recovery limits for the determination of VAL in pharmaceutical tablet, artificial urine and in serum samples.*

Sample	VAL ($\times 10^{-8}$ M)	Tablet added ($\times 10^{-8}$ M)	[a]Found ($\times 10^{-8}$ M)	Average recovery (%)	[a]RSD (%)
Tablet(5mg /100 mL)	1.0	1.0	1.96	98.2	1.3
	1.0	2.0	2.03	102.3	0.9
	1.0	4.0	4.98	96.8	1.2
Urine sample	2.0	-	1.95	95.2	0.8
	3.0	-	2.96	98.4	1.7
	5.0	-	5.13	101.2	1.1
Serum	2.0	-	1.96	96.8	1.6
	3.0	-	3.02	104.1	0.9
	5.0	-	4.98	95.4	1.6

[a] Mean value of six measurements

3.4. Conclusions

Present work, an electrodissolution–induced deposition of chitosan protected Au nanoparticle on conducting polymer (*p*-AHP) coated CPE has been developed by altering a polarization technique for the quantitative determination of the anti-viral drug VAL. The film of AuNPs coated polymer (*p*-AHP) extraordinarily enhanced the current response and has given a low oxidation overpotential for VAL. In the electrode system, both polymerization of the polymer on CPE and as well as dissolution of the AuNPs on polymer film has been the responsibility for electron-transfer across the electrode surface and for a very good electrocatalytic response. The sensor was capable for VAL detection up to nanomolar levels, even though a high concentration (4.0 μM) major organic interferents present in the solution and it had shown good recoveries for direct determination from physiological fluids and pharmaceutical formulations satisfactorily.

CHAPTER 4

Facile electrochemically reduced GO-CNT nanocomposite as sensitive probe for *in-vitro* determination of nitrofurantoin in biological fluids

4.1. Introduction

Nitrofurantoin (NFT) is the most extensively recommended antibiotic drug to treat urinary tract infection (UTI) caused by *E.coli* and *Enterococcus* pathogen [261], and it is mainly used against the microbial attacks on gallbladder located in the lower part of the urinary system [262,263]. However, over dosage of NFT could cause serious health concerns on human beings such as flatulence, abdominal pain, headache, depression, vomit, diarrhea and hepatotoxicity [264]. Moreover, NFT is prescribed specifically for UTI in pregnant women, and over dosage of NFT leads to directly affect the child's red blood cells [265]. Furthermore, NFT is used widely in the preparation of feed materials of farm animals, fish and poultry, because of its potential activity against a wide spectrum of bacterial infections, low cost and high efficiency. On prolonged usage, NFT and its metabolites were found to accumulate in animal tissues, and the animal produces were found to affect humans on consumption. Prolonged consumption of these animal produces is expected to cause mutagenic and carcinogenic effects in humans. Consequently, some of the countries like United States, China, European Union, Japan and Australia banned NFT usage due to its carcinogenic and mutagenic effects[264,266]. Subsequently, quality control mechanisms to evaluate food products and animal feed materials and to control even illegal usage of NFT are indispensable.

Thus, it is highly warranted to determine active concentrations of NFT in pharmaceutical formulations, physiological fluids of patients, meats, food products and animal feeds. Analytical tools capable of direct, rapid and on-site determination of trace levels of NFT directly from complex sample matrices are highly warranted in medical diagnosis, pharmaceutical industry and food quality control. Till to date, a number of analytical techniques have been developed for the quantification of NFT based on chemiluminescence[267,268], liquid chromatography [269], HPLC with fluorescence [270], luminescence [271], HPLC with mass spectrometry [272], thermometry [273] and electroanalysis[147,274]. Compared to all the other techniques, electroanalytical methods could provide a number of exceptional advantages, like miniaturization, rugged portable instrumentation, on-site analysis, low-cost disposable chips, short analytical time, compatible for automation and novice-friendly.

In the development of electrochemical sensor systems and electrocatalytic composite materials, CNTs have been playing vital role in combination with various nanomaterials, like metal nanoparticles [275], metal oxides [276], conducting polymers [277], etc. Electrochemical

determination of NFT has been investigated with the use of a variety of graphitic carbon materials. Screen printed carbon electrode with drop-coated lanthanum molybdate nanospheres (LMNSs/SPCE) was applied for the determination of NFT by DPV, and the low-detection-limit was 72 nM NFT [278]. A nanocomposite electrode fabricated with 3D flower-like NiO entrapped boron doped carbon nitride was analyzed by amperometry for NFT determination, and a low-detection-limit of 10 nM was observed [150]. A modified electrode comprised of nano-hydroxyapatite incorporated MWCNT-chitosan scaffolds showed a low-detection-limit of 1.3 nM NFT in steady-state amperometry analysis [279]. A nanocomposite electrode comprised of reduced graphene oxide/Fe_3O_4 nanorod composite exhibited a low-detection-limit of 1.14 nM for NFT determination in DPV experiments [147].

In recent years, nanocomposite materials developed with the combination of GO, rGO and CNT are explored intensively for various electrocatalytic applications to benefit from the synergistic effect of these efficient graphitic carbon materials. CNTs exhibit high surface area in 3D network but lack of dispersivity due to lower surface charge density. Functionalization of CNTs with hydroxyl and carboxyl moieties at edges and defect sites by oxidation was explored to increase the dispersivity. Graphene oxide possesses high edge density and amphiphilic in nature with good biocompatibility. MWCNT-GO composite benefits with high edge density, high dispersivity and high surface area in 3D network, and it alleviates the difficulty in GO to increase the edge density in 3D network, due to the synergistic effect between these two graphitic carbon materials[280]. The synergy between GO and MWCNT could impart excellent electronic and electrocatalytic properties to the composite, and the composite had exhibited enhanced electrocatalytic activities towards analytes and even enzymes[280,281]. MWCNT-GO nanocomposite prepared by simple sonication method was used as sensing platform for amperometric detection of glucose [280] and for simultaneous detection of dopamine and paracetamol [281]. A laminated structure of CNT-intercalated rGO/S has been designed by hydrothermal method to develop lithium-sulfur batteries with a high charging-rate and long lifetime[282]. A nanocomposite between CNT and rGO resulted by DC-pulse nitrogen atmospheric-pressure-plasma-jet (APPJ) process was investigated for gel-electrolyte supercapacitor applications and had shown an enhanced specific capacitance[283]. A composite CNT/rGO-CNF carbon aerogel formed by directional freeze-casting and freeze-drying process was highly promising for applications in flexible or wearable electronic devices and had exhibited

ultrahigh compressibility (up to 95% strain) and superior elasticity (94.6% height retention) for 50000 cycles [284]. Though hybrid CNT-rGO nanocomposites were also fabricated by various hydrothermal, solvothermal, chemical and microwave methods, they were not explored for electrochemical sensing of NFT yet, to the best of our knowledge. We have explored in this investigation the fabrication of hybrid ErGO-CNT nanocomposite electrode by electroreductive deposition of GO[285,286] as a simple, facile and cost-effective method for the determination of NFT.

In this work, we explored the development of electrochemically reduced graphene oxide-CNT nanocomposite (ErGO-CNT) modified GCE for highly sensitive and selective determination of an important antibiotic drug NFT. The main aim of the present study is to develop a cost-effective and straightforward electrochemical sensor and to apply it towards NFT determination in complex sample matrices. The fabricated ErGO-CNT composite has been characterized and evaluated by employing various surface analytical and electrochemical techniques, namely, scanning electron microscopy, cyclic voltammetry, DPV and steady-state amperometry. ErGO-CNT composite electrode has shown good electrochemical performance for NFT determination with enormous sensitivity, selectivity and excellent anti-interfering properties, and the detection limit, reproducibility, stability and applicability for physiological samples of the fabricated sensor were evaluated.

4.2. Experimental

4.2.1. Chemicals and materials

NFT, uric acid (UA), ascorbic acid (AA) and serotonin (5-HT) of high purity were utilized as obtained from TCI, Japan. MWCNTs (20–30 nm OD, 10–30 μm length and 95.2% content) were obtained from SRL, India. Phosphate buffer solution (PBS, 0.1 M) was prepared by mixing KH_2PO_4 and K_2HPO_4. All the reagents and solvents were of analytical grade and used without any purification process. MWCNTs have been functionalized with carboxyl groups by treating with 3 M HNO_3 subsequent the process described in our earlier publication [260] and in Chapter II. Double-distilled water treated with ultrahigh water purifier (ThermoFisher, USA) with the output 18 Mohm resistance has been utilized for all the aqueous solutions used for syntheses and electrochemical analyses. Human serum samples collected from a healthy donor have been utilized

to carry out the direct determination of NFT in spiked serum samples, and aliquots of the collected serum samples were stored at −20 °C prior to use.

4.2.2. Fabrication of sensor system

Glassy carbon electrode (CHI, USA; 3 mm diameter) was polished by using alumina slurry (down to 0.04 μm), then treated under ultra-sonication with DD water, aq. 1:1:1 v/v ethanol:H_2O:conc.HNO_3 and DD water sequentially and dried at RT. MWCNT (functionalized) was dispersed in DMF at 3 mg mL^{-1} level and sonicated for 1 h. The MWCNT ink was drop casted 5.0 microliters on cleaned GCE and then allowed it to dry at RT, and the electrode denoted henceforth as CNT/GCE. Graphene oxide (GO) has been prepared by following well-known modified Hummer's method [287]. GO dispersion (0.5 mg mL^{-1}) was prepared in aq. 0.1 M KCl. It was taken along with PBS (pH 5.0) in 1:1 v/v ratio in the electrochemical cell, and CNT/GCE was subjected for 10 cycles in the range of 0.2 to -0.8 V at 50 mV s^{-1} and is called henceforth as ErGO-CNT/GCE. Rotating disk glassy carbon electrode has also been modified similarly and denoted as ErGO-CNT/RDGCE, and the fabrication of the sensor surface has been illustrated in Scheme 4.1.

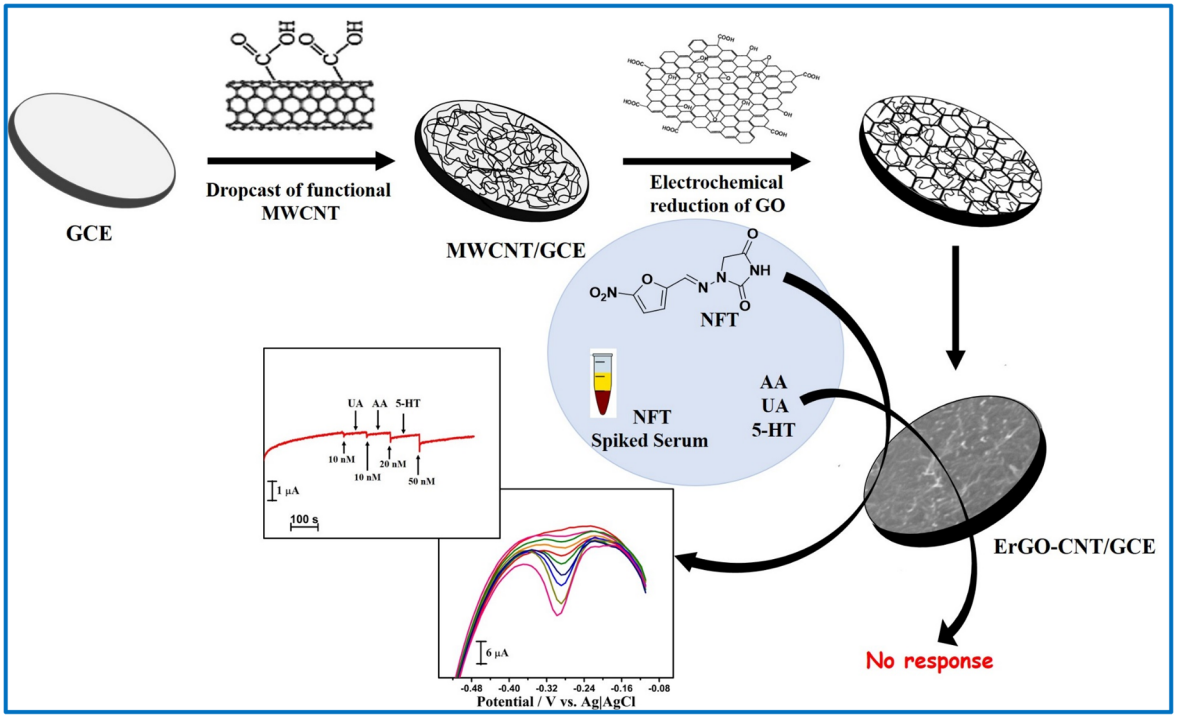

Scheme 4.1. *Schematic representation of ErGO-CNT/GCE fabrication*

4.2.3. Electrochemical analysis, surface imaging and X-ray diffraction (XRD) studies

Electrochemical workstation (CHI 619d, USA) has been used for all voltammetric and amperometric experiments. A two-compartment electrochemical cell of 20 mL volume was used with GCE, CNT/GCE, ErGO-CNT/GCE and ErGO-CNT/RDGCE as working electrode, Pt spiral as counter electrode and Ag|AgCl (3 N KCl) as reference electrode. All electrode potentials were referred against Ag|AgCl (3N KCl). PBS solutions of pH 5.0-9.0 were used as supporting electrolyte.

SEM images of the synthesized materials were recorded by using TESCAN VEGA-3 scanning electron microscope (Czech Republic) equipped with magnetron sputter coater (Quorum, SC7620 mini sputter coater, UK). By using sputter coater, a conductive nano-film of Au (~5 nm thick) was sputtered on the electrode surface before SEM imaging. Morphological images of the electrode surface were recorded at a reduced pressure of 0.10 milliPascal with magnification levels of up to 34,000 times. XRD spectrum of ErGO-CNT was recorded with the use of screen printed carbon electrode (SPCE) as the base electrode using Bruker AXS D8 diffractometer in the 2θ range of 6º - 90º with Cu K_α source of 1.5406 Å, step size of 0.01º and 0.3 s per step.

4.2.4. Preparation of serum samples

To assess the practical utility of the proposed sensor, human serum samples were prepared by using blood collected from healthy donors clotted, centrifuged at 3000 rpm for 15 min using Clinic Centrifuge LABPRO-140 and sterile-filtrated. Then, the collected serum sample was diluted 10 times using 0.1 M PBS for electrochemical analyses.

4.3. Results and discussion

4.3.1. SEM and XRD analyses

SEM images of CNT/GCE (A, B), GO (C, D) and ErGO-CNT/GCE (E, F) recorded at different magnification levels are shown in Fig. 4.1. In Fig. 4.1 (A, B), it was observed that a homogeneous spread of mesh like structure of the carbon nanotube matrix uniformly throughout the electrode surface. Figure 4.1 (C, D) showed nanothin flake-like structured nanosheets of GO. After the electrodeposition of ErGO on CNT/GCE electrode, the SEM images (Fig. 4.1 (E, F)) exhibited a homogeneous structure of nanothreads of CNT covered with an outerlayer of thin

flakes of ErGO, promoting close interactions between ErGO and CNTs at the interface and enhanced surface area of the electrode.

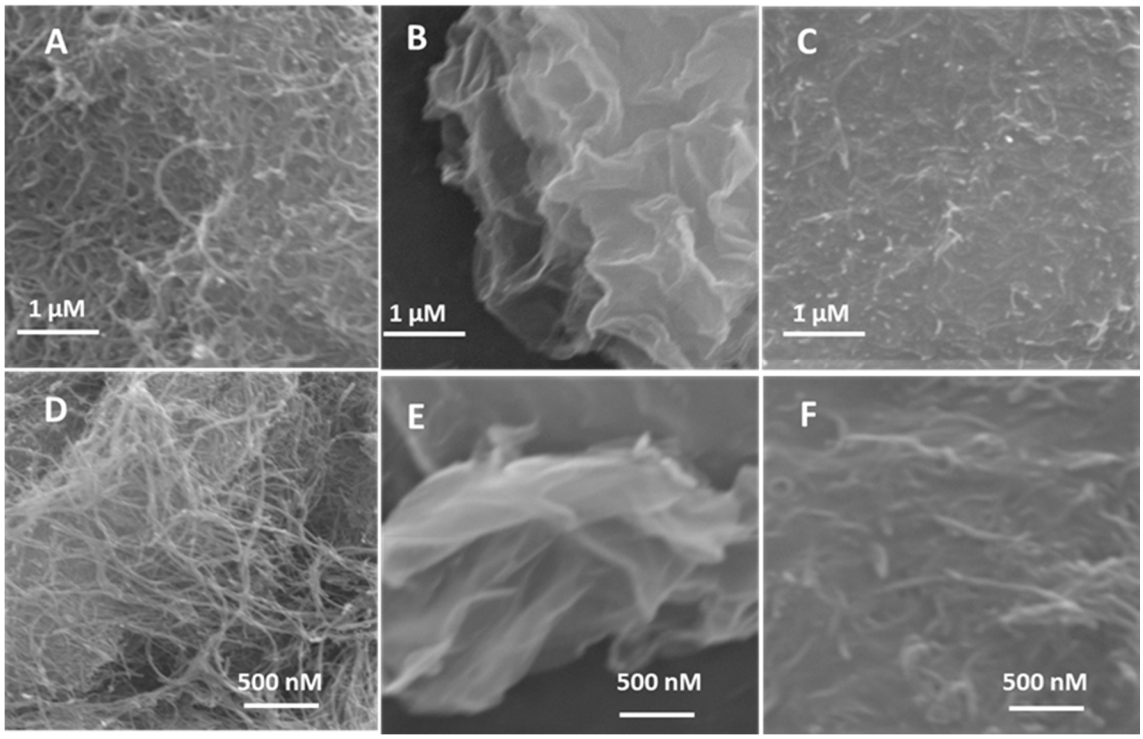

Fig. 4.1. *SEM images of CNT/GCE (A, B), GO (C, D) and ErGO-CNT/GCE (E, F) with different magnifications.*

XRD patterns of ErGO-CNT film and control materials have been recorded to analyze the fabrication of sensing platform and are shown in Fig. 4.2. CNT sample has shown a broad diffraction peak at 26.2˚ characteristic to the (002) plane and to the nanoparticulate nature of CNTs. GO has shown a quite sharp diffraction peak at 12.1˚ characteristic to the (002) plane with an interplanar distance of 7.3 Å. ErGO-CNT film was formed electrochemically on SPCE to record XRD spectrum. Control spectrum was recorded with bare SPCE, which has shown very sharp peaks of graphite at 26.7˚ and 53.4˚, corresponding to (002) and (004) planes of graphite, respectively [288]. XRD spectrum of ErGO-CNT has shown a very broad peak at 26.0˚, characteristic of reduced graphene oxide, and the absence of GO peak at 12.1˚ clearly confirms that GO was reduced effectively by the electrochemical reduction process.

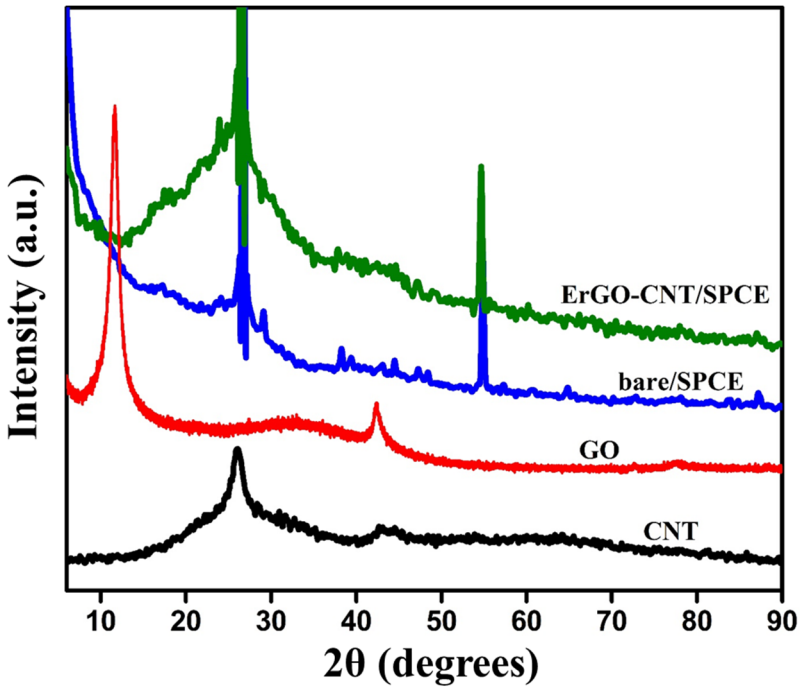

Fig. 4.2. *Powder XRD patterns recorded with CNT, GO, bare SPCE and ErGO-CNT/SPCE.*

4.3.2. Electrochemical characteristics of modified electrodes

Electroactive surface area (EASA) of ErGO-CNT/GCE, CNT/GCE and bare GCE was determined by recording CVs of 5 mM $K_3[Fe(CN)_6]$ in aq. 0.1 M KCl at different scan rates, and the obtained CVs are shown in Fig. 4.3. At all the electrodes, the plot of the peak current against the square root of scan rate was linear passing through the origin with a regression coefficient of $R^2 \geq 0.98$ (Fig. 4.3 (B)). From the slope of the plots, EASA of the electrodes was determined using Randles-Sevcik equation, using the diffusion coefficient (D) of $K_3[Fe(CN)_6]$ as 6.7 x 10^{-6} cm^2 s^{-1} [289].

$$i_p = 2.69 \times 10^5 \, n^{3/2} \, A \, D^{1/2} \, \upsilon^{1/2} \, C$$

where i_p refers the peak current, n is the number of electrons, A is the active surface area, C is the concentration of $K_3[Fe(CN)_6]$ and υ is the scan rate. EASA of bare GCE was determined to be 0.066 cm^2, which is nearly equal to the geometric area (0.071 cm^2) of GCE electrode. EASA of ErGO-CNT/GCE and CNT/GCE are 0.200 cm^2 and 0.111 cm^2, respectively, and are nearly 3.1 and 1.7 times higher compared to the geometric area. The exceptionally high EASA of ErGO-

CNT/GCE by 3.1 times clearly demonstrates the importance of ErGO-CNT composite for high surface area and confirms indirectly the porous nature of the composite on the electrode.

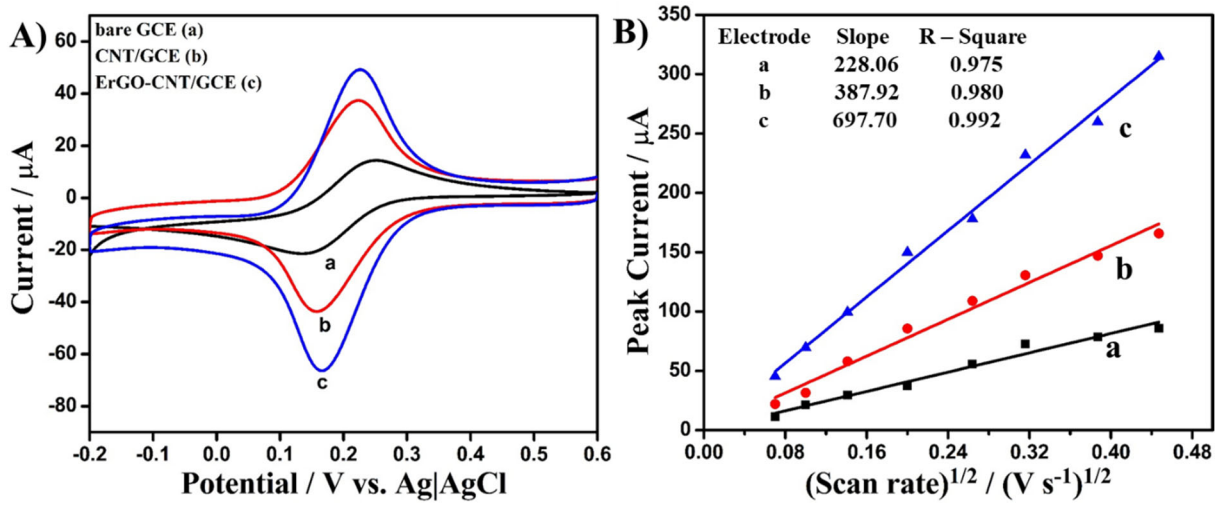

Fig. 4.3. *(A) CVs of $K_3[Fe(CN)_6]$ recorded at bare GCE (a), CNT/GCE (b) and ErGO-CNT/GCE (c) in aq. 5 mM $K_3[Fe(CN)_6]$ + 0.1 KCl; Scan rate = 10 mV s^{-1}. (B) Plot of the peak current against the square root of scan rate.*

Electrochemical responses of the modified electrodes towards the detection of NFT were investigated by CV studies, and the CVs of bare GCE, CNT/GCE and ErGO-CNT/GCE recorded in 0.1 M PBS (pH 7.0) containing 50 µM NFT at 50 mV s^{-1} scan rate are shown in Fig. 4.4. In the absence of NFT, there is no characteristic peak at any of the electrodes, but we observed a quasi-reversible redox reaction in the presence of NFT with the cathodic peak predominantly at all the electrodes. The cathodic peak potentials for the reduction of NFT at CNT/GCE and ErGO-CNT/GCE are -0.35 V and -0.310 V, respectively. Compared to bare GCE, the cathodic peak potential for NFT reduction at ErGO-CNT/GCE is shifted to less negative potentials by 0.1 V, and this decrease in over potential reveals the promotion and enhancement of the electroreduction of NFT at ErGO-CNT/GCE. Consequently, the cathodic peak current of NFT reduction at ErGO-CNT/GCE (-63.5 µA) is enormously high and is nearly 40 times high compared to that at bare GCE (-1.6 µA). Though the EASA of ErGO-CNT/GCE is only 3.1 times higher compared to bare GCE, the high peak current of NFT at ErGO-CNT/GCE by ~ 40 times clearly infers the high electrocatalytic activity of ErGO-CNT towards NFT and the exceptionally enhanced electronic interactions and enhanced electron-transfer between ErGO-CNT and NFT at the interface. The observed low over potential and extremely high peak current clearly reveal the enhanced electron-

conduction pathway at the interfacial ErGO-CNT composite thin film and enhanced interactions between the electrode and the substrate, promoting facile electron-transfer at the interface towards the reduction of NFT.

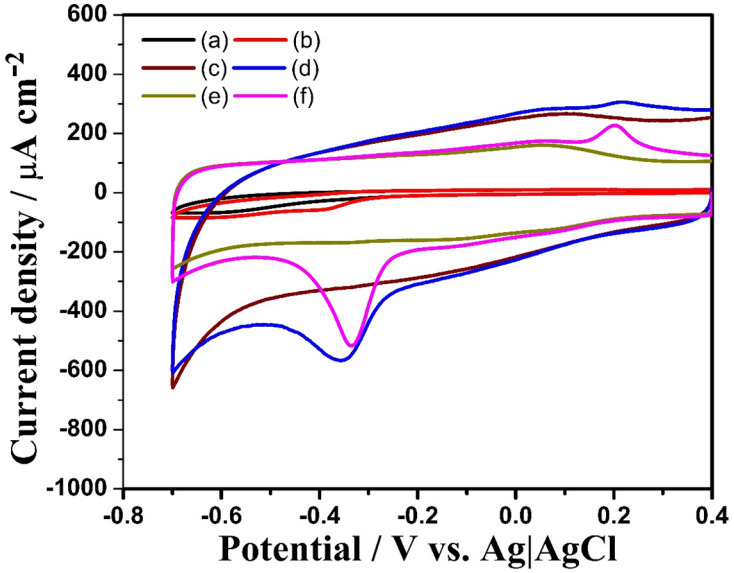

Fig. 4.4. *CVs of NFT recorded in PBS (pH 7.0) in the presence (b,d,f) and absence (a,c,e) of 50 μM NFT at bare GCE (a,b), CNT/CPE (c,d) and ErGO-CNT/CPE (e,f). Scan rate = 50 mV* s^{-1}.

Effect of the electrolyte pH on NFT reduction has been analyzed by recording CVs of 50 μM NFT at ErGO-CNT/GCE in PBS of different pH values of 5.0, 6.0, 7.0, 8.0 and 9.0, and the results are shown in Fig. 4.5 (A). A series of well-shaped CVs of NFT reduction were observed in the tested range of pH 5.0-9.0. With the increase in pH of buffer solution, the peak potential shifts gradually to more negative potentials (Fig. 4.5 (A)). The cathodic peak current and the peak potential were plotted against the pH, and the plots are shown in Fig. 4.5 (B). The observed CV curves confirm that the electrochemical response of NFT was pH dependent and that the hydrogen ions involve in the reduction and electron-transfer of NFT. Slope of the E_p vs. pH plot was observed to be 0.051 V/pH. The slope of the plot is nearing to 0.059 V/pH, indicating that both the number of electrons and the number of protons involved in the electrochemical reduction of NFT are equal (*vide infra*). It has been found that the highest peak current was observed at pH 7.0 (Fig. 4.5 B)). Based on this pH variation studies, PBS of pH 7.0 was chosen as supporting electrolyte for further analyses.

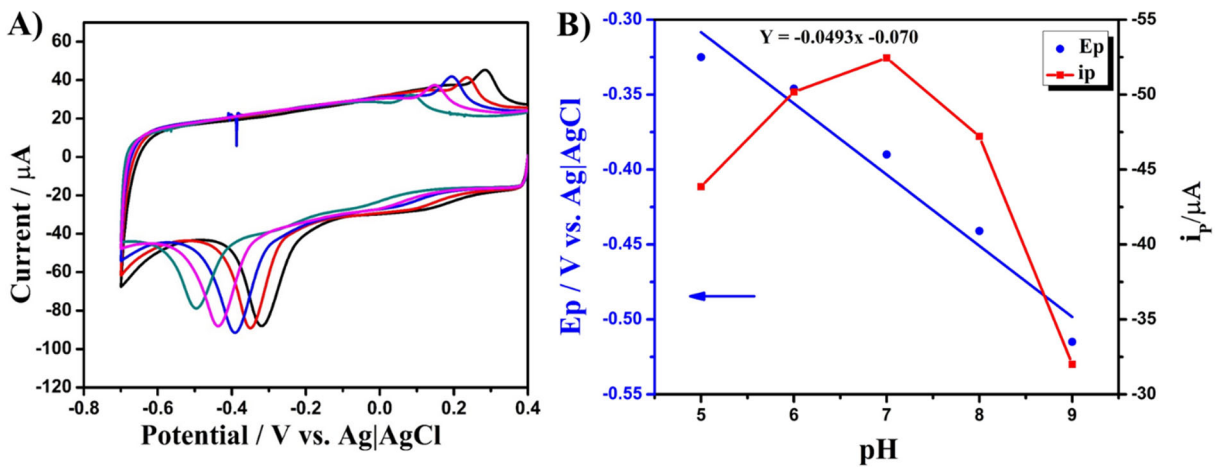

Fig. 4.5. *(A) CVs of 50 µM NFT in PBS buffer of different pH values (5.0 – 9.0) at ErGO-CNT/GCE; scan rate = 50 mV s^{-1}. (B) Plot of the peak potential and peak current against pH.*

Electrochemical reduction of NFT was investigated at ErGO-CNT/GCE in 0.1 M PBS (pH 7.0) containing 50 µM NFT by recording CVs at potential sweep rates of 5 - 300 mV s^{-1} (Fig. 4.6 (A)). A plot between the cathodic peak current and the square root of scan rate, $\upsilon^{1/2}$, has been constructed (Fig. 4.6 (B)). The peak current increased gradually with increasing scan rate and is linearly proportional to the square root of scan rate, $\upsilon^{1/2}$. The plot between i_p vs $\upsilon^{1/2}$ is passing through origin, as shown in Fig. 4.6 (B). These results show that the electrochemical reduction of NFT at ErGO-CNT/GCE followed diffusion-controlled process. The cathodic peak potential for NFT reduction shifts to more negative potentials with the increase in scan rate (Fig. 4.6 (A)), and the plot between the cathodic peak potential and ln(υ) is linear with the regression coefficient R^2 = 0.9915. From the plot between peak potential vs. ln(υ), the number of electrons involved in the electrodic process can be calculated according to Laviron's equation[290].

$$E_p = E' + (RT/\alpha nF)\ln(RTK/\alpha nF) + (RT/\alpha nF)\ln(\upsilon) \quad \text{.....} \quad 4.1$$

The slope of the E_p vs. ln(υ) plot, b = (RT/αnF), where 'b' is the slope, 'α' is the charge transfer coefficient and 'n' is the number of electrons. From the slope of the plot (Fig. 4.6 (C)), the value of 'αn' is calculated as 1.71. Electron transfer coefficient 'α' could be calculated from the equation, $\alpha = 47.7\ \text{mV}/(E_p - E_{p/2})$, where E_p is the peak potential and $E_{p/2}$ is the potential at which the current is half of the peak current. The value of 'α' is determined to be 0.48, and thus 'n' determined to be

3.6. Thus, the total number of electrons involved in NFT reduction is 4. Consequently, from E_p vs. pH studies, the electroreduction of NFT is ascertained to be a four-electron four-proton transfer process (*vide supra*). Electroreduction of NFT involved the reduction of a nitro group 'R-NO_2' into corresponding hydroxylamine group 'R-NH(OH)' [291], and it has been illustrated in Scheme 4.2.

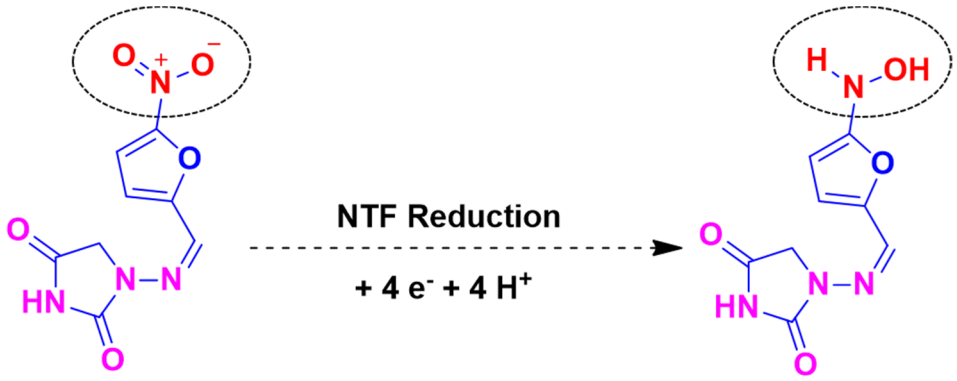

Scheme 4.2. Schematic representation of the electrochemical reduction of NFT involving the reduction of NO_2 group.

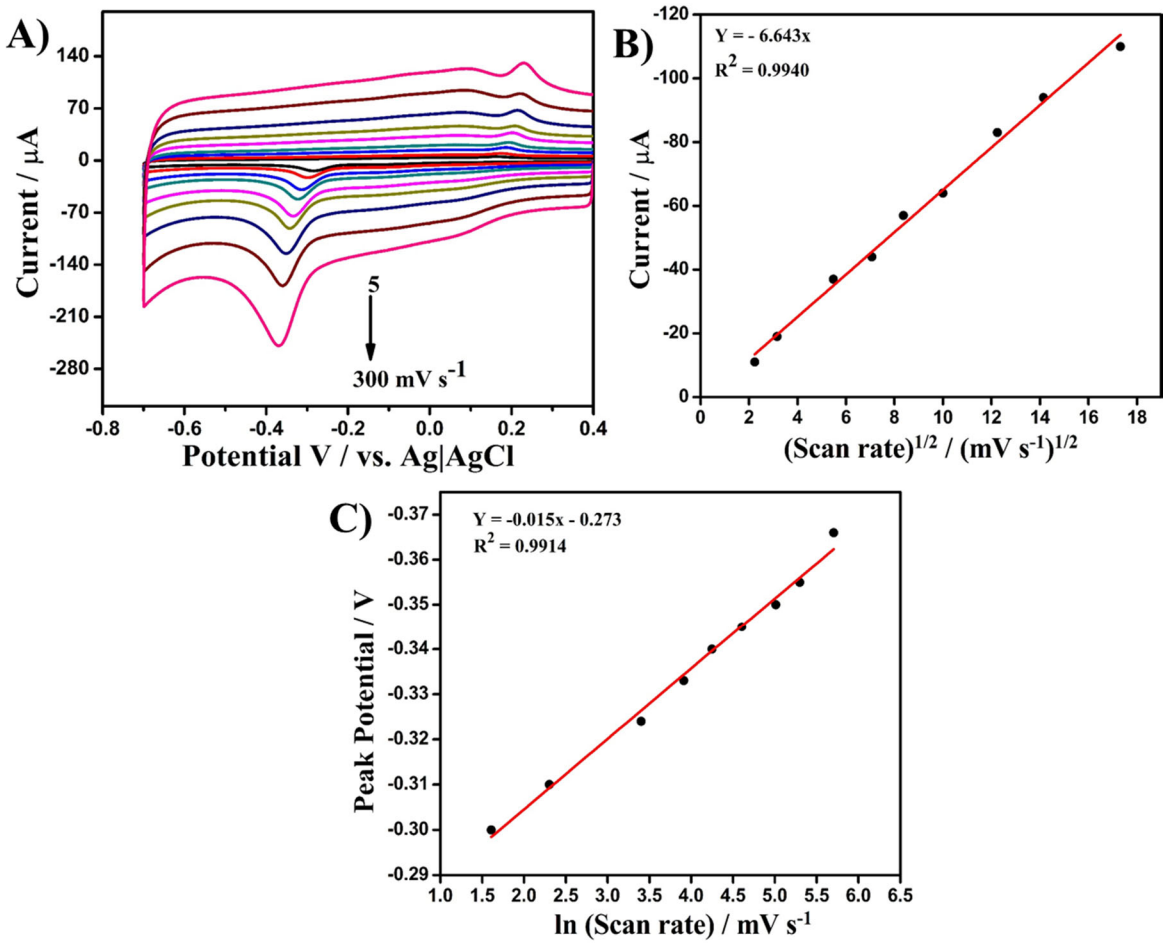

Fig. 4.6. *(A) CVs of 50 µM NFT in PBS buffer (pH 7.0) at ErGO-CNT/GCE with different scan rates (5, 10, 30, 50, 70, 100, 150, 200 and 300 mV s^{-1}). (B) Plot of the peak current against the square root of scan rate. (C) Plot of E_p vs. ln(scan rate).*

4.3.3. Determination of NFT by DPV

Efficiency and performance of the modified ErGO-CNT/GCE electrode towards the detection of NFT was examined by DPV technique. Under optimized conditions of 50 ms pulse width, 5 ms sample width, 120 mV pulse height, 5 mV increment and 150 ms pulse period of DPV, a good DPV profile was observed with the peak potential of –0.28 V at ErGO-CNT/GCE. The DPV measurements were performed using ErGO-CNT/GCE in PBS in the range of 0.02 to 2 µM, and the resultant voltammograms are shown in Fig. 4.7(A). The calibration plot of peak current vs. concentration of NFT is shown in Fig. 4.7(B). The cathodic peak current increased with NFT concentration in parabolic manner, and consequently two linear regions were observed in the plot, as shown in Fig. 4.7(B), with the linear regression coefficients, $R^2 = 0.9843$ for lower concentration

range 0.02 – 0.3 µM and R^2 = 0.9895 for higher concentration range 0.5 – 2.0 µM of NFT. Such a parabolic increase in the peak current was reported earlier in several electrochemical sensors[226,264,278]. The parabolic increase in the peak current was observed probably due to a slow heterogeneous electron transfer at the interface. Thus, at increased high concentrations, all the molecules diffusing to the electrode could not undergo electrodic reaction and consequently the peak current didn't increase proportionately.

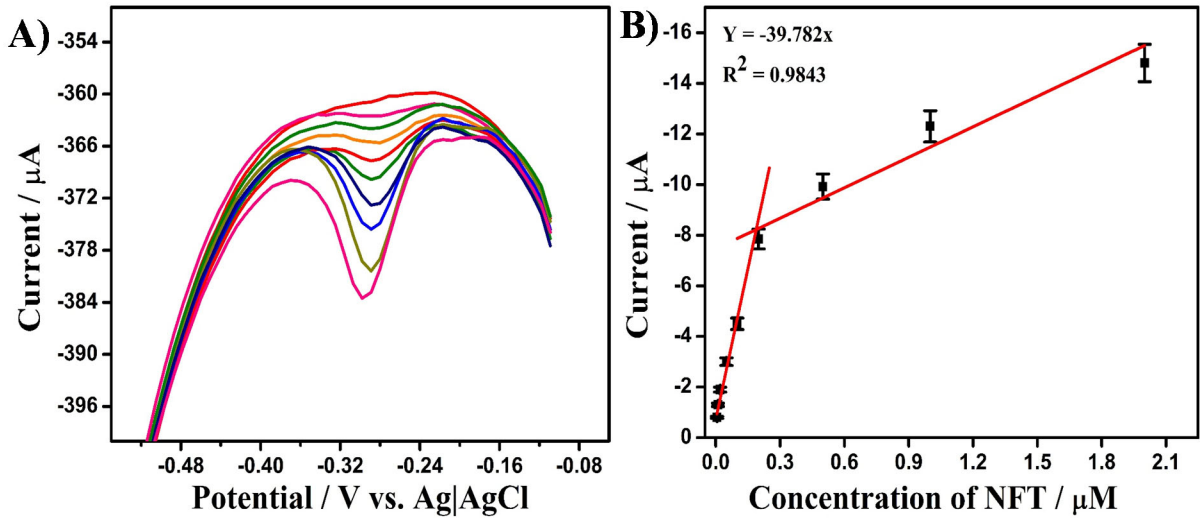

Fig. 4.7. *(A) DPVs of NFT in PBS buffer (pH 7.0) at different concentrations (0.02 to 2.0 µM) at ErGO-CNT/GCE. (B) Plot of the peak current against the concentration of NFT.*

ErGO-CNT/GCE electrode was stable and exhibited constant current responses for repeated analysis at a particular concentration of the analyte. The DPVs recorded repeatedly three times for 2 µM NFT by using a single ErGO-CNT/GCE electrode are shown in Fig. 4.8, and the peak currents were constant with a standard deviation of only 1.9%. This investigation demonstrates that ErGO-CNT/GCE was stable for electroanalysis of NFT and was resistant to electrode fouling or to the adsorption of degraded products on the electrode surface. Performance of the present sensor for the quantification of NFT was further evaluated by steady-state amperometric analyses.

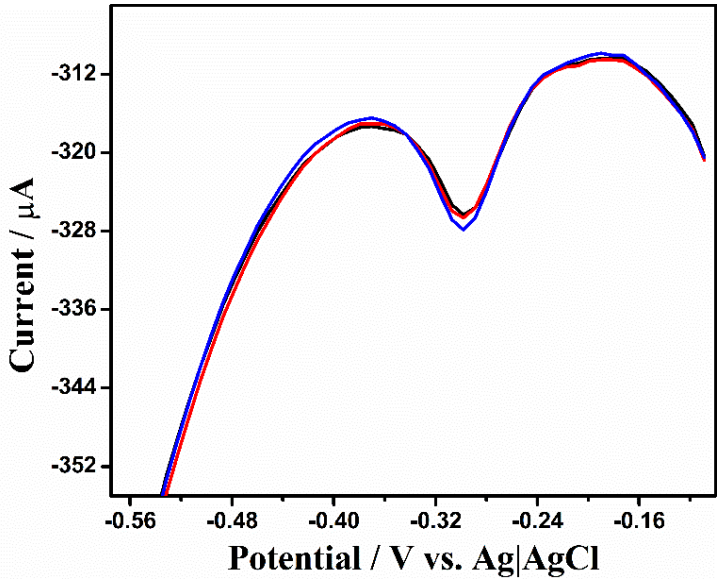

Fig. 4.8. *DPVs recorded at ErGO-CNT/GCE in the presence of 2.0 µM NFT in PBS (pH 7.0) for three different runs.*

4.3.4. Amperometric i-t curve studies

Steady-state amperometric i-t curve analysis under hydrodynamic conditions is the most important technique in electrochemical methods for sensor applications, and the result outputs from this study like stability, sensitivity, selectivity, reproducibility, etc. could be extended easily to flow-injection-analysis (FIA), where automated multiple-sample analyses and continuous monitoring could well be executed. Amperometry experiments under hydrodynamic conditions were conducted with the use of rotating disk electrode. At the optimized condition of -0.4 V and rotating speed of 1200 rpm, we examined the steady-state amperometric response towards the detection of NFT at ErGO-CNT/RDGCE. Stock solution of NFT in PBS was added sequentially to the electrolyte at increased concentration levels at regular intervals of ~30 s, and the observed amperometric results are shown in Fig. 4.9 (A). A well-defined increase in cathodic current was observed promptly immediate to each addition of NFT at ErGO-CNT/RDGCE, and the cathodic current attains the steady-state within 4 s from the addition of NFT. The increase in cathodic current was plotted against the concentration of NFT. The plot of amperometric current response against NFT concentration was linear from 0.005 to 2.81 µM with the correlation coefficient R^2 = 0.9906 (Fig. 4.9 (B)). Even the addition of as low as 5 nM NFT has given a good response (see Fig. 4.9 (inset)) in cathodic current with an overwhelming signal-to-noise ratio (S/N) of 6, and the

low-detection-limit of NFT at ErGO-CNT/RDGCE was confirmed to be 1.87 nM (S/N = 3) with the analysis time as low as 5 s.

Sensitivity of the present sensor system has been compared with the previous literature reports using the specific current density, and the present sensor system was found to exhibit a superior specific current density of 36.3 μA μM^{-1} cm^{-2}, which is at least 3 times higher than those reported with different electrochemical sensors. Lanthanum molybdate nanospheres ($La_2(MoO_4)_3$) employed SPE exhibited a specific current density of 2.94 μA μM^{-1} cm^{-2} [278]. Sensitivity of the 3D flower-like NiO entrapped boron doped carbon nitride was 1.15 μA μM^{-1} cm^{-2} [150]. A high sensitivity of 9.59 μA μM^{-1} cm^{-2} was reported for NFT using nitrogen-doped carbon quantum dots embedded Co_3O_4 with MWCNTs[292]. The results of the present study regarding method, linear range, limit of detection and sensitivity were compared with the literature reports, involving various electrochemical methods, modified electrodes and other analytical techniques employed to detect NFT (Table 4.1). Low-detection-limit of the present sensor, 1.87 nM, with the analysis time of 5 s is superior compared to that of various modified electrochemical sensors and also to that of the other analytical methods, based on bulky laboratory-based sophisticated instruments (Table 4.1). Low-detection-limit obtained in this study is superior by one to three orders of magnitude (~10-1000 times) compared to various electrochemical sensor systems employing electrodes based on boron-doped diamond, carbon quantum dots, carbon nanofiber, 3D neodymium molybdate, etc.[145,149,264,274,278,293,294]. Only a few electrochemical sensor systems have shown very equivalent or superior low-detection-limits (1.0 - 1.3 nM) compared to that of the present sensor (1.9 nM) [147,279,295]. Low-detection-limit of this study is nearly 2 to 4 times superior compared to those reported with chromatographic methods employing sophisticated HPLC and LC-MS analytical instruments[272,296]. The present sensor system fabricated by simple and facile drop-casting followed by electroreductive deposition of rGO exhibited excellent low-detection-limit and sensitivity to the antibiotic NFT due to the synergistic effect of the high surface area of both CNT and ErGO nanomaterials and to the enhanced interactions resulted probably by electrodeposition. The fabricated electrochemical sensor is further investigated for interference, stability and direct real-sample analysis in human serum.

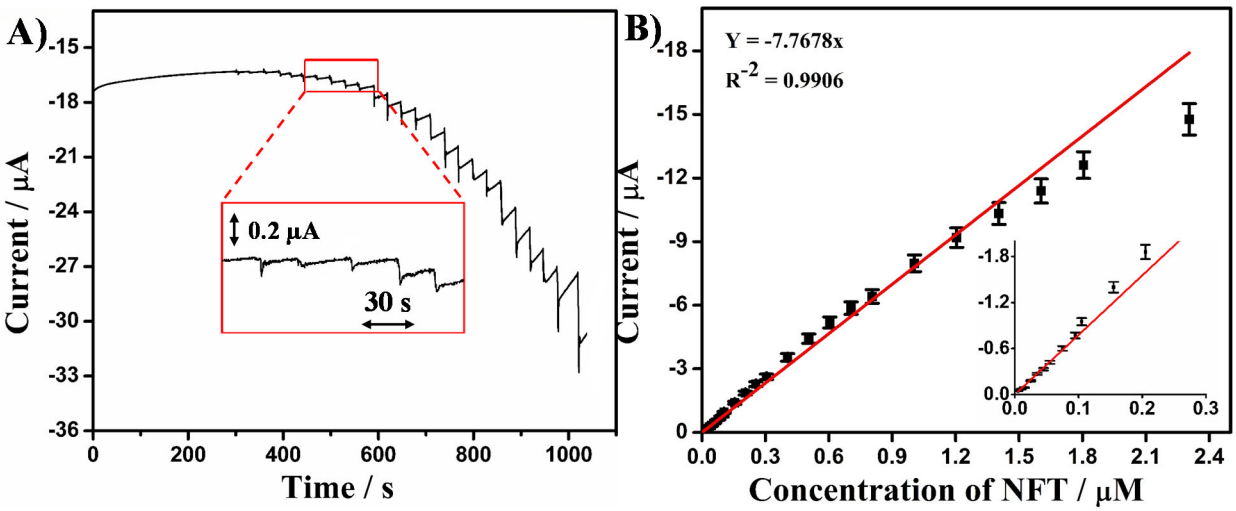

Fig. 4.9. *(A) Steady state current–time analysis at ErGO-CNT/RDGCE rotated at 1200 rpm in PBS (pH 7.0) to the additions of NFT from 0.005 to 2.81 µM. Every addition increases the concentration of NFT at regular intervals of ~ 30 s.* E_{app} *= -0.4 V. (B) Plot of the increase in cathodic current vs. NFT concentration.*

Table 4.1. Comparison of the results of NFT determination by various electrochemical methods, modified electrodes and the other analytical methods.

Electrode	Method	Linear range	LOD	Reference
m-AgSAE	DPV	0.2 – 100 µM	81 nM	[291]
rGO/Fe_3O_4Nanorod/GCE	DPV	0.005 – 100 µM	1.14 nM	[147]
GCE/PAMT/dsDNA	DPV	2 – 25 mg L^{-1} (8.4 – 105 µM)	0.65 mg L^{-1} (2.7 µM)	[292]
BDDFE	SWV	0.54 – 5.66 µM	-	[294]
NiO/BCN	Amperometry	0.05 – 230.0 µM	10.0 nM	[150]
HA NPs/MWCNT-CHI	Amperometry	0.005 – 982.1 µM	1.3 nM	[279]
LMNSs/SPCE	DPV	0.01 – 144 µM	72 nM	[278]
$Nd_2Mo_3O_9$/SPCE	DPV	0.1 – 481 µM	16 nM	[246]
N-CQD@Co_3O_4/MWCNT	DPV	0.05 – 1220 µM	44 nM	[295]
$LuVO_4$/GRS	Amperometry	0.008 – 256 µM	1 nM	[149]
CNF/SPCE	LSV using FIA	19.1 – 76.2 ng mL^{-1} (80.3 – 320.2 nM)	11.4 mL^{-1} (47.9 nM)	[274]
n.a.	HPLC-MS	7 – 60 µg kg^{-1} (29.4 – 252.1 nM)	1.69 µg kg^{-1} (7.10 nM)	[272]
n.a.	LC-MS	0.5 – 40 µg kg^{-1} (2.1 – 168 nM)	1 µg kg^{-1} (4.2 nM)	[295]
n.a.	LC-ESIMS	0 – 2.0 µg kg^{-1} (0 – 8.2 nM)	0.12 µg kg^{-1} (0.504 nM)	[296]
ErGO-CNT/GCE	Amperometry	0.005 – 2.81 µM	1.87 nM	present work

AgSAE - Ag Solid Amalgam Electrode; PAMT - Poly-(5-amino-2-mercapto-1,3,4-thiadiazole); BDDFE - Boron-doped diamond film electrode; BCN - Boron doped carbon nitride; HA NPs - Hydroxyapatite nanoparticles; CHI - chitosan hydrogels; N-CQD - Nitrogen-doped carbon quantum dots; GRS - Graphene sheets; CNF - Carbon nanofiber; *n.a.* - Not applicable.

4.3.5. Interference analysis

Selectivity of the sensor system was investigated by analyzing the electrochemical response of ErGO-CNT/RDGCE for NFT in the presence of a few important biologically active interferents, such as AA, UA and 5-HT. These physiological compounds in serum were selected for the interference study, considering that they are small molecular compounds similar to NFT and are electrochemically active. Steady-state amperometric responses of ErGO-CNT/RDGCE to the additions of 10, 20 and 50 nM NFT were investigated along with the additions of 10 fold concentrations of AA, UA and 5-HT at regular time intervals of ~30 s, and the results are shown in Fig. 4.10. Immediate to the additions of NFT, the current increased cathodically and attained a plateau within 5 s, whereas no characteristic current change was observed to the additions of all the interferents at the 10-fold concentrations. In the presence of the interferents, the cathodic current response for NFT exhibited only 4.5% deviation in total compared to NFT alone detection. The physiological compounds, AA, UA and 5-HT, didn't exhibit any current response at the applied potential of -0.4 V, because they could be electrochemically active widely at more positive potentials of > +0.1 V [297]. This observation shows that the various physiological compounds were electrochemically inactive at ErGO-CNT/RDGCE with the applied potential of -0.4 V. Further, the observation of an equivalent current response for NFT irrespective to the coexistence of the interferents indicated that the nanocomposite ErGO-CNT graphitic carbon matrix would be resistant for adsorption and accumulation of physiological compounds and interferents at the electrode interface and that it restricted electrode fouling/poisoning. From the above amperometric investigations, the results clearly reveal that the fabricated ErGO-CNT/RDGCE sensor is good for selective NFT detection even in the presence of electroactive biological interferences.

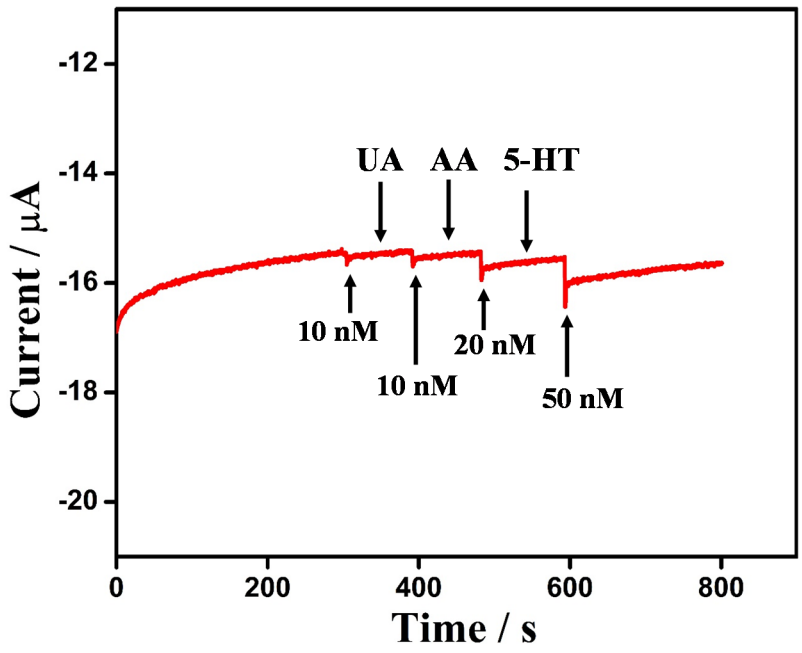

Fig. 4.10. *(A) Steady-state amperometric response of ErGO-CNT/RDGCE to the additions of 10, 10, 20 and 50 nM NFT and to the additions of 10 fold excess concentrations of interfering compounds such as UA, AA and 5-HT in 0.1 M PBS (pH 7.0) under continuous stirring at 1200 rpm, mimicking flow-cell conditions.*

4.3.6. Repeatability and reusability

Repeatability of the ErGO-CNT modified GCE was analyzed by recording the amperometric response of 50 nM NFT in PBS. To examine the repeatability of the modified electrode, we successfully measured 20 consecutive measurements using single electrode in the period of 14 days and found that the current response decreased by ~3.9 % only. It is clearly showing that the ErGO-CNT system has good repeatability and stability to multiple usage. Reproducibility of the present system has been evolved by analyzing the peak current of 50 nM NFT by using five independent ErGO-CNT/GCE electrodes. The RSD of the peak current of five electrodes was found to be 2.8% for the determination NFT in multiple experiments, showing excellent reproducibility of the sensor system. From the above evidences, we can conclude that the present biosensor is highly reproducible and reusable for the detection of NFT.

4.3.7. Determination of NFT in human serum

The developed sensor system was demonstrated so far to possess a wide dynamic linear range, good stability, selectivity and high sensitivity. In this study, practical feasibility of the present sensor for NFT determination in serum samples were investigated by steady-state amperometry under hydrodynamic conditions, which is mimic to FIA methodology, and thus the developed sensing strategy could be smoothly and immediately transferred to FIA system, apt for multiple samples and automated analysis. Steady-state amperometric current response recorded with ErGO-CNT/RDGCE in diluted human serum for the additions of NFT in the range of 0.005 to 1.505 µM is shown in Fig. 4.11(A). On the addition of NFT, the current increased cathodically and reached a steady-state within 4 s from the addition of NFT. The increase in cathodic current was plotted against NFT concentration (Fig. 4.11(B)), and the plot is linear to the concentration of NFT in the range of 0.005 to 1.505 µM ($R^2 = 0.998$). The cathodic current response of the electrode towards NFT in serum is very much equivalent to that observed in pure PBS alone. In overall, the developed ErGO-CNT modified electrode could be employed successfully for the determination of NFT in real physiological samples *in-vitro* with negligible interferences.

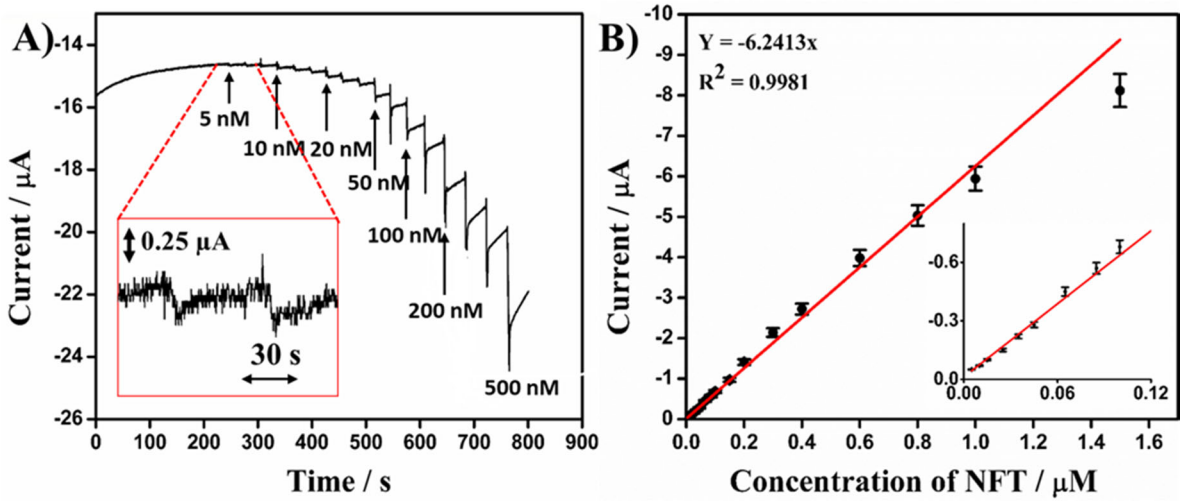

Fig. 4.11. *(A) Steady state current–time analysis at ErGO-CNT/RDGCE in 10 times diluted human serum to the additions of NFT from 0.005 to 1.505 µM. Every addition increases the concentration of NFT at regular intervals of ~ 30 s. E_{app} = -0.4 V. (B) Plot of the increase in cathodic current vs. NFT concentration.*

4.4. Conclusions

Development of an electrochemical sensor capable for highly sensitive and selective determination of NFT with an analysis time of mere 5 s was demonstrated. The methodology adopted here for sensor fabrication involved drop-casting step followed by electrodeposition, and it was very simple, facile and environmental-benign approach to achieve controlled thin graphene film. The steady-state current–time analysis probed here under hydrodynamic conditions could prompt to swiftly transfer the sensor performances and strategy to direct multiplex analyses of samples using automated FIA systems. The proposed method was successfully employed for the determination of NFT *in-vitro* in real sample analyses of diluted human serum samples, and the sensitivity of the fabricated sensor is at least 3 times superior compared to various electrochemical sensors reported. The exceptionally enhanced sensitivity and electrocatalytic activity combined with the simple and controlled fabrication process could be extended further to electrocatalytic applications in fuel cells, methanol oxidation, carbon dioxide conversion, etc., employing simultaneous electroreductive deposition of rGO and metals. The developed electrochemical sensor system could be extended for practical applications in the analyses of pharmaceutical dosages and medical diagnosis.

CHAPTER 5

Gold nanoparticle incorporated conducting polymer layer on carbon nanotube matrices for sensitive detection of serotonin in presence of dopamine *in-vitro*

5.1. Introduction

Neurotransmitters are endogenous chemicals that enable neurotransmission. Development of an electrochemical biosensor for direct detection of serotonin (5-HT), a neurotransmitter agent, from physiological fluids has been investigated. There is a great interest in order to determine neurotransmitters by developing electrochemical techniques. 5-HT is a monoamine neurotransmitter which is produced by serotonergic neurons in central nervous system, brain and intestines. It transmits messages between nerve cells and plays a major role in emotive system such as regulation of sleep, mood, appetite and sexuality. Deficit of 5-HT leads to several conditions such as migraine, depression, poor memory, bipolar disorder and anxiety. A high level of 5-HT marked toxicity and potential fatal effect is known as serotonin syndrome, and thus there is necessary to determine and continuously monitor of 5-HT in patients. There are several conventional chromatographic and spectrophotometric techniques such as spectrophotometry [298], HPLC [299], capillary electrophoresis [300] and LC-MS [301] for detection of 5-HT in physiological and pharmaceutical samples. But these techniques are time-taking, expensive, bulky non-portable instrumentation and even difficult to handle. From the past few years, electrochemical techniques are advanced for the detection of trace level of specific target analytes of even low-molecular-weight and from even complex sample matrices due to their high sensitive, selective, less time taken, portability and easy to operate characteristics.

In recent years, usage of versatile nanomaterials such as graphene, graphene oxide, carbon nanotubes, metal nanoparticles, etc. to modify electrode surface has contributed to the theme of many research in biological analysis by using electrochemical techniques. Carbon nanotube is one of the extensively used material for electrode surface modification in the area of electrochemical sensors and biosensors [260,302,303]. Due to the unique properties of CNTs, such as good electrical conductivity, high chemical stability and high adsorption properties, these are used in sensors towards electrochemical sensing of biological compounds. Functionalized CNT surface itself has carboxyl (-COOH), carbonyl (-C=O) and hydroxyl (-OH) functional groups, making these type of materials an outstanding support that can be adapted with several materials, including metal nanoparticles and conducting polymers.

In recent years, conducting polymers have attracted curiosity because of their reactivity, biocompatibility and potential for applications in various diverse fields, such as electrochemical materials, corrosion protection [304,305], photocatalysis [306,307] and sensors[308,309]. Fabrication of electrodes by using conducting polymer is an emerging method in the area of electrochemical sensors and biosensors due to their high compatibility with metal nanoparticles and biological molecules. Conducting polymers have extended π-orbital system which can easily promote the electrons from one end of polymer to other, which enhances the catalytic properties of the sensor. Kinetics of electrodic processes can be improved by depositing a thin film of conducting polymer on the electrode surface. The ability and biocompatibility of the sensor system could be influenced by the thickness of the polymer. Compared to other chemical methods, electrochemical polymerization method is simple and best technique for the formation of thin layers on the electrode surface with desirable thickness.

Composites of metal nanoparticles with different types of materials such as carbon materials[297][310] and polymers[311] have seen wide range of applications in nanoscience and technology. Especially gold nanoparticle composites show a significant role in biosensors due to their high strength, stability, excellent electron conductivity and unique surface chemistry. Gold nanoparticles freely allow the electron flow into the materials and established high catalytic activity in both reactions oxidation and reduction. Problem with the nanoparticle is particle aggregation, which is the response for the decrease in conductivity, active surface area and catalytic activity. Therefore, to overcome this problem, different types of approaches have been established to avoid the aggregation of the particles, such as surfactant stabilizers, polymer coating, thiol-ligand coating and polymer capping agents [312] .

The main aim of the present studies is to propose a simple, sensitive and selective method for detection of the important drug and neurotransmitter, serotonin, by using voltammetric and hydrodynamic amperometric techniques. In this study, electro-oxidation of serotonin has been investigated at AuNPs decorated conducting polymer interface. The detection of serotonin in artificial urine and pharmaceutical samples indicating that the present sensor system in this study might be implemented in quality control laboratories plus therapeutic drug monitoring in clinical and pharmaceutical industries.

5.2. Experimental

5.2.1. Chemicals

Serotonin and dopamine were obtained from Tokyo Chemical Industry, Japan, $HAuCl_4$ from Sigma-Aldrich, USA and 2-amino-5-mercapto-1,3,4-thiadiazole from Sisco Research Laboratories, India. Other chemicals used in this study were analytical grade (min. 99.5% purity). PBS was prepared by mixing 1 M KH_2PO_4 and 1 M K_2HPO_4 to pH 3.0 – 9.0. Double-distilled water treated with Ultrahigh water purifier (Thermo Fisher Scientific, USA) with the final resistance of 18 Mohm was utilized all throughout the investigation and for the preparation of aqueous solutions.

5.2.2. Functionalization of MWCNT

MWCNTs has been functionalized according to the procedure reported[260] earlier with a slight variation. Pristine MWCNT was added to 3 M HNO_3, sonicated for few minutes and heated to 60 °C for 24 h under constant stirring. During the acid treatment, it is oxidized at side-wall defect sites and at nanotube ends to form carboxyl groups. The obtained solid black precipitate was centrifuged, and the centrifugate was washed repeatedly with water until the supernatant becomes pH 7.0. The resultant *f*-CNT was dried at 80 °C in hot-air oven.

5.2.3. Fabrication of AuNPs/*poly*-AMT/*f*-CNT electrode

At first, we polished GCE (CHI, USA; 3 mm diameter) with Al_2O_3 slurry (down to 40 nm), washed with double distilled water thoroughly, then sonicated in 1:1 aq. Ethanol, 3N HNO_3 and double distilled water sequentially and finally dried at RT. Chitosan solution was prepared (0.25% w/v) by dispersing 0.25 g chitosan powder in 100 mL 1% v/v aq. CH_3COOH and was treated with ultra-sonication for 20 min at RT. Then, 5 mg functionalized CNT was added in 1 mL chitosan and dispersed it properly with ultra-sonication for 1 h. 9.0 µL of synthesized chitosan *f*-CNT ink was casted on cleaned GCE, dried at RT for further modification and denoted as *f*-CNT/GCE. After this, the *f*-CNT/GCE have been polymerised with a conducting polymer of 2-amino-5-mercapto-1,3,4-thiadiazole (AMT) by potentiodynamic polarization method. For this, the *f*-CNT/GCE is placed in 1 mM AMT + 0.5 M H_2SO_4 and ten consecutive cycles were swept between -0.2 to +1.6 V vs. Ag|AgCl (3N KCl) at a scan rate of 100 mV s^{-1}. A thin film of *poly*-AMT formed on the surface of *f*-CNT/GCE and denoted as *poly*-AMT/*f*-CNT/GCE. Next, AuNPs were

deposited on *poly*-AMT/*f*-CNT/GCE by potentiostatic technique using 10 mM gold solution ($HAuCl_4$) in 0.1 M H_2SO_4 as supporting electrolyte by applying potential at -0.2 V vs. Ag|AgCl (3 N KCl) for 100 s. The resultant electrode hereafter denoted as AuNPs/*p*-AMT/*f*-CNT/GCE, dried at RT for analysis.

5.2.4. Characterization

SEM images of the electrode surface were recorded with TESCAN VEGA-3 SEM (Czech Republic) operating at 10-30 kV equipped by the magnetron sputter coater (Quorum, SC7620, UK). Morphological images of the electrode surface were recorded at a reduced pressure of 0.10 milliPascal with magnification levels of up to 20,000 times.

5.2.5. Electrochemical analysis

Electrochemical potentiostat/galvanostat (CHI instruments, USA) has been used for all voltammetric and amperometric experiments. A conventional 10 mL volume one-compartment three-electrode cell has been used with the GCE modified working electrode, Pt wire counter and Ag|AgCl (3 N KCl) reference electrode. All the electrode potentials have been referred against Ag|AgCl (3N KCl). PBS (pH 7.0) has been used for all electrochemical experiments as the supporting electrolyte.

5.3. Results and discussion

5.3.1. Surface morphology

Surface morphology of *f*-CNT/GCE and AuNPs/*p*-AMT/*f*-CNT/GCE electrodes was characterized by SEM analysis, and the respective SEM images shown in Fig. 5.1(A, B). In Fig. 5.1(A), we observed a well homogeneous distribution of carbon nanotubes network on the surface of GCE. In the SEM image of AuNPs/*poly*-AMT/*f*-CNT/GCE, nanowire shaped carbon nanotubes were fully covered uniformly on GCE along with the spherical shaped AuNPs incorporated conducting polymer layer of poly-AMT all over the surface. Discrete Au nanoparticles of uniform size and shape were seen throughout the surface. The chemical composition of AuNPs/*p*-AMT/*f*-CNT/GCE was examined by using EDX studies (Fig. 5.1(C)). EDX analysis of AuNPs/*p*-AMT/*f*-CNT/GCE is evidently showing the carbon, gold, sulfur and oxygen peaks with the weight ratios of 83.85, 6.68, 5.32 and 4.15, respectively. Elemental mapping of the respective elements evidently reveals that the Au element is distributed evenly throughout the poly-AMT matrix (Fig. 5.1(D)).

The appearance of the Au and S along with the carbon on the surface of AuNPs/*p*-AMT/*f*-CNT/GCE is corroborating the formation poly-AMT layer with the incorporation of Au nanoparticles.

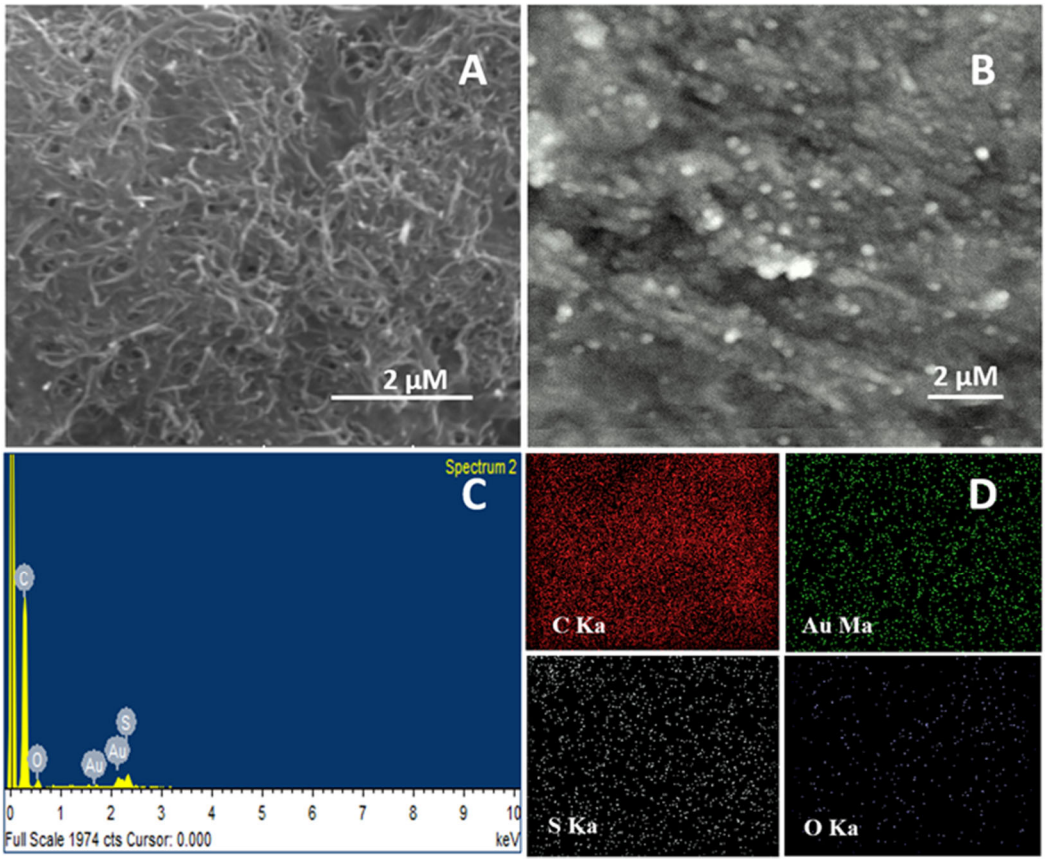

Fig. 5.1. *SEM images of f-CNT/GCE and AuNPs/poly-AMT/f-CNT/GCE electrodes (A, B). C) EDX spectrum and D) Elemental mapping of C, Au, S and O of AuNPs/poly-AMT/f-CNT/GCE.*

5.3.1. Electrodeposition of *p*-AMT and AuNPs

A thin film of AuNPs/*p*-AMT was formed on the surface of *f*-CNT/GCE electrode by applying two successive electrodepositions of *poly*-AMT and AuNPs. For the deposition of *poly*-AMT at first, *f*-CNT/GCE is placed in 1 mM AMT + 0.5 M H_2SO_4 and is swept ten cycles between -0.2 to +1.6 V at the scan rate 100 mV s^{-1}, and the observed CVs are shown in Fig. 5.2(A). The oxidation peak of the AMT appeared at +1.10 V in the first cycle. In the very next cycle, the oxidation peak potential increased nearly 20 mV and appeared at +1.12 V with a considerable decrease in peak current. For the cycles 4 to 6, we observed a very meagre amount of current is decreasing in each cycle, which indicates that the oxidative AMT polymerization occurred on the surface of *f*-CNT/GCE and that the electroactive polymerization decreased and stabilized at the

end of 6 cycles. In further cycles, the anodic peak current remained constant revealing that the polymerization extent remained constant to the additions of each new cycle and finally the electrode denoted as *p*-AMT/*f*-CNT/GCE. Figure 5.2(B) shows the chronoamperometry profile for electrodeposition of Au at the applied potential of -0.2 V. The cathodic current for electrodeposition of Au from $HAuCl_4$ solution decreased drastically in the beginning and attained near steady-state above 80 s. The electrodeposition was carried out for 100 s, and the electrode is denoted as AuNPs/*p*-AMT-*f*-CNT/GCE.

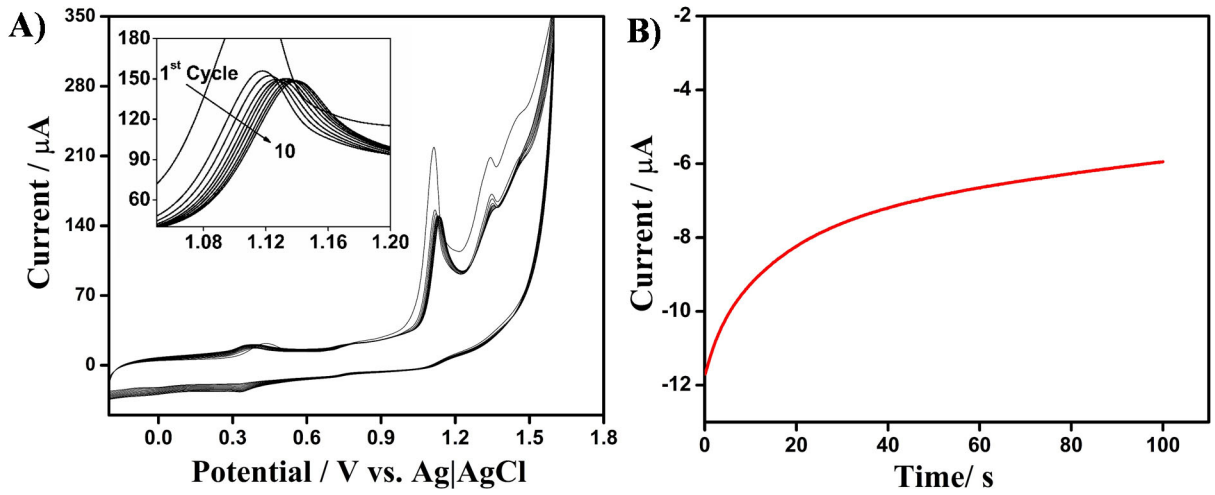

Fig 5.2. *(A) Potentiodynamic deposition of 2-amino-5-mercapto-1,3,4-thiadiazole (1 mM) in 0.1 M H_2SO_4 through 10 cycles on f-CNT/GCE; Scan rate 100 mV s^{-1}. (B) Chronoamperometry profile of potentiostatic deposition of AuNPs from 10 mM $HAuCl_4$ at -0.2 V in 0.1 M H_2SO_4 for 100 s.*

5.3.3. Oxidation of serotonin at AuNPs/*p*-AMT/*f*-CNT/GCE

CV measurements of 5-HT were carried out at AuNPs/*p*-AMT/*f*-CNT/GCE in PBS (pH 7.0) containing 5.0×10^{-5} M 5-HT at 100 mV s^{-1} scan rate (Fig. 5.3). In presence of 5-HT, an irreversible oxidation peak was observed at all *f*-CNT/GCE, *p*-AMT/*f*-CNT/GCE and AuNPs/*p*-AMT/*f*-CNT/GCE electrodes at +0.34 V, but, in the absence of 5-HT, no specific peak was observed at any of the electrodes. AuNPs/*p*-AMT/*f*-CNT/GCE has shown the highest peak current compared to *p*-AMT/*f*-CNT/GCE and *f*-CNT/GCE. It could be credited to the increase in surface area of the electrode, which could be verified from the high capacitive current of AuNPs/*p*-AMT/*f*-CNT/GCE electrode. The peak current at AuNPs/*p*-AMT/*f*-CNT/GCE is higher by more than three

times compared to that at *p*-AMT/*f*-CNT/GCE, and the over potential for oxidation of 5-HT at AuNPs/*p*-AMT/*f*-CNT/GCE is nearly 50 mV is less compared to the other electrode.

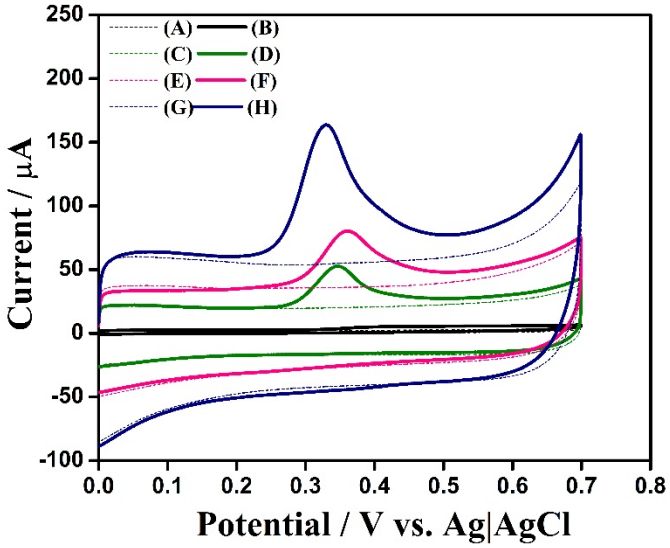

Fig. 5.3. *CVs of 5-HT recorded in PBS (pH 7.0) in the presence (b, d, f, h) and absence (a, c, e, g) of 50 µM 5-HT at bare GCE (a, b), f-CNT/GCE (c, d), poly-AMT/f-CNT/GCE (e, f) and AuNPs/poly-AMT/ f-CNT/GCE (g, h). Scan rate = 100 mV* s^{-1}.

Influence of the potential scan rate on the electrochemical behaviour of 5-HT at *AuNPs/poly-AMT/f-CNT/GCE* was studied (Fig. 5.4). We recorded CVs of 5-HT at different scan rates from 5 - 200 mV s^{-1}. The anodic peak current increased gradually with increasing scan rate, and the peak potential shifted towards more positive potential and is linearly dependent on ln(scan rate) (Fig. 5.4(D)). The anodic peak current was plotted against the square root of scan rate ($\upsilon^{1/2}$), and a linear plot passing through the origin with R^2 = 0.9972 obtained (Fig. 5.4 (B)). The results indicate that 5-HT oxidation at AuNPs/*p*-AMT/f-CNT/GCE is controlled by diffusion process.

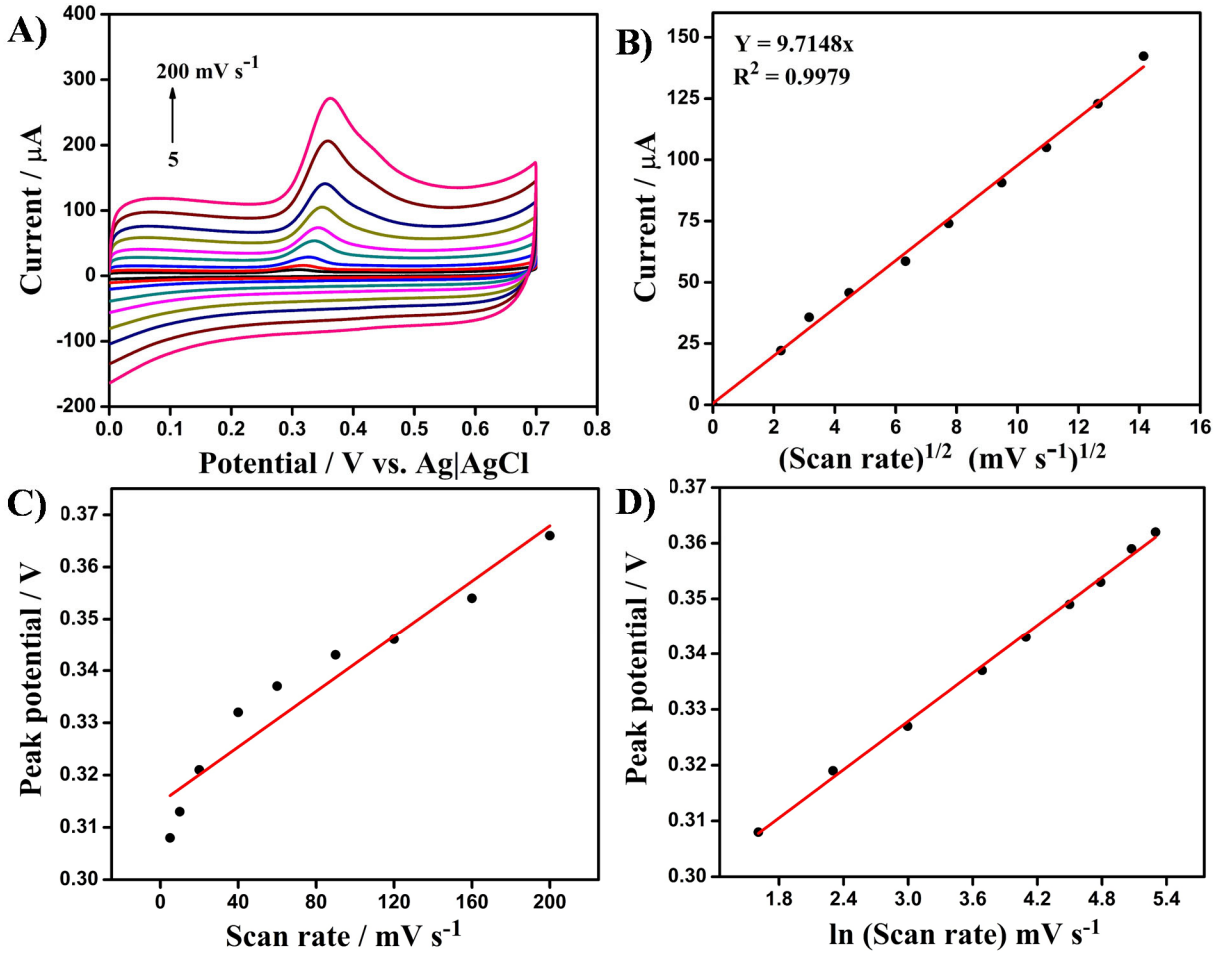

Fig. 5.4. *(A) CVs of 50.0 × 10^{-6} M serotonin in PBS buffer (pH 7.0) at AuNPs/poly-AMT/f-CNT/GCE; scan rate = 5, 10, 20, 40, 60, 90, 120, 160 and 200 mV s^{-1}. (B) Plot of i_p vs. square root of scan rate. (C) Plot of E_p vs. scan rate. (D) Plot of E_p vs. ln(scan rate).*

5.3.4. pH Studies

The effect of pH on 5-HT oxidation at the fabricated electrode AuNPs/*p*-AMT/*f*-CNT/GCE has been verified by CV at different pH 3.0-9.0 (Fig. 5.5(A)). We found that the increase in pH of buffer solution modulated the anodic peak of 5-HT. The anodic peak potential decreased gradually with increasing pH of buffer solution, and the plots of E_p vs. pH and i_p vs. pH are shown in Fig. 5.5(B). The peak current is maximum at pH 7.0 and is nearly same between pH 7.0-9.0, and the peak potential is optimum at pH 7.0. Thus, the pH 7.0 is preferred good for further analysis considering the oxidation peak position and the peak current at pH 7.0.

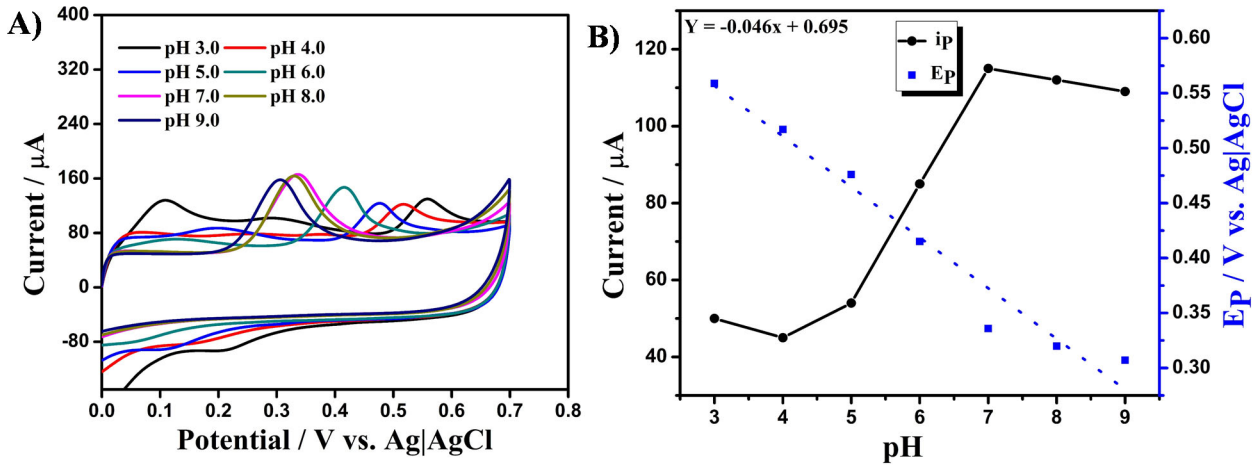

Fig. 5.5. *A) CVs of 50 µM 5-HT in PBS of different pH (3.0 – 9.0) at AuNPs/poly-AMT/f-CNT/GCE; scan rate = 100 mV s^{-1}. (B) Plot of peak potential and peak current against pH.*

5.3.5. Determination of serotonin by SWV studies

We performed SWV to investigate the electrochemical performance of AuNPs/*p*-AMT/*f*-CNT/GCE towards the determination of 5-HT. For a good voltammetric profile, the best optimum parameters: potential window +0.16 to +0.56 V, amplitude = 25 mV, step width = 4 mV, and frequency = 10 Hz. SWVs were recorded at AuNPs/*p*-AMT/*f*-CNT/GCE in PBS pH 7.0 containing 5-HT 0.015 – 5.0 µM, and the SWVs are shown in Fig. 5.6(A). A fine oxidation peak of 5-HT was observed at the potential of + 0.32 V, and the peak current of 5-HT increased gradually with increasing the concentration of 5-HT. The plot of anodic peak current vs. 5-HT concentration is linear (Fig 5.6(B)) in 0.015 – 5.0 µM concentration range. The linear regression equation is: i (µA) = 8.537 $C_{5\text{-HT}}$ (µM) with R^2 = 0.986. Low-detection-limit of the present sensor system is determined to be 7.8 nM by considering the change in peak current with three relative standard deviations (RSDs). Compared to other various reported electrochemical methods with different electrode modification and analytical methods, the LOD of the present electrode system is far superior, as shown in Table 5.1.

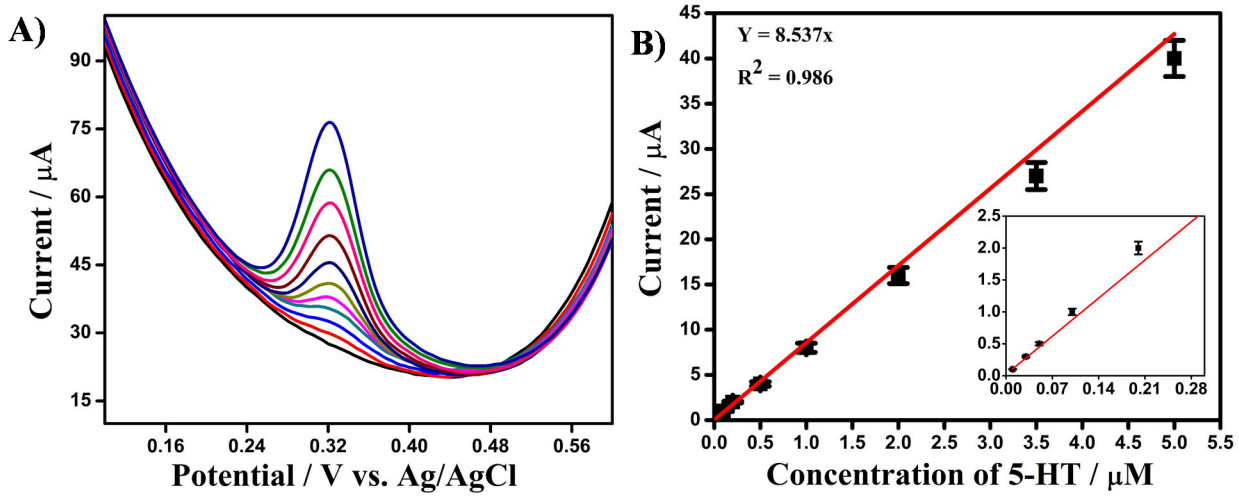

Fig. 5.6. *(A) SWVs of 5-HT in PBS (pH 7.0) at different concentrations (0.015 to 5.0 µM) recorded using AuNPs/poly-AMT/f-CNT/GCE. (B) Plot of peak current against concentration of 5-HT.*

5.3.6. Amperometric i-t curve analysis

Further, the detection of 5-HT has been demonstrated by amperometric analysis at the AuNPs/poly-AMT/*f*-CNT/GCE modified electrode. Figure 5.7 shows the amperometric i-t curve analysis of 5-HT detection in constant uniformly stirred PBS solution at the applied potential of +0.3 V. The steady-state current at AuNPs/*poly*-AMT/*f*-CNT/GCE with the initial addition of 50 nM 5-HT is showing good anodic current response and with each further successive additions of various concentrations with a sample interval of ~50 s. The plot of amperometric current response against the concentration of 5-HT has linear profile from 50 nM to 2.15 µM with a regression coefficient of 0.9572 as shown in Fig. 5.7(A). The limit of detection at AuNPs/*poly*-AMT/*f*-CNT/GCE modified electrode was found to be 18 nM. Electrocatalytic activity of the present sensor system has been further studied towards the detection of 5-HT in presence of a high interferential biological molecule, dopamine, and in diluted serum samples.

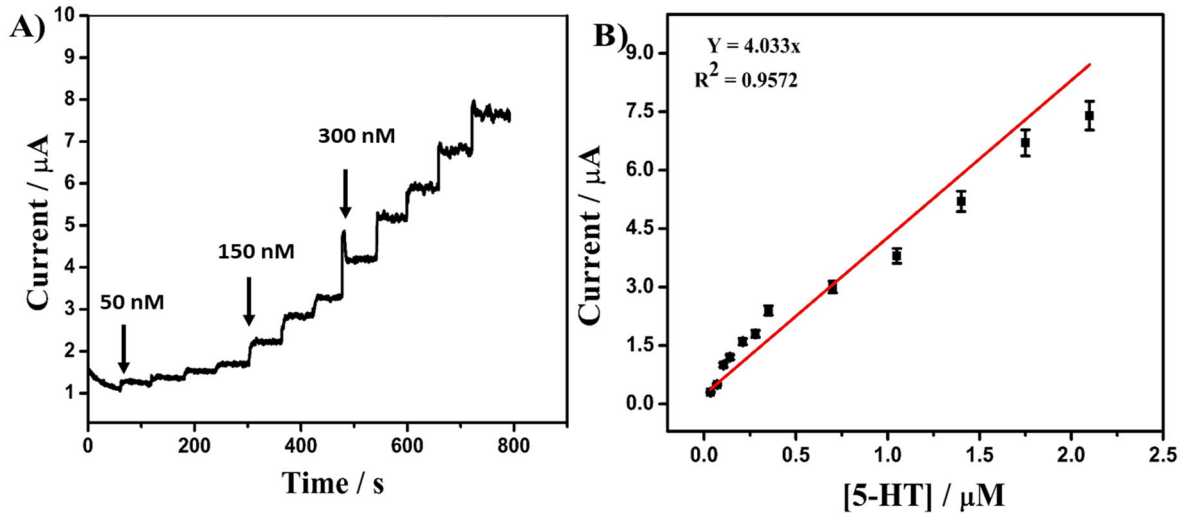

Fig. 5.7. *(A) Steady state current–time analysis at AuNPs/poly-AMT/f-CNT/GCE in PBS (pH 7.0) to the additions of 5-HT. Every addition increases 5-HT concentration at regular intervals of ~ 50 s. Eapp = +0.3 V. (B) Plot of the increase in anodic current vs. 5-HT concentration.*

Table 5.1. *Detection of 5-HT using electrochemical and various analytical methods.*

Electrode	Method	Linear range	Limit of detection	Reference
MCM-41-COOH/Au@nano-CILPE	SWV	0.2 – 20 μM	100 nM	[313]
Pt/MWCNT/PPy/AgNPs	DPV	0.50 - 5.0 μM	0.15 nM	[314]
DDF-CNT-TiO_2/IL/GC	DPV	1.0 – 650.0 μM	154 nM	[315]
GCE/MWCNT-NiO	SWV	5.98 - 62.8 μM	118 nM	[316]
GCE/MWCNT-ZnO	SWV		129 nM	
GCE/MWCNT-Fe_3O_4	SWV		166 nM	
PEDOT:PSS/TPyP– 3IP/FTO	CV	-	0.23 μM	[317]
NiO/CNT/PEDOT/GCE	DPV	0.3 – 35 μM	63 nM	[318]
RoMWCNT/GC	PDV	5 – 210 μM	460 nM	[319]
IL–DC–CNT/GC	DPV	5.0 – 900.0 μM	2 μM	[320]
Polymelamine/EPPGS	SWV	0.1 – 100 μM	30 nM	[321]
G-g-PLA-Pd/GCE	Amperometry	0.1–100.0 μM	80 nM	[322]
AuNPs/poly-AMT/ f-CNT/GCE	SWV	0.015 – 5 μM	7.8 nM	Present work

MCM-41-COOH/Au@nano-CILPE - MCM-41-COOH-carboxyl-functionalized mesoporous molecular sieve; DDF - 9-(1,3-dithiolan-2-yl)-6,7-dihydroxy-3,3-dimethyl-3,4- dihydrodibenzo[b,d]furan-1(2H)-one; TPyP– tetrakis(4-pyridyl)-21H,23H-porphyrin 3IP/FTO - bifunctional molecule, 3-iodopropionate Fluorine-doped tin oxide ; IL–DC–CNT – Ionic liquid 7-(1,3-dithiolan-2-yl)-9,10-dihydroxy-6H-benzofuro[3,2-c]chromen-6-one carbon nanotubes ; G-g-PLA - poly(lactic acid).

5.3.7. Interference studies

Electrochemical performance of 5-HT has been investigated in the presence of an important electroactive biological component dopamine (DA) at the fabricated AuNPs/p-AMT/*f*-CNT/GCE electrode by using SWV method. Figure 5.8 shows the SWVs resulted in the mixture of 4 mM DA and 5-HT at different concentrations of (2.0 – 8.0 µM) at modified electrode in PBS (pH 7.0). Oxidation peak of 5-HT did not change by the presence of DA in solution. Even at the high concentration 4000 µM DA in the solution, the oxidation peak current of 5-HT increased gradually with 5-HT concentration without any influence on the current response. From the above results, we could confirm that the suggested AuNPs/*p*-AMT/*f*-CNT/GCE sensor could be implemented for the determination of 5-HT even in the existence of various electroactive interferents along with 5-HT in solution.

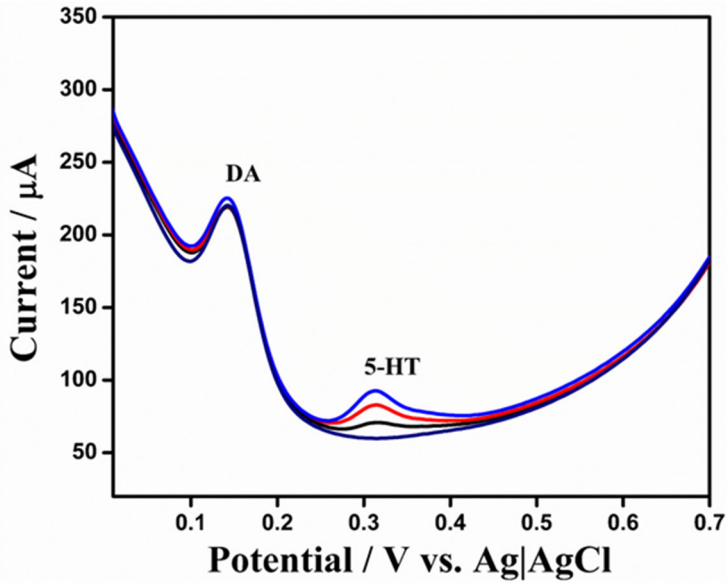

Fig. 5.8. *SWVs recorded at AuNPs/poly-AMT/f-CNT/GCE with 5-HT at different concentrations (0, 2.0, 5.0 and 8.0 µM) in the presence of DA 4.0 mM in PBS (pH 7.0).*

Table 5.2. Recovery limits for the detection of 5-HT in serum samples.

Sample	5-HT (× 10^{-6} M)	Found (× 10^{-6} M)	Average recovery (%)	RSD (%)
Serum	0.1	0.11	102.3	1.4
	0.5	0.51	101.0	0.8
	1.0	0.98	99.5	1.7

5.3.8. Real sample analysis

Finally, the fabricated electrochemical sensor has been studied in order to explore real-world utilisation. Serotonin recovery from human serum was examined by adding 5-HT into diluted human serum samples. Figure 5.9 shows the SWVs of AuNPs/p-AMT/*f*-CNT/GCE recorded in diluted serum sample in the presence of 0.1, 0.5, 1.0 and 2.0 µM 5-HT. The respective anodic peak to 5-HT oxidation appeared at +0.32 V, and the peak current increased with 5-HT concentration. The recovery of 5-HT form diluted serum at different concentrations of 5-HT varied from 99.5% to 102.3 % (Table 5.2) and is quite satisfactory. In the absence of 5-HT, a weak anodic peak observed at +0.24 V is characteristic to the uric acid present in real sample of human serum.

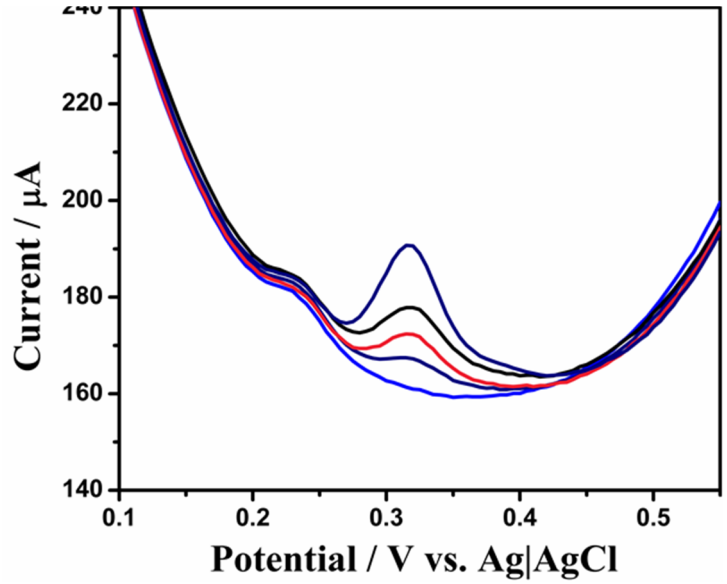

Fig. 5.9. *SWV analysis in diluted human serum (20 times) impregnated with 5-HT at various concentrations (0, 0.1, 0.5, 1.0 and 2.0 µM).*

5.3.9. Reproducibility and Reusability

Performance of the AuNPs/*p*-AMT/*f*CNT/GCE sensor in terms of stability, reproducibility and repeatability to determination of 5-HT was examined by SWV technique. SWVs of 1.0 μM 5-HT were analysed at a single AuNPs/*p*-AMT/*f*-CNT/GCE over a period of 10 days, and, the electrode was stored at ambient laboratory condition when not in use. Peak current of the recorded SWVs decreased merely 3.7% in about 30 measurements. This observations reveals that the excellent stability and reusability of the present sensor. Further, we examined the reproducibility of the fabricated electrode by using six independently fabricated AuNPs/*p*-AMT/*f*-CNT/GCE electrodes to multiple measurements of 5-HT. The peak current of the SWVs of 1.0 μM 5-HT analysed at these electrodes varied to the range of 2.6% only. It is clearly confirming that the modified electrode system is highly reproducible to 5-HT analysis. From the observations, we conclude that the reusability and reproducibility of the AuNPs incorporated polymer electrode are quite satisfactory.

5.4. Conclusions

In the present work, an electrodeposition of nanoAu crystals onto conducting polymer film deposited on CNT electrode has been explored for the quantitative determination of the important neurotransmitter agent, serotonin. The AuNPs/*p*-AMT film extraordinarily improved the current response and exhibited the oxidation peak of 5-HT at low overpotential region. In the electrode system, both polymerization of the polymer on CNT and as well as deposition of AuNPs on the polymer film have been responsible for the efficient electron-transfer across the surface and for very good electrocatalytic response. The present sensor was capable for determination of 5-HT in nanomolar levels even in the presence of highly electroactive interferents and with excellent recovery limits for direct determination of 5-HT from biological fluids with a very less analysis time of 20 s. The fabricated sensor showed good stability, high sensitivity towards 5-HT detection and simple fabrication method. With all these advantages, the present system fabricated with AuNPs, conducting polymer and CNT could be extended for detection of other important biomarkers and pharmaceutical drugs.

CHAPTER 6

Summary and Conclusions

6.1 **Summary**

The Introduction chapter was focussed on describing the concepts of chemical sensors starting from the principles, functioning, latest advances and the state-of-the-art. Various types of chemical sensors were discussed based upon their principles, and applications of chemical sensors towards the monitoring of target molecules have been discussed in detail. A brief discussion on CMEs and literature reports on different types of materials used in chemical modification of electrodes have been given. Various electrochemical strategies for the detection of diverse pharmaceutical drug molecules, anti-bacterial, anti-viral, anti-cancer, anti-depressant agents, etc. were critically reviewed. Necessity for the development of electrochemical sensors for the specific detection of trace levels of vital drug molecules was emphasized and the objectives of the present study were defined. Development of electrochemical sensors for selected drugs such as *Methotrexate, Valacyclovir, Nitrofurantoin* and *Serotonin* were defined as the objectives of the present study. Electrochemical techniques have been elucidated as efficient transduction methods towards the development of sensors for the above selected pharmaceutical drugs.

In *Chapter 2*, a simple and low-cost reusable electrochemical sensor has been fabricated for sensitive determination of the important chemotherapy agent Methotrexate (MTX). Electrochemical response of the developed acid functionalized carbon nanotube past electrode (*f*-CNTPE) was investigated towards the detection of MTX by using different electrochemical techniques, cyclic voltammetry (CV), differential pulse voltammetry (DPV), square wave voltammetry (SWV) and amperometry. The CNTPE electrode exhibited electrocatalytic activity towards MTX oxidation, and the overpotential is reduced by ~70 mV to +0.82 V. The electrocatalytic current is enhanced nearly three times of magnitude. With SWV technique, a parabolic calibration plot over the concentration range of 10 - 1500 nM MTX was achieved, and the biosensor could detect as low as 2.9 nM with SWV and 3.7 nM by steady-state amperometric analysis with an analysis time of ~10 s. The modified electrode exhibited very good selectivity towards the specific recognition of MTX. The electrochemical biosensor detected MTX *in-vitro* directly from spiked drug formulations, artificial urine and diluted serum samples as low as ≤ 1.0 µM with good recovery limits.

In Chapter 3, a fast and facile electrochemical sensor for the detection of an important anti-viral drug, valacyclovir (VAL), has been fabricated by electrodissolution-induced deposition of nanoAu particle on conducting polymer, poly-(3-amino-5-hydroxypyrazole) (*poly*-AHP) coated carbon paste electrode. The AuNPs/*poly*-AHP film was developed on carbon paste electrode (CPE) by adopting a simple potentiodynamic and potentiostatic polarization techniques. The fabricated *AuNPs/poly-AHP/CPE* electrode surface was characterized by electronic spectroscopy, XRD, SEM and EDX, and the diameter of AuNPs was ~35 nm by different methods. Electrochemical capability of *AuNPs/poly-AHP* modified CPE for valacyclovir detection was investigated by cyclic voltammetry, differential pulse voltammetry, chronoamperometry and electrochemical impedance analysis. The nanoAu decorated conducting polymer electrode was efficient for electrocatalysis of VAL. Peak current of the DPVs established a linear determination range of 5 – 80 nM VAL. Practical utility of the developed *AuNPs/poly-AHP/CPE* biosensor has been demonstrated for VAL detection from undiluted urine, pharmaceutical and human serum samples with good recovery limits.

In Chapter 4, a highly sensitive electrochemical sensor with a hybrid nanocomposite comprised of electrochemically reduced graphene oxide and CNT as sensor interface has been fabricated for nitrofurantoin. ErGO-CNT nanocomposite was characterized by XRD, scanning electron microscopy (SEM) for its chemical and structural information. The electrochemical response of the fabricated ErGO-CNT nanocomposite modified GCE towards NFT detection was investigated by CV, chronoamperometry and DPV. Nanothin flake-like structured nanosheets of ErGO with uniform deposition over porous CNT matrix was responsible for the enhanced catalytic electron transfer mediation towards the reduction of NFT. The amperometric i-t curve analysis was carried out for the determination of NFT under hydrodynamic conditions, and a limit of detection of 1.87 nM obtained with the linear determination range of 0.005 – 2.81 μM NFT. Practical applicability has been demonstrated for NFT determination in diluted serum with very good recovery limits.

In Chapter 5, an electrochemical sensor established by incorporating gold nanoparticles onto a conducting polymer layer on carbon nanotube matrices for serotonin (5-HT) detection. A thin film of a conducting polymer, poly-(2-amino-5-mercapto-1,3,4-thiadiazole) (*poly*-AMT), was formed on CNT/GCE by employing potentiodynamic polymerization technique. Further, AuNPs

was deposited by simple potentiostatic deposition from aq. $HAuCl_4$ on the surface of *poly*-AMT/*f*-CNT/GCE. The sensor surface has been characterized by SEM and EDX for structural and chemical properties of the electrode. Electrocatalytic activity of AuNPs/*poly*-AMT/*f*-CNT composite electrode for serotonin detection was examined by CV and SWV. A linear determination range of 0.015 – 24 μM 5-HT was demonstrated by SWV analysis with detection limit of 7.8 nM. Practical utility of AuNPs/*poly*-AMT/*f*-CNT biosensor from diluted serum has been demonstrated with very good recovery limits.

In the development of electrochemical sensors of the selected drug molecules, the plausible electrodic reaction mechanism involved in the determination of the drug molecules were discussed. Performance of the electrochemical sensors fabricated successfully in the present study for the selected pharmaceutical drugs have been compiled and presented in Table 6.1 together with the details of low-detection-limit, linear concentration range of detection and real sample analyses.

6.2 Conclusions

In this research work, a number of electrochemical sensors have been fabricated with the use of different carbon nanotube based hybrid nanocomposite modified electrodes, and quite excellent low-detection-limits were established. Further, a variety of materials such as gold nanoparticles, conducting polymers, syntheses and deposition of graphenes by chemical and electrochemical methods, graphitic carbon, carbon nanotubes and biopolymers were investigated effectively in developing the electrochemical biosensors. Pharmaceutical drugs of different molecular weights, different functional groups, different molecular structures and of very wide application fields have been chosen and analysed in this study.

Table 6.1: *Summary of the developed electrochemical sensors for selected drugs and their respective performances.*

Analyte	Sensor Platform	LOD (nM)			Linear Range (µM)	Real Sample Analysis
		SWV	DPV	Amp		
MTX	*f*-CNTPE	2.9	--	3.7	0.01 – 1.5	Artificial Urine, Pharmaceutical Tablet, Blood serum
NFT	ErGO-CNT/GCE	--	13.7	1.87	0.005 – 2.81	Serum
VAL	AuNPs/poly-AHP/CPE	--	1.89	2.5	0.005 – 0.08	Artificial Urine, Pharmaceutical Injection, Blood serum
5-HT	AuNPs/poly-AMT/ f-CNT/GCE	7.8	--	18	0.015 – 5.0	Serum

All the fabricated electrochemical sensor systems have shown low-detection-limits as low as nanomolar concentration levels and the analysis time periods are less than 10 s. With the use of a combination of conducting polymer and nanoAu particles, the low-detection-limit achieved in the present study have shown variation depending on the nature of the conducting polymer. A right choice of the combinations of conducting polymer seems essential in achieving very good low-detection-limits. The developed sensor systems clearly established that low-detection-limits of nanomolar concentrations and analytical time periods of less than few seconds could be effectively achieved with various kinds of pharmaceutical drugs of small molecules. All these results clearly established the versatility, efficiency and applicability of the electrochemical sensors based on various hybrid nanocomposite based CMEs for detection of selected pharmaceutical drugs and further provided confidence for efforts in future to develop electrochemical sensors for the analysis and sensitive detections of diverse target groups such as biomarkers, environmental pollutants and food toxins by employing highly catalytic nanostructured materials based CMEs.

References

[1] R. Sabourian, S. Z. Mirjalili, N. Namini, F. Chavoshy, M. Hajimahmoodi, M. Safavi, *Analytical Biochemistry* **2020**, *610*, 113891.

[2] I. Klimczak, A. Gliszczynska-Świglo, *Food Chemistry* **2015**, *175*, 100.

[3] J. Ma, Z. Yao, L. Hou, W. Lu, Q. Yang, J. Li, L. Chen, *Talanta* **2016**, *161*, 686.

[4] B. Yilmaz, U. Ciltas, *Journal of Pharmaceutical Analysis* **2015**, *5*, 153.

[5] J. Chang, X. Wang, J. Wang, H. Li, F. Li, *Analytical Chemistry* **2019**, *91*, 3604.

[6] S. Cinti, M. Basso, D. Moscone, F. Arduini, *Analytica Chimica Acta* **2017**, *960*, 123.

[7] L. Tian, K. Qian, J. Qi, Q. Liu, C. Yao, W. Song, Y. Wang, *Biosensors and Bioelectronics* **2018**, *99*, 564.

[8] S. Eissa, M. Siaj, M. Zourob, *Biosensors and Bioelectronics* **2015**, *69*, 148.

[9] M. Z. H. Khan, M. R. Hasan, S. I. Hossain, M. S. Ahommed, M. Daizy, *Biosensors and Bioelectronics* **2020**, *166*, 112431.

[10] M. Alafeef, K. Dighe, P. Moitra, D. Pan, *ACS Nano* **2020**, *14,* 17028.

[11] Y. Zhou, Y. Fang, R. Ramasamy, *Sensors* **2019**, *19*, 392.

[12] Y. Zhao, Q. Zhai, D. Dong, T. An, S. Gong, Q. Shi, W. Cheng, *Analytical Chemistry* **2019**, *91*, 6569.

[13] J. Shi, C. Chan, Y. Pang, W. Ye, F. Tian, J. Lyu, Y. Zhang, M. Yang, *Biosensors and Bioelectronics* **2015**, *67*, 595.

[14] Y. Jeong, Y.-M. Kook, K. Lee, W.-G. Koh, *Biosensors and Bioelectronics* **2018**, *111*, 102.

[15] J. C. Pickup, F. Hussain, N. D. Evans, O. J. Rolinski, D. J. S. Birch, *Biosensors and Bioelectronics* **2005**, *20*, 2555.

[16] C. Li, G. Shi, *Journal of Photochemistry and Photobiology C: Photochemistry Reviews* **2014**, *19*, 20.

[17] M. Stanisavljevic, S. Krizkova, M. Vaculovicova, R. Kizek, V. Adam, *Biosensors and Bioelectronics* **2015**, *74*, 562.

[18] O. S. Wolfbeis, *Journal of Materials Chemistry* **2005**, *15*, 2657.

[19] W. Peng, Y. Qin, W. Li, M. Chen, D. Zhou, H. Li, J. Cui, J. Chang, S. Xie, X. Gong, B. Tang, *ACS Sensors* **2020**, *5*, 1912.

[20] C.-H. Huang, Y. Il Park, H.-Y. Lin, D. Pathania, K. S. Park, M. Avila-Wallace, C. M. Castro, R. Weissleder, H. Lee, *ACS Nano* **2019**, *13*, 11698.

[21] K. Lukyanenko, I. Denisov, V. Sorokin, A. Yakimov, E. Esimbekova, P. Belobrov, *Chemosensors* **2019**, *7*, 16.

[22] Y. Chen, C. Huang, B. Hellmann, Z. Jin, X. Xu, G. Xiao, *Food Chemistry* **2020**, *309*, 125691.

[23] J. Zhou, S. Chen, F. Sun, P. Luo, Q. Du, S. Zhao, *Journal of Chromatography B* **2015**, *1006*, 65.

[24] A. R. A. Rahman, S. Foo, S. Goel, *Procedia Chemistry* **2009**, *1*, 1091.

[25] M. Li, S. K. Cushing, N. Wu, *The Analyst* **2015**, *140*, 386.

[26] S. Kim, T. G. Kim, S. H. Lee, W. Kim, A. Bang, S. W. Moon, J. Song, J.-H. Shin, J. S. Yu, S. Choi, *ACS Applied Materials & Interfaces* **2020**, *12*, 7897.

[27] Y. Wu, Y. He, X. Yang, R. Yuan, Y. Chai, *Sensors and Actuators B: Chemical* **2018**, *275*, 260.

[28] J. Ju, C.-M. Hsieh, Y. Tian, J. Kang, R. Chia, H. Chang, Y. Bai, C. Xu, X. Wang, Q. Liu, *ACS Sensors* **2020**, *5*, 1777.

[29] M. D. Porter, R. J. Lipert, L. M. Siperko, G. Wang, R. Narayanan, *Chemical Society Reviews* **2008**, *37*, 1001.

[30] L. Guerrini, D. Graham, *Chemical Society Reviews* **2012**, *41*, 7085.

[31] J. Kneipp, H. Kneipp, K. Kneipp, *Chemical Society Reviews* **2008**, *37*, 1052.

[32] L. Tang, W. Chen, B. Chen, R. Lv, X. Zheng, C. Rong, B. Lu, B. Huang, *Sensors and Actuators B: Chemical* **2021**, *327*, 128944.

[33] Q. Chen, N. Feng, X. Huang, Y. Yao, Y. Jin, W. Pan, D. Liu, *ACS Omega* **2020**, *5*, 18818.

[34] X. Zheng, R. Fan, C. Li, X. Yang, H. Li, J. Lin, X. Zhou, R. Lv, *Sensors and Actuators B: Chemical* **2019**, *283*, 659.

[35] M. A. Cooper, V. T. Singleton, *Journal of Molecular Recognition* **2007**, *20*, 154.

[36] J. Tamayo, P. M. Kosaka, J. J. Ruz, Á. San Paulo, M. Calleja, *Chem. Soc. Rev.* **2013**, *42*, 1287.

[37] S. Sun, Y. Wei, H. Wang, Y. Cao, B. Deng, *Talanta* **2018**, *179*, 213.

[38] A. Bossi, S. A. Piletsky, P. G. Righetti, A. P. F. Turner, *Journal of Chromatography A* **2000**, *892*, 143.

[39] M. Shanmuganathan, P. Britz-McKibbin, *Analytica Chimica Acta* **2013**, *773*, 24.

[40] K. M. Mayer, J. H. Hafner, *Chemical Reviews* **2011**, *111*, 3828.

[41] E. L. Gool, I. Stojanovic, R. B. M. Schasfoort, A. Sturk, T. G. van Leeuwen, R. Nieuwland, L. W. M. M. Terstappen, F. A. W. Coumans, *Clinical Chemistry* **2017**, *63*, 1633.

[42] M. Lutfiyah, W. Aji Eko Prabowo, A. Melati, *Journal of Physics: Conference Series* **2020**, *1445*, 012005.

[43] C. M. Das, Q. Ouyang, X.-Q. Dinh, P. Coquet, K.-T. Yong, *Optics Communications* **2020**, *458*, 124748.

[44] W. O. Nyang'au, A. Setiono, M. Bertke, H. Bosse, E. Peiner, *Sensors* **2019**, *19*, 4758.

[45] M. SoltanRezaee, M. Bodaghi, *Scientific Reports* **2020**, *10*, 1.

[46] C. Li, X. Ma, Y. Guan, J. Tang, B. Zhang, *ACS Sensors* **2019**, *4*, 3034.

[47] V. Perumal, U. Hashim, *Journal of Applied Biomedicine* **2014**, *12*, 1.

[48] Z. Wang, M. Kimura, T. Ono, *Thermochimica Acta* **2018**, *668*, 110.

[49] B. Xie, B. Danielsson, In *Handbook of Biosensors and Biochips*; John Wiley & Sons, Ltd: Chichester, UK, 2008.

[50] I. Satoh, Y. Iijima, *Sensors and Actuators B: Chemical* **1995**, *24*, 103.

[51] Y. Yao, X. Chen, H. Guo, Z. Wu, *Applied Surface Science* **2011**, *17*, 7778.

[52] J. Xi, J. Y. Chen, *Journal of Biochips & Tissue Chips* **2013**. *S5*, 1.

[53] W.-Y. Tsai, P.-L. Taberna, P. Simon, *Journal of the American Chemical Society* **2014**, *136*, 8722.

[54] A. Alassi, M. Benammar, D. Brett, Quartz crystal microbalance electronic interfacing systems: A review. *Sensors (Switzerland)* **2017**, *17,* 1.

[55] S. J. Patil, N. Duragkar, V. R. Rao, *Sensors and Actuators, B: Chemical* **2014**, *192,* 444.

[56] D. Bhatia, H. Sharma, R. S. Meena, V. R. Palkar, *Sensing and Bio-Sensing Research* **2016**, *9*, 45.

[57] K. R. Buchapudi, X. Huang, X. Yang, H. F. Ji, T. Thundat, *Analyst* **2011**, *136,* 1539.

[58] S. Abdellaoui, M. Bekhouche, A. Noiriel, R. Henkens, C. Bonaventura, L. J. Blum, B. Doumèche, *Chemical Communications* **2013**, *49*, 5781.

[59] B. D. Leca-Bouvier, A. Sassolas, L. J. Blum, *Analytical and Bioanalytical Chemistry* **2014**, *406*, 5657.

[60] S. Jesny, S. Menon, K. Girish Kumar, *RSC Advances* **2016**, *6*, 75741.

[61] D. Talarico, F. Arduini, A. Amine, I. Cacciotti, D. Moscone, G. Palleschi, *Analytical and Bioanalytical Chemistry* **2016**, *408*, 7299.

[62] P. Kalimuthu, S. A. John, *Talanta* **2010**, *80*, 1686.

[63] S. Nagarajan, R. Vairamuthu, R. Angamuthu, G. Venkatachalam, *Journal of Electroanalytical Chemistry* **2019**, *846*, 113156.

[64] R. Sivasubramanian, M. V. Sangaranarayanan, *Sensors and Actuators B: Chemical* **2015**, *213*, 92.

[65] S. Abdellaoui, A. Noiriel, R. Henkens, C. Bonaventura, L. J. Blum, B. Doumèche, *Analytical Chemistry* **2013**, *85*, 3690.

[66] J. A. V. Albelda, A. Uzunoglu, G. N. C. Santos, L. A. Stanciu, *Biosensors and Bioelectronics* **2017**, *89*, 518.

[67] R. S. Dey, C. R. Raj, *ACS Applied Materials & Interfaces* **2013**, *5*, 4791.

[68] B. Manna, C. Retna Raj, *Journal of Materials Chemistry B* **2016**, *4*, 4585.

[69] N. S. K. Gowthaman, M. A. Raj, S. A. John, *ACS Sustainable Chemistry & Engineering* **2017**, *5*, 1648.

[70] S.-A. Jin, S. Poudyal, E. E. Marinero, R. J. Kuhn, L. A. Stanciu, *Electrochimica Acta* **2016**, *194*, 422.

[71] K. Toko, *Measurement Science and Technology* **1998**, *9*, 1919.

[72] Q. Zhai, L. W. Yap, R. Wang, S. Gong, Z. Guo, Y. Liu, Q. Lyu, J. Wang, G. P. Simon, W. Cheng, *Analytical Chemistry* **2020**, *92*, 4647.

[73] J. Bobacka, *Electroanalysis* **2006**, *18*, 7.

[74] E. Lindner, B. D. Pendley, *Analytica Chimica Acta* **2013**, *762*, 1.

[75] S. M. Usman Ali, O. Nur, M. Willander, B. Danielsson, *Sensors and Actuators B: Chemical* **2010**, *145*, 869.

[76] L. Torsi, M. Magliulo, K. Manoli, G. Palazzo, *Chemical Society Reviews* **2013**, *42*, 8612.

[77] H. Li, W. Shi, J. Song, H.-J. Jang, J. Dailey, J. Yu, H. E. Katz, *Chemical Reviews* **2019**, *119*, 3.

[78] A. M. Bond, R. G. Compton, D. A. Fiedler, G. Inzelt, H. Kahlert, H. Lohse, M. Lovric, S. K. Lovric, F. Marken, A. Neudeck, U. Retter, F. Scholz, Z. Stojek, *Electroanalytical Methods Guide to Experiments and Applications 2nd, revised and extended edition*; 2009, 1.

[79] F. Scholz, *Fresenius J Anal Chem* (**1990**), 136, 138.

[80] D. C. Grahame, *Chemical Reviews* **1947**, *41*, 441.

[81] D. D. Macdonald, *Electrochimica Acta* **2006**, *51*, 1376.

[82] C. R. Lowe, In *Handbook of Biosensors and Biochips*; John Wiley & Sons, Ltd: Chichester, UK, 2008.

[83] C. Lyons, *Annals New York Academy of Sciences* **1962**, *102,* 29.

[84] S. Arisawa, T. Arise, R. Yamamoto, **1992**, *209*, 259.

[85] P. Preparations, *Journal compilation* C **2005**, *364,* 99.

[86] M. Diaconu, S. C. Litescu, G. L. Radu, *Microchimica Acta* **2011**, *172*, 177.

[87] D. W. G. Morrison, M. R. Dokmeci, U. Demirci, **2008**.

[88] Z. Yang, C. Zhang, J. Zhang, W. Bai, *Biosensors and Bioelectronics* **2014**, *51,* 268.

[89] P. Das, M. Das, S. R. Chinnadayyala, I. M. Singha, P. Goswami, *Biosensors and Bioelectronics* **2016**, *79*, 386.

[90] R. B. Rakhi, P. Nayak, C. Xia, H. N. Alshareef, *Scientific Reports* **2016**, *6*, 36422.

[91] H. H. Nguyen, S. H. Lee, U. J. Lee, C. D. Fermin, M. Kim, *Materials* **2019**, *12*, 121.

[92] W. Wen, X. Yan, C. Zhu, D. Du, Y. Lin, *Analytica Chemistry* **2017,** *89,* 138.

[93] S. Akbari Nakhjavani, B. Khalilzadeh, P. Samadi Pakchin, R. Saber, M. H. Ghahremani, Y. Omidi, *Biosensors and Bioelectronics* **2018**, *122,* 8.

[94] R. Khan, M. Pal, A. V. Kuzikov, T. Bulko, E. V. Suprun, V. V. Shumyantseva, *Materials Science and Engineering: C* **2016**, *68*, 52.

[95] P. A. B. Ferreira, M. C. M. Araujo, C. M. Prado, R. A. de Lima, B. A. G. Rodríguez, R. F. Dutra, *Colloids and Surfaces B: Biointerfaces* **2020**, *189*, 110834.

[96] D. Tang, J. Tang, B. Su, J. Ren, G. Chen, *Biosensors and Bioelectronics* **2010**, *25,* 1658.

[97] P. B. Luppa, L. J. Sokoll, D. W. Chan, *Clinica chimica acta* **2001,** *314,* 1.

[98] G. Şenocak, In *Climate Change 2013 - The Physical Science Basis*; Intergovernmental

Panel on Climate Change, Ed.; Cambridge University Press: Cambridge, 2019; pp. 1–30.

[99] Y. Zhu, P. Chandra, K. M. Song, C. Ban, Y. B. Shim, *Biosensors and Bioelectronics* **2012**, *36,* 29.

[100] S. Li, C. Li, Y. Wang, H. Li, F. Xia, *Analytical Chemistry* **2020**, *92,* 13427.

[101] W. Kim, J. S. Lee, J. Jang, *ACS Applied Materials & Interfaces* **2020**, *12*, 20882.

[102] C. Alexander, H. S. Andersson, L. I. Andersson, R. J. Ansell, N. Kirsch, I. A. Nicholls, J. O'Mahony, M. J. Whitcombe, *Journal of Molecular Recognition* **2006**, *19*, 106.

[103] J. J. BelBruno, *Chemical Reviews* **2019**, *119*, 94.

[104] M. A. Beluomini, J. L. da Silva, A. C. de Sá, E. Buffon, T. C. Pereira, N. R. Stradiotto, *Journal of Electroanalytical Chemistry* **2019**, *840*, 343.

[105] B. Hatamluyi, A. Hashemzadeh, M. Darroudi, *Sensors and Actuators B: Chemical* **2020**, *307*, 127614.

[106] Y. Cao, T. Feng, J. Xu, C. Xue, *Biosensors and Bioelectronics* **2019**, *141*, 111447.

[107] L. Torrance, A. Ziegler, H. Pittman, M. Paterson, R. Toth, I. Eggleston, *Journal of Virological Methods* **2006**, *134*, 164.

[108] M. Fahie, C. Chisholm, M. Chen, *ACS Nano* **2015,** *9*, 1089.

[109] Rajesh, Z. Gao, R. Vishnubhotla, P. Ducos, M. D. Serrano, J. Ping, M. K. Robinson, A. T. C. Johnson, *Advanced Materials Interfaces* **2016**, *3*, 1600124.

[110] S. Iijima, *Nature* **1991**, *354*, 56.

[111] W. Yu, L. Sisi, Y. Haiyan, L. Jie, *RSC Advances* **2020**, *10*, 15328.

[112] A. Ambrosi, C. K. Chua, A. Bonanni, M. Pumera, *Chemical Reviews* **2014**, *114*, 7150.

[113] H. Y. Mao, S. Laurent, W. Chen, O. Akhavan, M. Imani, A. A. Ashkarran, M. Mahmoudi, *Chemical Reviews* **2013**, *113*, 3407.

[114] D. A. C. Brownson, D. K. Kampouris, C. E. Banks, *Chemical Society Reviews* **2012**, *41*, 6944.

[115] M. Pumera, *Chemical Society Reviews* **2010**, *39*, 4146.

[116] Y. Liu, X. Dong, P. Chen, *Chem. Soc. Rev.* **2012**, *41*, 2283.

[117] S. Guo, S. Dong, *Chemical Society Reviews* **2011**, *40*, 2644.

[118] V. Georgakilas, M. Otyepka, A. B. Bourlinos, V. Chandra, N. Kim, K. C. Kemp, P. Hobza, R. Zboril, K. S. Kim, *Chemical Reviews* **2012**, *112*, 6156.

[119] D. Chen, H. Feng, J. Li, *Chemical Reviews* **2012**, *112*, 6027.

[120] H. Naarmann, In *Ullmann's Encyclopedia of Industrial Chemistry*; Wiley-VCH Verlag GmbH & Co. KGaA: Weinheim, Germany, 2000; Vol. 29, pp. 6.5-621.

[121] A. Malinauskas, *Synthetic Metals* **1999**, *107*, 75.

[122] J. Heinze, B. A. Frontana-Uribe, S. Ludwigs, *Chemical Reviews* **2010**, *110*, 4724.

[123] N. Gupta, S. Sharma, I. A. Mir, D. Kumar, *Journal of Scientific and Industrial Research* **2006**, *65*, 549.

[124] L. Zhang, L. Wang, *Journal of Solid State Electrochemistry* **2013**, *17*, 691.

[125] S. Guo, E. Wang, *Nano Today* **2011**, *6*, 240.

[126] L. Rassaei, F. Marken, M. Sillanpää, M. Amiri, C. M. Cirtiu, M. Sillanpää, *TrAC Trends in Analytical Chemistry* **2011**, *30*, 1704.

[127] F. Wang, S. Hu, *Microchimica Acta* **2009**, *165*, 1.

[128] P. Mäki-Arvela, D. Y. Murzin, *Applied Catalysis A: General* **2013**, *451*, 251.

[129] A. Kolmakov, M. Moskovits, *Annual Review of Materials Research* **2004**, *34*, 151.

[130] T.-F. Kang, F. Wang, L.-P. Lu, Y. Zhang, T.-S. Liu, *Sensors and Actuators B: Chemical* **2010**, *145*, 104.

[131] P. Raveendran, J. Fu, S. L. Wallen, *Journal of the American Chemical Society* **2003**, *125*, 13940.

[132] T. Wang, J.-S. Hu, W. Yang, H.-M. Zhang, *Electrochemistry Communications* **2008**, *10*, 814.

[133] B. C. Sih, M. O. Wolf, *Chemical Communications* **2005**, 3375.

[134] M. K. Corbierre, R. B. Lennox, *Chemistry of Materials* **2005**, *17*, 5691.

[135] S. Bhat, U. Maitra, *Journal of Chemical Sciences* **2008**, *120*, 507.

[136] P. Rameshkumar, R. Ramaraj, *Journal of Applied Electrochemistry* **2013**, *43*, 1005.

[137] K.-J. Huang, D.-J. Niu, X. Liu, Z.-W. Wu, Y. Fan, Y.-F. Chang, Y.-Y. Wu, *Electrochimica Acta* **2011**, *56*, 2947.

[138] H. Hosseini, H. Ahmar, A. Dehghani, A. Bagheri, A. R. Fakhari, M. M. Amini,

Electrochimica Acta **2013**, *88*, 301.

[139] V. K. Gupta, M. L. Yola, M. S. Qureshi, A. O. Solak, N. Atar, Z. Üstündağ, *Sensors and Actuators B: Chemical* **2013**, *188*, 1201.

[140] S. Hu, Y. Wang, X. Wang, L. Xu, J. Xiang, W. Sun, *Sensors and Actuators B: Chemical* **2012**, *168*, 27.

[141] N. Karimian, M. B. Gholivand, G. Malekzadeh, *Journal of Electroanalytical Chemistry* **2016**, *771*, 64.

[142] M. Dehghani, N. Nasirizadeh, M. E. Yazdanshenas, *Materials Science and Engineering: C* **2019**, *96*, 654.

[143] P. Sagar, M. Srivastava, R. Prakash, S. K. Srivastava, *Analytical Methods* **2020**, *12*, 3014.

[144] M. Abrishamkar, S. E. Tilami, S. H. Kaldozakh, A. Branch, K. Science, **2020**, *3*, 767.

[145] G. Muthusankar, R. K. Devi, G. Gopu, *Biosensors and Bioelectronics* **2020**, *150*, 111947.

[146] D. Dechtrirat, P. Yingyuad, P. Prajongtat, L. Chuenchom, C. Sriprachuabwong, A. Tuantranont, I.-M. Tang, *Microchimica Acta* **2018**, *185*, 261.

[147] B. He, J. Li, *Analytical Methods* **2019**, *11*, 1427.

[148] J. N. Baby, B. Sriram, S.-F. Wang, M. George, *ACS Sustainable Chemistry & Engineering* **2020**, *8*, 1479.

[149] T. Kokulnathan, S.-M. Chen, *Journal of Hazardous Materials* **2020**, *384*, 121304.

[150] T. Kokulnathan, T.-J. Wang, *Composites Part B: Engineering* **2019**, *174*, 106914.

[151] B. Karuppaiah, R. Ramachandran, S. M. Chen, S. Wan-Ling, J. Y. Wan, *New Journal of Chemistry* **2020**, *44,* 46.

[152] M. Annalakshmi, S. Sumithra, S. M. Chen, T. W. Chen, X. H. Zheng, *New Journal of Chemistry* **2020**, *44,* 10604.

[153] A. Todakar, N. P. Shetti, U. S. Devarushi, S. M. Tuwar, *Materials Today: Proceedings* **2019**, *18*, 550.

[154] U. S. Devarushi, N. P. Shetti, S. D. Bukkitgar, S. M. Tuwar, *Russian Journal of Electrochemistry* **2018**, *54,* 869.

[155] B. R. Adhikari, M. Govindhan, A. Chen, *Sensors (Switzerland)* **2015**, *15*, 22490.

[156] R. Jain, P. Pandey, *Ionics* **2015**, *21*, 3279.

[157] G. A. Saleh, H. F. Askal, I. H. Refaat, A. H. Naggar, F. A. M. Abdel-aal, *Arabian Journal*

of Chemistry **2016**, *9*, 143.

[158] B. R. Adhikari, M. Govindhan, H. Schraft, A. Chen, *Journal of Electroanalytical Chemistry* **2016**, *780,* 241.

[159] P. S. Dorraji, F. Jalali, *Materials Science and Engineering: C* **2016**, *61*, 858.

[160] N. P. Shetti, D. S. Nayak, S. J. Malode, R. M. Kulkarni, *Sensing and Bio-Sensing Research* **2017**, *14*, 39.

[161] P. Tarlekar, A. Khan, S. Chatterjee, *Journal of Pharmaceutical and Biomedical Analysis* **2018**, *151*, 1.

[162] M. Hamtak, L. Fotouhi, M. Hosseini, P. S. Dorraji, *Journal of The Electrochemical Society* **2018**, *165*, B632.

[163] N. P. Shetti, S. J. Malode, D. S. Nayak, R. R. Naik, G. T. Kuchinad, K. R. Reddy, S. S. Shukla, T. M. Aminabhavi, *Microchemical Journal* **2020**, *155,* 104727.

[164] N. F. Atta, A. Galal, Y. M. Ahmed, *Journal of Electroanalytical Chemistry* **2019**, *838*, 107.

[165] P. Ranganathan, B. Mutharani, S. M. Chen, P. Sireesha, *Journal of Physical Chemistry C* **2019**, *123,* 12211.

[166] S. D. Bukkitgar, N. P. Shetti, *Materials Science and Engineering: C* **2016**, *65*, 262.

[167] F. M. Zahed, B. Hatamluyi, F. Lorestani, Z. Es'haghi, *Journal of Pharmaceutical and Biomedical Analysis* **2018**, *161,* 12.

[168] D. Lima, G. N. Calaça, A. G. Viana, C. A. Pessôa, *Applied Surface Science* **2018**, *427,* 742.

[169] B. Mutharani, P. Ranganathan, S. M. Chen, *Sensors and Actuators, B: Chemical* **2020**, *304,* 127361.

[170] B. Hatamluyi, Z. Es'haghi, F. Modarres Zahed, M. Darroudi, *Sensors and Actuators, B: Chemical* **2019**, *286,* 540.

[171] V. P. Pattar, S. T. Nandibewoor, *RSC Advances* **2015**, *5,* 34292.

[172] M. Fouladgar, *Journal of The Electrochemical Society* **2018**, *154,* 104654.

[173] M. Rahimi-Nasrabadi, F. Ahmadi, H. Beigizadeh, M. S. Karimi, A. Sobhani-Nasab, Y. Joseph, H. Ehrlich, M. R. Ganjali, *Microchemical Journal* **2020**, *154,* 104654.

[174] A. A. Ensafi, F. Rezaloo, B. Rezaei, *Journal of the Taiwan Institute of Chemical Engineers* **2017**, *78,* 45.

[175] R. Šelešovská, L. Janíková-Bandžuchová, J. Chýlková, *Electroanalysis* **2015**, *27*, 42.

[176] J. Chen, B. Fu, T. Liu, Z. Yan, K. Li, *Electroanalysis* **2018**, *29,* 1.

[177] Y. Wei, L. Luo, Y. Ding, X. Si, Y. Ning, *Bioelectrochemistry* **2014**, *98*, 70.

[178] N. Jandaghi, S. Jahani, M. Kazemipour, M. M. Foroughi, A. F. A. abad, K. Mohammadi, F. Borhani, *Synthetic Metals* **2019**.

[179] T. W. Chen, U. Rajaji, S. M. Chen, B. S. Lou, N. Al-Zaqri, A. Alsalme, F. A. Alharthi, S. Y. Lee, W. H. Chang, *Ultrasonics Sonochemistry* **2019**, *58,* 104664.

[180] H. Zhou, G. Ran, J.-F. Masson, C. Wang, Y. Zhao, Q. Song, *Biosensors and Bioelectronics* **2018**, *105*, 226.

[181] N. Jandaghi, S. Jahani, M. M. Foroughi, M. Kazemipour, M. Ansari, *Microchimica Acta* **2020**, *187,* 24.

[182] Z. Deng, H. Li, Q. Tian, Y. Zhou, X. Yang, Y. Yu, B. Jiang, Y. Xu, T. Zhou, *Microchemical Journal* **2020**, *157*, 105058.

[183] M. Colleoni, A. Rocca, M. T. Sandri, L. Zorzino, G. Masci, F. Nolè, G. Peruzzotti, C. Robertson, L. Orlando, S. Cinieri, F. de Braud, G. Viale, A. Goldhirsch, *Annals of Oncology* **2002**, *13*, 73.

[184] C. J. Poole, H. M. Earl, L. Hiller, J. A. Dunn, S. Bathers, R. J. Grieve, D. A. Spooner, R. K. Agrawal, I. N. Fernando, A. M. Brunt, S. M. O'Reilly, S. M. Crawford, D. W. Rea, P. Simmonds, J. L. Mansi, A. Stanley, P. Harvey, K. McAdam, L. Foster, R. C. F. Leonard, C. J. Twelves, *New England Journal of Medicine* **2006**, *355*, 1851.

[185] M. Kuroda, T. Kotake, H. Akaza, S. Hinotsu, T. Kakizoe, *Japanese Journal of Clinical Oncology* **1998**, *28*, 497.

[186] H. L. Bleich, E. S. Boro, E. Frei, N. Jaffe, M. H. N. Tattersall, S. Pitman, L. Parker, *New England Journal of Medicine* **1975**, *292*, 846.

[187] J. E. Gach, R. A. Sabroe, M. W. Greaves, A. Kobza Black, *British Journal of Dermatology* **2001**, *145*, 340.

[188] A. U. Buzdar, C. Marcus, G. R. Blumenschein, T. L. Smith, *Cancer* **1985**, *55*, 2761.

[189] H. Aboleneen, J. Simpson, D. Backes, *Journal of Chromatography B: Biomedical Sciences and Applications* **1996**, *681*, 317.

[190] X. Liu, J. Liu, Y. Huang, R. Zhao, G. Liu, Y. Chen, *Journal of Chromatography A* **2009**, *1216*, 7533.

[191] I. A. Bernstein, S. G. Chakrabarti, **1969**, *15,* 1157.

[192] S. Chen, Z. Zhang, D. He, Y. Hu, H. Zheng, C. He, *Luminescence* **2007**, *22*, 338.

[193] J. Rodríguez Flores, G. C. Peñalvo, A. E. Mansilla, M. J. R. Gómez, *Journal of Chromatography B* **2005**, *819*, 141.

[194] H.-L. Cheng, S.-S. Chiou, Y.-M. Liao, C.-Y. Lu, Y.-L. Chen, S.-M. Wu, *Analytical and Bioanalytical Chemistry* **2010**, *398*, 2183.

[195] K. Fotoohi, T. Skärby, S. Söderhäll, C. Peterson, F. Albertioni, *Journal of Chromatography B* **2005**, *817*, 139.

[196] L. van Haandel, J. F. Stobaugh, *Analytical and Bioanalytical Chemistry* **2010**, *397*, 1841.

[197] S. Chen, Z. Zhang, *Spectrochimica Acta Part A: Molecular and Biomolecular Spectroscopy* **2008**, *70*, 36.

[198] S. Fang, C. P. Lollo, C. Derunes, M. J. LaBarre, *Journal of Chromatography B* **2011**, *879*, 3612.

[199] M. B. Gholivand, F. Ahmadi, A. Sohrabi, *Electroanalysis* **2007**, *19*, 2465.

[200] L. Hosseinzadeh, S. Abassi, F. Ahmadi, *Analytical Letters* **2007**, *40*, 2693.

[201] F. Wang, Y. Wu, J. Liu, B. Ye, *Electrochimica Acta* **2009**, *54*, 1408.

[202] Y. Guo, Y. Chen, Q. Zhao, S. Shuang, C. Dong, *Electroanalysis* **2011**, *23*, 2400.

[203] L. Gao, Y. Wu, J. Liu, B. Ye, *Journal of Electroanalytical Chemistry* **2007**, *610*, 131.

[204] R. Xing, H. Yang, S. Li, J. Yang, X. Zhao, Q. Wang, S. Liu, X. Liu, *Journal of Solid State Electrochemistry* **2017**, *21*, 1219.

[205] K. Y. Goud, A. Hayat, G. Catanante, M. Satyanarayana, K. V. Gobi, J. Louis, *Electrochimca Acta,* **2017**, *244*, 96.

[206] J. Amani, M. Maleki, A. Khoshroo, A. Sobhani-Nasab, M. Rahimi-Nasrabadi, *Analytical Biochemistry* **2018**, *548*, 53.

[207] J. Amani, A. Khoshroo, M. Rahimi-Nasrabadi, *Microchimica Acta* **2018**, *185*, 79.

[208] R. Xing, L. Tong, X. Zhao, H. Liu, P. Ma, J. Zhao, X. Liu, S. Liu, *Sensors and Actuators B: Chemical* **2019**, *283*, 35.

[209] A. Khoshroo, L. Hosseinzadeh, A. Sobhani-Nasab, M. Rahimi-Nasrabadi, H. Ehrlich, *Journal of Electroanalytical Chemistry* **2018**, *823*, 61.

[210] A. Babaei, A. R. Taheri, *Sensors and Actuators B: Chemical* **2013**, *176*, 543.

[211] B. Zhang, D. Huang, X. Xu, G. Alemu, Y. Zhang, F. Zhan, Y. Shen, M. Wang,

Electrochimica Acta **2013**, *91*, 261.

[212] S. Wang, Z. Qi, H. Huang, H. Ding, *Analytical Letters* **2012**, *45*, 1658.

[213] G. RIVAS, M. RUBIANES, M. RODRIGUEZ, N. FERREYRA, G. LUQUE, M. PEDANO, S. MISCORIA, C. PARRADO, *Talanta* **2007**, *74*, 291.

[214] L. Agüí, P. Yáñez-Sedeño, J. M. Pingarrón, *Analytica Chimica Acta* **2008**, *622*, 11.

[215] M. E. Ghica, R. Pauliukaite, O. Fatibello-Filho, C. M. A. Brett, *Sensors and Actuators B: Chemical* **2009**, *142*, 308.

[216] S. Murugesan, K. Myers, V. R. Subramanian, *Applied Catalysis B: Environmental* **2011**, *103*, 266.

[217] G. Oliveira, B. Janegitz, V. Zucolotto, O. Fatibello-Filho, *Open Chemistry* **2013**, *11*, 1837.

[218] S. Phal, B. Lindholm-Sethson, P. Geladi, A. Shchukarev, S. Tesfalidet, *Analytica Chimica Acta* **2017**, *987*, 15.

[219] Y. Wang, H. Liu, F. Wang, Y. Gao, *J. solid state Electrochem,* **2012**, *16,* 3227.

[220] F. Wang, Y. Wang, K. Lu, X. Wei, B. Ye, *J. Electroanal. Chem*, **2012**, *674*, 83.

[221] E. M. Materon, A. Wong, O. Fatibello-Filho, R. C. Faria, *Journal of Electroanalytical Chemistry* **2018**, *827*, 64.

[222] Y. Wang, J. Xie, L. Tao, H. Tian, S. Wang, H. Ding, *Sensors and Actuators B: Chemical* **2014**, *204*, 360.

[223] D. A. El-Hady, M. M. Seliem, R. Gotti, N. A. El-Maali, *Sensors and Actuators B: Chemical* **2006**, *113*, 978.

[224] T. Brooks, C. W. Keevil, *Letters in Applied Microbiology* **1997**, *24*, 203.

[225] V. S. Kumar, M. Satyanarayana, K. Y. Goud, K. V. Gobi, *Clean Technologies and Environmental Policy* **2018**, *20*, 759.

[226] M. Satyanarayana, K. Koteshwara Reddy, K. Vengatajalabathy Gobi, *Electroanalysis* **2014**, *26*, 2365.

[227] D. N. Travessa, F. S. da Silva, F. H. Cristovan, A. M. Jorge Jr., K. R. Cardoso, *Materials Research* **2014**, *17*, 687.

[228] H. Sharma, D. C. Agarwal, A. K. Shukla, D. K. Avasthi, V. D. Vankar, *Journal of Raman Spectroscopy* **2013**, *44*, 12.

[229] S. Hrapovic, E. Majid, Y. Liu, K. Male, J. H. T. Luong, *Analytical Chemistry* **2006**, *78*, 5504.

[230] E. Laviron, *Journal of Electroanalytical Chemistry and Interfacial Electrochemistry* **1979**, *101*, 19.

[231] M. Satyanarayana, K. Y. Goud, K. K. Reddy, K. V. Gobi, *Electrochimica Acta* **2015**, *178*, 608.

[232] Y. Wei, L. Luo, Y. Ding, X. Si, Y. Ning, *Bioelectrochemistry* **2014**, *98*, 70.

[233] B. Shah, T. Lafleur, A. Chen, *Faraday Discussions* **2013**, *164*, 135.

[234] A. Savaşer, C. K. Özkan, Y. Özkan, B. Uslu, S. A. Özkan, *Journal of Liquid Chromatography & Related Technologies* **2003**, *26*, 1755.

[235] R. K. Singla, A. Mitra, F. H. Assaleh, B. R. Chandu, *Scientia Pharmaceutica* **2014**, *82*, 617.

[236] D. Sathis Kumar, B. D. N. Prashanthi, A. Harani, P. Anusha, *Jurnal Teknologi* **2015**, *76*.

[237] A. El-Zaher, R. EL-Bagary, F. Morsy, M. Mostafa, *Analytical Chemistry Insights* **2014**, 41.

[238] C. H. A. Kumar, T. A. Kumar, B. M. Gurupadayya, S. N. Sloka, **2010**, *2*, 278.

[239] J. S. Reddy, I. E. Chakravarth, K. Prabhavathi, **2011**, *3*, 773.

[240] R. Kanneti, R. Rajesh, J. R. Aravinda Raj, P. A. Bhatt, *Chromatographia* **2009**, *70*, 407.

[241] D. Khalafallah, N. Akhtar, O. Y. Alothman, H. Fouad, K. Abdelrazek khalil, *Solid State Sciences* **2017**, *71*, 51.

[242] C. Zhang, C. Hua, G. Wang, M. Ouyang, C. Ma, *Electrochimica Acta* **2010**, *55*, 4103.

[243] R. Solmaz, *Progress in Organic Coatings* **2011**, *70*, 122.

[244] V. M. Cristante, S. M. A. Jorge, J. P. S. Valente, M. J. Saeki, A. O. Florentino, P. M. Padilha, *Thin Solid Films* **2007**, *515*, 5334.

[245] M. Satyanarayana, K. Yugender Goud, K. Koteshwara Reddy, K. Vengatajalabathy Gobi, *Electrocatalysis* **2017**, *8*, 214.

[246] Z. Linting, L. Ruiyi, L. Zaijun, X. Qianfang, F. Yinjun, L. Junkang, *Sensors and Actuators B: Chemical* **2012**, *174*, 359.

[247] G. Wang, R. Han, X. Su, Y. Li, G. Xu, X. Luo, *Biosensors and Bioelectronics* **2017**, *92*, 396.

[248] G. C. Pedro, F. D. S. Gorza, R. J. da Silva, K. T. O. do Nascimento, J. C. Medina-Llamas, A. E. Chávez-Guajardo, J. J. Alcaraz-Espinoza, C. P. de Melo, *Analytica Chimica Acta* **2019**, *1047*, 214.

[249] X. Liu, Q. Han, Y. Zhang, X. Wang, S. Cai, C. Wang, R. Yang, *Applied Surface Science* **2019**, *471*, 929.

[250] J. Han, M. Wang, Y. Hu, C. Zhou, R. Guo, *Progress in Polymer Science* **2017**, *70*, 52.

[251] T. S. Martins, J. L. Bott-Neto, P. A. Raymundo-Pereira, E. A. Ticianelli, S. A. S. Machado, *Sensors and Actuators B: Chemical* **2018**, *276*, 378.

[252] R. K. Gupta, M. P. Srinivasan, R. Dharmarajan, *Materials Letters* **2012**, *67*, 315.

[253] P. Kannan, S. A. John, *Electrochimica Acta* **2011**, *56*, 7029.

[254] S. S. Nair, S. A. John, T. Sagara, *Electrochimica Acta* **2009**, *54*, 6837.

[255] H. Huang, X. Yang, *Biomacromolecules* **2004**, *5*, 2340.

[256] D. Tarinc, A. Golcu, *Russian Journal of Electrochemistry* **2015**, *51*, 149.

[257] B.-R. Adhikari, M. Govindhan, H. Schraft, A. Chen, *Journal of Electroanalytical Chemistry* **2016**, *780*, 241.

[258] R. Jain, P. Pandey, *Ionics* **2015**, *21*, 3279.

[259] B. Uslu, S. A. Özkan, Z. Şentürk, *Analytica Chimica Acta* **2006**, *555*, 341.

[260] S. Kummari, V. S. Kumar, M. Satyanarayana, K. V. Gobi, *Microchemical Journal* **2019**, *148*, 626.

[261] R. E. Ritts, *Journal of Antimicrobial Chemotherapy* **1990**, *26*, 31.

[262] A. E. Muller, E. M. Verhaegh, S. Harbarth, J. W. Mouton, A. Huttner, *Clinical Microbiology and Infection* **2017**, *23*, 355.

[263] M. S. Bader, M. Loeb, A. A. Brooks, *Postgraduate Medicine* **2017**, *129*, 242.

[264] J. Vinoth Kumar, R. Karthik, S.-M. Chen, K.-H. Chen, S. Sakthinathan, V. Muthuraj, T.-W. Chiu, *Chemical Engineering Journal* **2018**, *346*, 11.

[265] L. Lebid, *Ukrainian Journal of Nephrology and Dialysis* **2017**, *54*, 126.

[266] U. Athikomrattanakul, M. Katterle, N. Gajovic-Eichelmann, F. W. Scheller, *Biosensors and Bioelectronics* **2009**, *25*, 82.

[267] Q. Wang, Y.-C. Liu, Y.-J. Chen, W. Jiang, J.-L. Shi, Y. Xiao, M. Zhang, *Anal. Methods* **2014**, *6*, 4414.

[268] W. Liu, C. Zhao, Y. Zhang, S. Lu, J. Liu, R. Xi, *Journal of Agricultural and Food Chemistry* **2007**, *55*, 6829.

[269] V. Arancibia, *Talanta* **2003**, *61*, 377.

[270] L.-Q. Sheng, M.-M. Chen, S.-S. Chen, N.-N. Du, Z.-D. Liu, C.-F. Song, R. Qiao, *Food Additives & Contaminants: Part A* **2013**, *30*, 2114.

[271] H. Li, J. Ren, X. Xu, L. Ning, R. Tong, Y. Song, S. Liao, W. Gu, X. Liu, *The Analyst* **2019**, *144*, 4513.

[272] D. Wilasinee, P. Sutthivaiyakit, S. Sutthivaiyakit, *Analytical Letters* **2015**, *48*, 1979.

[273] U. Athikomrattanakul, N. Gajovic-Eichelmann, F. W. Scheller, *Analytical Chemistry* **2011**, *83*, 7704.

[274] P. Salgado-Figueroa, P. Jara-Ulloa, A. Alvarez-Lueje, J. A. Squella, *Electroanalysis* **2013**, *25*, 1433.

[275] M. Satyanarayana, K. Y. Goud, K. K. Reddy, V. S. Kumar, K. V. Gobi, *Materials Science and Engineering: C* **2019**, *101*, 103.

[276] S. Vetri Selvi, *International Journal of Electrochemical Science* **2019**, *14*, 6454.

[277] W. Zhang, S. Cao, Z. Wu, M. Zhang, Y. Cao, J. Guo, F. Zhong, H. Duan, D. Jia, *Sensors* **2019**, *20*, 149.

[278] B. Karuppaiah, R. Ramachandran, S.-M. Chen, S. Wan-Ling, J. Y. Wan, *New Journal of Chemistry* **2020**, *44*, 46.

[279] S. Velmurugan, S. Palanisamy, T. C-K Yang, M. Gochoo, S.-W. Chen, *Ultrasonics Sonochemistry* **2020**, *62*, 104863.

[280] S. Palanisamy, S. Cheemalapati, S.-M. Chen, *Materials Science and Engineering: C* **2014**, *34*, 207.

[281] S. Cheemalapati, S. Palanisamy, V. Mani, S.-M. Chen, *Talanta* **2013**, *117*, 297.

[282] J. Yuan, X. Zheng, L. Jiang, D. Yao, G. He, H. Chen, J. Che, *Materials Letters* **2018**, *219*, 68.

[283] F.-H. Kuok, H.-H. Chien, C.-C. Lee, Y.-C. Hao, I.-S. Yu, C.-C. Hsu, I.-C. Cheng, J.-Z. Chen, *RSC Advances* **2018**, *8*, 2851.

[284] X. Peng, K. Wu, Y. Hu, H. Zhuo, Z. Chen, S. Jing, Q. Liu, C. Liu, L. Zhong, *Journal of Materials Chemistry A* **2018**, *6*, 23550.

[285] V. Mani, B. Devadas, S.-M. Chen, *Biosensors and Bioelectronics* **2013**, *41*, 309.

[286] H. Tong, J. Zhu, J. Chen, Y. Han, S. Yang, B. Ding, X. Zhang, *Journal of Solid State Electrochemistry* **2013**, *17*, 2857.

[287] V. Sunil Kumar, S. Kummari, K. Yugender Goud, M. Satyanarayana, K. Vengatajalabathy Gobi, *International Journal of Hydrogen Energy* **2020**, *45*, 1018.

[288] F. T. Johra, J.-W. Lee, W.-G. Jung, *Journal of Industrial and Engineering Chemistry* **2014**, *20*, 2883.

[289] S. Hrapovic, E. Majid, Y. Liu, K. Male, J. H. T. Luong, *Analytical Chemistry* **2006**, *78*, 5504.

[290] E. Laviron, *Journal of Electroanalytical Chemistry and Interfacial Electrochemistry* **1979**, *101*, 19.

[291] W. Richard, D. Evrard, P. Gros, *Journal of Electroanalytical Chemistry* **2012**, *685*, 109.

[292] G. Aydoğdu, G. Günendi, D. K. Zeybek, B. Zeybek, Ş. Pekyardımcı, *Sensors and Actuators B: Chemical* **2014**, *197*, 211.

[293] Z. Krejčová, J. Barek, V. Vyskočil, *Electroanalysis* **2015**, *27*, 185.

[294] P. de Lima-Neto, A. N. Correia, R. R. Portela, M. da S. Julião, G. F. Linhares-Junior, J. E. S. de Lima, *Talanta* **2010**, *80*, 1730.

[295] N.-N. Du, M.-M. Chen, L.-Q. Sheng, S.-S. Chen, H.-J. Xu, Z.-D. Liu, C.-F. Song, R. Qiao, *Journal of Chromatography A* **2014**, *1327*, 90.

[296] L. Rodziewicz, *Journal of Chromatography B* **2008**, *864*, 156.

[297] M. Satyanarayana, K. Y. Goud, K. K. Reddy, K. V. Gobi, *Electrochimica Acta* **2015**, *178*, 608.

[298] Q. Jin, L. Shan, J. Yue, X. Wang, *Food Chemistry* **2008**, *108*, 779.

[299] B. A. Patel, M. Arundell, K. H. Parker, M. S. Yeoman, D. O'Hare, *Journal of Chromatography B* **2005**, *818*, 269.

[300] D. A. Román, A. S. Carretero, C. C. Blanco, A. F. Gutiérrez, *Biomedical Chromatography* **2004**, *18*, 422.

[301] X. Huang, G. Mazza, *Critical Reviews in Food Science and Nutrition* **2011**, *51*, 269.

[302] V. Schroeder, S. Savagatrup, M. He, S. Lin, T. M. Swager, *Chemical Reviews* **2019**, *119*, 599.

[303] G. RIVAS, M. RUBIANES, M. RODRIGUEZ, N. FERREYRA, G. LUQUE, M. PEDANO, S. MISCORIA, C. PARRADO, *Talanta* **2007**, *74*, 291.

[304] K. Vinothkumar, M. G. Sethuraman, *Materials Today Communications* **2018**, *14*, 27.

[305] L. Jiang, J. A. Syed, H. Lu, X. Meng, *Journal of Alloys and Compounds* **2019**, *770*, 35.

[306] C. Wang, Z.-Y. Hu, H. Zhao, W. Yu, S. Wu, J. Liu, L. Chen, Y. Li, B.-L. Su, *Journal of Colloid and Interface Science* **2018**, *521*, 1.

[307] U. Riaz, S. M. Ashraf, J. Kashyap, *Materials Research Bulletin* **2015**, *71*, 75.

[308] Z. Linting, L. Ruiyi, L. Zaijun, X. Qianfang, F. Yinjun, L. Junkang, *Sensors and Actuators B: Chemical* **2012**, *174*, 359.

[309] G. Wang, R. Han, X. Su, Y. Li, G. Xu, X. Luo, *Biosensors and Bioelectronics* **2017**, *92*, 396.

[310] M. H. Ghanbari, F. Shahdost-Fard, H. Salehzadeh, M. R. Ganjali, M. Iman, M. Rahimi-Nasrabadi, F. Ahmadi, *Microchimica Acta* **2019**, *186*, 641.

[311] J. Han, M. Wang, Y. Hu, C. Zhou, R. Guo, *Progress in Polymer Science* **2017**, *70*, 52.

[312] T. S. Martins, J. L. Bott-Neto, P. A. Raymundo-Pereira, E. A. Ticianelli, S. A. S. Machado, *Sensors and Actuators B: Chemical* **2018**, *276*, 378.

[313] Y. Li, Y. Ji, B. Ren, L. Jia, G. Ma, X. Liu, *Materials Research Bulletin* **2019**, *109*, 240.

[314] I. Cesarino, H. V Galesco, S. A. S. Machado, *Materials Science and Engineering: C* **2014**, *40*, 49.

[315] M. Mazloum-Ardakani, A. Khoshroo, *Electrochimica Acta* **2014**, *130*, 634.

[316] O. E. Fayemi, A. S. Adekunle, E. E. Ebenso, *Sensing and Bio-Sensing Research* **2017**, *13*, 17.

[317] M. Song, S. Kim, N. Ki Min, J. Jin, *Biosensors and Bioelectronics* **2014**, *52*, 411.

[318] D. Sun, H. Li, M. Li, C. Li, H. Dai, D. Sun, B. Yang, *Sensors and Actuators B: Chemical* **2018**, *259*, 433.

[319] M. C. Bonetto, F. F. Muñoz, V. E. Diz, N. J. Sacco, E. Cortón, *Electrochimica Acta* **2018**, *283*, 338.

[320] M. Mazloum-Ardakani, A. Khoshroo, *Journal of Electroanalytical Chemistry* **2014**, *717–718*, 17.

[321] P. Gupta, R. N. Goyal, *Talanta* **2014**, *120*, 17.

[322] H. S. Han, J. You, H. Jeong, S. Jeon, *Applied Surface Science* **2013**, *284*, 438.

LIST OF PUBLICATIONS & BIO-DAT

LIST OF PUBLICATIONS & BIO-DA

Publications in Peer-Reviewed/Refereed International Journals

1. *Direct electrochemical determination of methotrexate using functionalized carbon nanotube paste electrode as biosensor for in-vitro analysis of urine and dilute serum samples*
   Shekher Kummari, V. Sunil Kumar, M. Satyanarayana, K. Vengatajalabathy Gobi
   Microchemical Journal 148 (2019) 626–633 ***(IF 4.56)***

2. Facile Electrochemically Reduced GO-CNT as Sensitive Probe for Determination of Nitrofurantoin in Biological Fluids
   Shekher Kummari, V. Sunil Kumar, K. Vengatajalabathy Gobi
   Electroanalysis 32 (2020) 2452-2462 ***(IF 2.54)***

3. A review on recent developments in optical and electrochemical aptamer-based assays for mycotoxins using advanced nanomaterials *(Review)*
   K. Yugender Goud, K. Koteshwara Reddy, M. Satyanarayana, **Shekher Kummari,** K. Vengatajalabathy Gobi
   Microchimica Acta (2020) 187:29 ***(IF 6.23)***

4. One-pot synthesis of $Pd_{20-x}Au_x$ nanoparticles embedded in nitrogen doped graphene as highperformance electrocatalyst toward methanol oxidation
   V. Sunil Kumar, **Shekher Kummari,** K. Yugender Goud, M. Satyanarayana, K. Vengatajalabathy Gobi
   International journal of hydrogen energy 45 (2020) 1018 – 2019 ***(IF 4.93)***

5. *Electrodissolution-induced deposition of nanoAu particles on poly-(3-amino-5-hydroxypyrazole) coated carbon paste electrode for highly sensitive detection of Valacyclovir in physiological samples.*
   Shekher Kummari, *V. Sunil Kumar, Yugender Goud, K. Vengatajalabathy Gobi*
   Sensors and Actuators B: (Communicated)

6. *Electropolymerized Conducting Polymer on Multi-Walled Carbon Pasta Electrode as a Sensing Matrix for the Sensitive Detection of an Anti-Viral Drug Valganciclovir in Human Biological Samples.*
   Shekher Kummari, V. Sunil Kumar, K. Vengatajalabathy Gobi
   (Manuscript under preparation)

Book chapter

Metal oxide-metal nanocomposite-modified electrochemical sensors for toxic chemicals

K. Koteshwara Reddy, K. Yugender Goud, M. Satyanarayana, S. Kummari, V. S. Kumar, H. Bandal, T. Jayaramudu, R. Pyarasani, H. Kim, J. Amalraj, K. V. Gobi *

Book chapters in Metal Oxide Series, Elsevier, 2021. pp. 79-137.

BIO-DATA

Shekher Kummari

Contact Address
S/O. K. Balaiah
Regulapally
Bejjanki (Mandal)
Siddipet (District) – 505473
Telangana, India.
E-mail: shekar.kummari1@gmail.com
shekarnitw@student.nitw.ac.in
Mobile: +91-9966408954

Objective: To be professionally associated with an organization, where I can utilize my Doctoral Research experience in solving the practical challenges and achieve the goals of the organization

Academic Qualifications:

January 2016 – Present : Research Scholar (PhD Student)
Under the supervision of **Professor. K. V. Gobi**, Department of Chemistry, National Institute of Technology Warangal, Telangana, India

Research Topic: "*Development of Hybrid Graphitic Carbon Nanocomposites as Sensing Platform for Pharmaceutical Drugs in-vitro in Biological Fluids"*
Status: To be awarded (Thesis submitted)

July 2011 – May 2013 : Master of Science in Chemistry
University College of Science, Osmania University, Telangana, India
Cumulative Grade Point Average (CGPA): **6.3** (First Class)

June 2007 – April 2011 : Bachelor of Science (Chemistry, Zoology and Fisheries)
Osmania University, Siddipet, Telangana, India
Percentage of Marks: **59.63 (Second Class)**

June 2005 – March 2007 : Intermediate (Botany, Zoology, Physics and Chemistry)
Board of Intermediate Education, Andhra Pradesh, India
Percentage of Marks: **62.8 (First Division)**

June 2004 – March 2005 : Secondary School Certificate (High School)
Board of Secondary Education, Andhra Pradesh, India
Percentage of Marks: **78.8 (First Division)**

Professional Summary:

- **Ph.D. Research Fellow** at National Institute of Technology, Warangal, Telangana, India, from January 2016 to till date.

Personal Details:

- Name : Shekher Kummari.
- Father's Name : Balaiah
- Date of Birth : 10-05-1990
- Gender : Male
- Marital Status : Unmarried
- Nationality : Indian
- Languages Known : Telugu, English and Hindi

Achievements:

- Qualified Graduate Aptitude Test in Engineering (**GATE**) 2015.
- Secured 154th rank in Osmania University Entrance Test **(OU)** 2011 for M.Sc. Admissions.

Technical Skills:

- Expertise in utilizing the software - Microsoft Office, Ngraph, Origin etc., Chemistry Related software - ChemDraw Ultra 12.0, HyperChem Release - 8.0.9, X'Pert HighScore Plus.
- Expertise in MENDELEY Reference Manager.

Expertise in Instrumental Techniques:

- Electrochemical Impedance Analyzer, Zahner-Elektrik (IM6e), GmbH, Germany
- Electrochemical Workstation, Sinsil CHI 619D and CHI6132e.
- UV-Visible Spectrophotometers, Analytik Jena Specord 205 and Shimadzu 1601
- FTIR Spectrophotometer, PerkinElmer
- Raman spectrometer, HR800 LabRAM confocal

- Differential Scanning Calorimeter, Q10 TA instruments, USA
- Scanning Electron Microscope, VEGA3, Tescon, USA
- Other small instruments relevant for materials characterization and analysis

Research Interests:

- Biosensors and Electrochemical Sensors
- Nanostructured Materials
- Nano-composites towards Practical Applications of Electrochemistry.
- Electrochemical Techniques

Other Capabilities:

- Capable of carrying out both collaborative and independent research
- Motivated strong ethics and providing efficient service
- Very good interpersonal and communication skills along with management skills
- Good experience in writing technical papers, presentations and reports
- Guided many post-graduate students for their projects